MOTOROLA Government Electronics Division

FINAL REPORT
AROD GEODETIC FEASIBILITY ANALYSIS PROGRAM

SCOTTSDALE, ARIZONA 85252

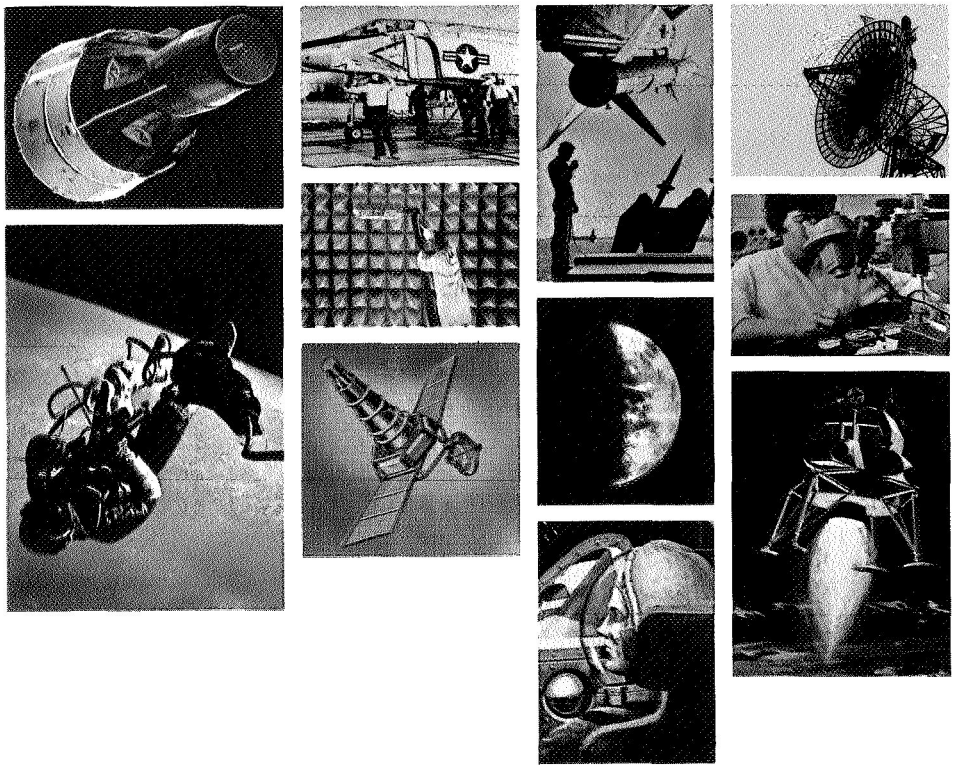

CONTRACT NASW-1794

26 November 1969

Approved By

K. Porter, Chief Engineer
Space Systems Laboratory

Prepared By

Stanley W. Attwood,
Senior Engineer
Advanced Development Section

FINAL REPORT
AROD GEODETIC FEASIBILITY ANALYSIS PROGRAM

Presented to
NASA Headquarters
Washington, D. C.

MOTOROLA • Government Electronics Division • 8201 E. McDOWELL ROAD, SCOTTSDALE, ARIZ. 85252

ABSTRACT

AROD GEODETIC FEASIBILITY ANALYSIS

This is the final report on an analysis to evaluate the potential performance of AROD as a satellite geodetic survey instrument. This analysis reviews four principle areas: (1) Equipment performance, (2) Propagation effects, (3) Geometrical effects, and (4) The benefits of advanced data processing.

The first two areas were evaluated by Motorola. The latter two through simulation were studied by DBA Systems under sub-contract to Motorola.

The main results of the study are that the ranging capability of the AROD System and advanced methods of propagation correction largely remove ranging error from geodetic survey. The principle source of error is the definition of orbital parameters and strength of figures. Geodetic survey to accuracies of 1 meter are possible with a relatively few number of passes.

TABLE OF CONTENTS

TABLE OF CONTENTS (CONT.)

TABLE OF CONTENTS (CONT.)

LIST OF ILLUSTRATIONS

LIST OF ILLUSTRATIONS (CONT.)

LIST OF TABLES

SECTION I

1.0 INTRODUCTION

This is the final report on the AROD Geodetic Survey Feasibility Analysis done under contract no. NASW-1794 for NASA Headquarters. The purpose of the study was to evaluate the potential performance of AROD (Advanced Range and Orbit Determination) system used for satellite geodetic survey.

There are four basic parts to the study:

1. An evaluation of the AROD hardware performance,
2. A review and numerical estimate of propagation error,
3. The effects of geometry, and
4. The benefits of advanced data processing.

The first two parts of the evaluation were performed by Motorola. The evaluation of geometrical and data processing effects was performed under sub-contract to Motorola by DBA Systems. This latter work is reported in total in Section 5.0 of this report. All other sections of this report were prepared by Motorola. The final conclusion as to the overall capability and advantages of AROD as a geodetic survey tool are the opinions of Motorola.

The basic conclusion to be reached on the basis of the results of this study program is that AROD can indeed provide geodetic survey to an accuracy of the order of one meter with reasonable geometry and number of satellite passes such as 10. In addition, because of its small size and weight, it is operationally attractive and requires a minimum of data processing to achieve the stated performance.

The theoretical performance is as good as or better than other systems now in use. Therefore, AROD should be considered seriously for application as a satellite geodetic survey tool.

SECTION II

2.0 SCOPE OF THE STUDY AND RECOMMENDATIONS

The analysis study program was restricted in scope in each of the four areas of investigation. In the area of the evaluation of equipment performance, the effort was confined to a thorough review of the extensive laboratory test evaluation performed under the AROD development program for NASA Marshall Space Flight Center. [2] In addition, throughout the present study, the AROD equipment was tested periodically to measure any latent drift or change in equipment accuracy with age. The equipment performance is reported in Sections 4.1 and 4.2.

In the area of propagation the study was confined to a review of the literature and where appropriate a review of methods currently used. In the latter case, no operational methods were found which were appropriate to the frequency band used or with the accuracy necessary for geodetic survey. Two experimental methods, one by NBS and one by DBA Systems, were reviewed as applicable. These are covered for both tropospheric effects and ionospheric effects in Sections 4.4 and 4.5. No experimental verification was contemplated.

The areas of geometry and data processing are interrelated and were studied as a single entity. This study was confined to a limited number of geometrical cases, employing a fixed altitude satellite typical of current experimental survey satellites. There was no intention to compare or contrast various geodetic survey systems. However, the study was so directed that the results may be compared readily with both theoretical analysis and field tests using other systems such as SECOR and optical methods. The geometry and station locations are those used in previous tests. The passes were chosen to resemble those actually used in the past.

Results of theoretical error models and simulations in the past have generally proven to be somewhat optimistic. Although every effort has been made to be accurate throughout this study, only an operational flight test will provide the ultimate evaluation of AROD as a geodetic survey tool. On the basis of the results projected by this study program, this is recommended.

SECTION III

3.0 AROD SYSTEM DESCRIPTION

3.1 INTRODUCTION

A complete functional description of the AROD system is contained in the AROD System Description Report[1]. This section presents a brief summary of the basic concepts and principles of AROD as they are applicable to its use for geodetic survey. The purpose of this description is three-fold. First, it should provide some insight into the objectives and general characteristics of AROD and how it can be used operationally. Second, the description serves as a basis for defining equipment measurement error sources whose effect is analyzed to develop an error model. Third, the description defines certain system parameters that were specified for the feasibility model objectives but which might be changed for geodetic survey applications.

The AROD program was originally a part of the Saturn 5 program. Due to program delay, the AROD development was removed from the Saturn 5 program and in December 1964, Motorola was awarded a contract to develop a feasibility demonstration model of the AROD as an advanced technology and development program. There were two principle goals in this contract. First, to develop a system to determine range and range rate in the vehicle from four ground stations simultaneously with very high equipment accuracy. The system was to be completely

automatic and unattended and to require no calibration other than initial alignment for a mission life of two years. The operational requirements were tailored for earth orbit Saturn 5 missions. Second, to develop as small, light weight, and low power a vehicle equipment as possible consistent with the 1964 state-of-the-art in packaging and components.

Although not developed for geodetic survey, the system that evolved is potentially capable of providing excellent geodetic survey performance using both satellite and aircraft terminals. That is the reason for this evaluation study.

3.2 GENERAL DESCRIPTION AND OPERATIONAL CHARACTERISTICS

AROD is a vehicle based radio frequency system which provides near real time range and range rate data from multiple ground-based transponder sites. These are determined from measurements of time delay and doppler. Computation of the vehicle position and its velocity vector can be performed on a separate vehicle computer using the data obtained by simultaneous interrogation of three or more ground sites. The ground stations are completely automatic and require no external timing or synchronization other than the signals from the orbiting vehicle.

The AROD system has been designed with a high degree of flexibility to make it adaptable to a wide variety of missions and applications. This flexibility includes frequency versatility to accommodate varying channel assignments and an adaptable program to determine the site acquisition sequence and criteria for advancing to a new site. Simultaneous tracking of three

stations while acquiring a new site is the normal mode of operation, each site being dropped on the basis of an increasing range exceeding a pre-programmed number, and a new site being selected from the vehicle program. This program can be preset or changed in flight.

Two radio frequency links between the vehicle and each transponding site are used to perform the AROD functions. A VHF down-link is used for station control and to accelerate the acquisition process. This link essentially performs the duties normally accomplished by the operator in a manned station. It provides an estimate of vehicle direction, vehicle velocity and approximate range, and the turn-on turn-off instructions. Provisions have been made to allow this link to do double duty as a telemetry communications channel simultaneously with its normal AROD functions.

A turn-around S-band link is used for the range and range rate measurements. The range is determined from the two-way time delay upon the S-band modulation, and the range rate is derived from the two-way doppler shift of the S-band carrier. Coherent frequency translation is used throughout to provide the desired accuracy. The range modulation is transmitted as ±90 degree phase reversals of the carrier and is derived from a binary pseudo-noise (PN) code.

The system is fully coherent in the tracking mode. All radio frequency carriers as well as the range modulation, the time generation, and measurement intervals are derived from a common

source located in the vehicle. This eliminates some sources of measurement error and also permits the use of each signal to aid the others during acquisition and tracking. It also provides the means of mutual assistance under conditions of high dynamics or abnormal signal reception.

The AROD functional subsystems and their interconnections are shown in block form in Figure 3.1-1. These subsystems perform the following services in the acquisition and tracking modes.

1. The Vehicle Frequency and Time Reference is the master time and frequency reference for the entire system. From one stable oscillator are derived the tracking frequencies, the control frequencies, the ranging signals, the time labels for the data readout, and all internal signals needed in the remainder of the system. The carrier frequency signals for the transmitters and the local oscillator signals for the tracking receivers are derived in the programmable frequency synthesizers.
2. The Vehicle System Control Logic controls the selection of stations, establishes the sequence of events during acquisition, and contains the memory necessary for station release at the proper range. This subsystem also contains the logic required to assign channels and to make decisions based on the reported tracking status in both the vehicle and transponder receivers.
3. The Vehicle Station Control Transmitter is a vhf transmitter which provides the transponder station with control

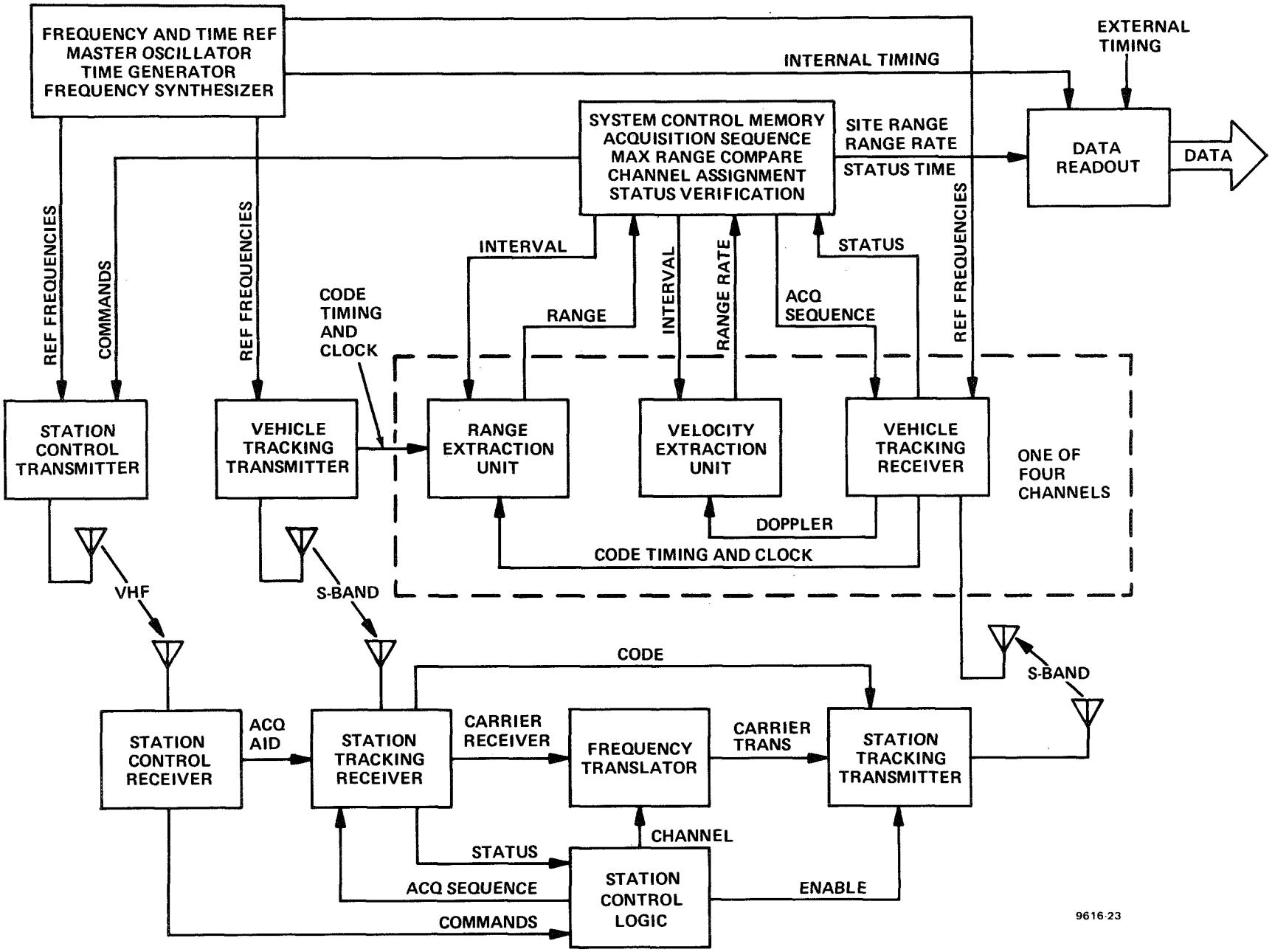

Figure 3.1-1. AROD Functional Subsystems

data, and assists the ground station in the acquisition of the tracking signal. The acquisition aids include minimization of spatial search, Doppler frequency search, and code timing search. This signal also provides an antisideband lockout aid to the station tracking receiver. The reception of a standby command by the Station Control Receiver automatically applies power to the remainder of the station equipment.

4. The S-Band Vehicle Tracking Transmitter is modulated with the Range Modulation signal for the determination of the vehicle position and velocity. To minimize equipment delays, the code timing and high speed clock are extracted near the modulator and delivered to the Range Extraction Unit.

5. The S-Band Vehicle Tracking Receiver contains four channels to process the multiple station return signals simultaneously. The receiver correlates the range modulation upon the received signals and extracts the Doppler velocity from each channel. The receiver also provides detection of the up-link data and provides operating status indications to the System Control Logic.

6. The Vehicle Range Extraction Unit contains the Transmitter Range Modulation Generator. The transmitted range modulation is compared against the received signals, and the time difference is computed. The time delay is sent to the data readout section and to the system control section where it is compared against the preset maximum range.

One of these units operates with each tracking receiver channel.

7. The Vehicle Velocity Extraction Unit contains a gated counter which extracts the S-Band Doppler shift for range rate determination. One of these units operates with each tracking receiver channel. As the gated time interval is determined from the same frequency source as the S-band carrier there is no bias error in the range rate extraction.

8. In the Vehicle Data Readout Section the information from the Range Extraction Units, the Velocity Extraction Units, the site identification, and the time of the readings are combined for readout to the vehicle computer or to telemetry. The readout rate is nominally four times per second and may be either internally synchronized or may be interrogated by an external non-synchronous timing signal.

9. The Station Control Receiver is the vhf receiver at each of the transponder stations. The receiver provides for the demodulation of control data, supplies a timing signal to the S-Band Tracking Receiver for coarse range correlation, and programs the tracking receiver to the expected Doppler shifted frequency.

10. The Transponder Station Control Logic decodes the control information, programs the Station Tracking Transmitter to the desired channel, and provides the sequencing necessary for mode control of the transponder station.

11. The Station Tracking Receiver receives the range modulated S-band signal from the vehicle and correlates the range modulation. The receiver is fully coherent to preserve the Doppler velocity information. A submultiple of the received carrier frequency is directed to the Station Frequency Translator for use in deriving the transmitted carrier.

12. The Station Frequency Translator contains the stable oscillator used in generating the reversed Doppler signal for initial retransmission to the vehicle. It also contains the circuitry necessary to generate any one of four possible coherent transmitter frequencies as directed by the Station Control Logic.

13. The Station Tracking Transmitter amplifies the desired channel carrier signal and modulates this signal with the recorrelated range modulation. The site identification and operating status codes are also applied to the transmitter.

3.3 BASIC AROD CONCEPTS AND PRINCIPLES

The previous section presented an overall description of the AROD System. Here the emphasis is placed upon four aspects of the system that are important to the potential capability of AROD as a geodetic survey tool. These are signal processing, time delay (Range) measurement, Doppler (Range Rate) measurement, and the role played by the vhf link.

The first three require some further description as they relate directly to range and range rate measurement accuracy. The vhf

command and control link provides several important operational functions. Its ability to do this for system parameters other than those currently contained in the equipment may be compromised.

The AROD system simultaneously measures the round trip delay from the vehicle to four ground based transponders. This concept eliminates the necessity for knowing the time relationship between transponder stations. This greatly simplifies the transponder terminals. All measurements are made with respect to the master oscillator in the vehicle. This oscillator or clock drives a time base generator which can be easily synchronized to an external source.

3.3.1 Signal Processing

Time delay variation of the equipment is the critical parameter for range measurement accuracy. Phase variation over the measurement interval is the important parameter in range rate measurements. Both are minimized in the AROD system by a unique signal processing technique. Correlation detection is used between the receiver reference and the received signal at a point as close to the antenna as possible. The tracking error signal is transformed into a form that is least sensitive to variations in the equipment parameters. Specifically the variations in equipment parameters lead to variation in gain of the tracking servo systems and not to variations in time delay or rapid variations of phase in the carrier tracking system. The basic principle can best be explained with a simplified system. A functional block diagram of such a system is presented in Figure 3.3-1.

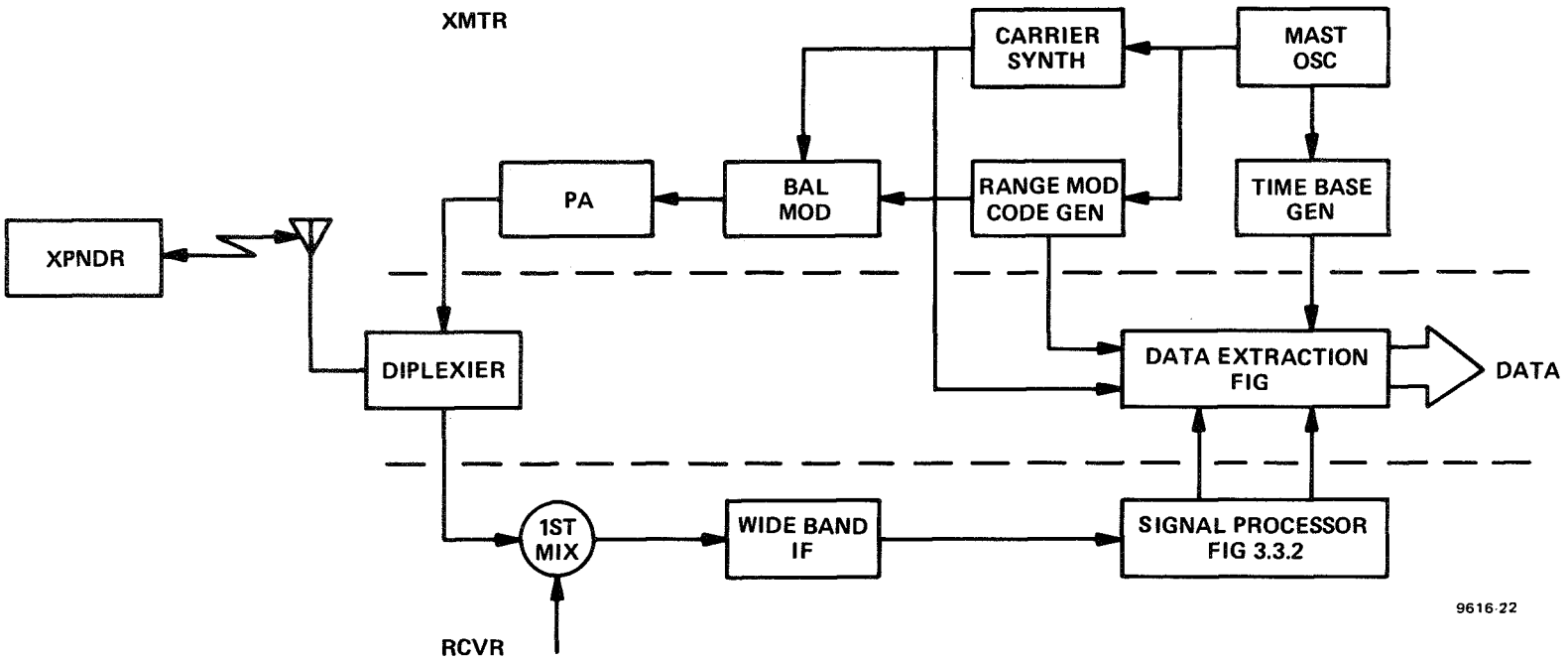

Figure 3.3-1
Signal Processing System

All frequencies are derived from a single master oscillator. A 6.4 MHz clock is derived and used to drive a pseudo-noise (PN) code generator. This code is the range modulation and bi-phase modulates the transmitter carrier. The composite signal is transmitted to the transponder where it is coherently translated and retransmitted back to the vehicle receiver. The received signal is coherently translated to an intermediate frequency and presented to the signal processing section of the receiver. The function of this unit is to demodulate the range modulation and doppler signal and present these signals to the data extraction units, where the estimate of range and range rate data is performed. The signal processor derives its advantages by developing a modulating loop error signal which is proportional to the magnitude and sign of the carrier component - phase shift and delays from the balanced demodulator only effect the open loop gain of the modulation tracking loop and are a second order effect. This fact will become evident by tracing the signal path through the signal processor.

The functional block diagram of the signal processing section is shown in Figure 3.3-2. The received signal is described as:

(1) $e_r = m_1(t) \sin(w_1 t + \theta_1)$

$m_1(t)$ = PN sequence with value +1 or -1

w_1 = intermediate frequency

θ_1 = phase angle of the received signal

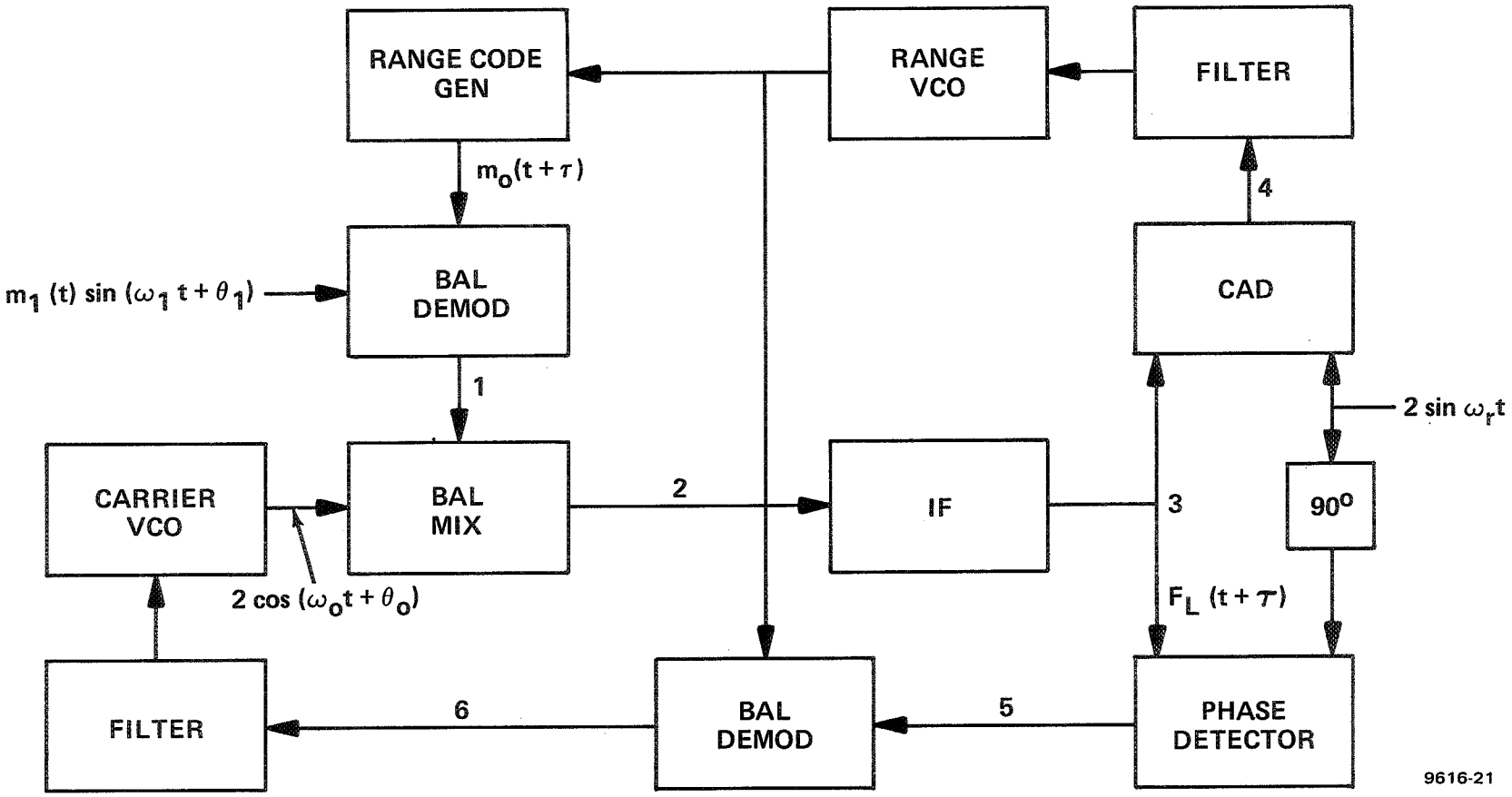

Figure 3.3-2. Functional Block Diagram of S-Band Signal Processor

The pseudo-noise code used in AROD is not a conventional PN code. It is a combination fast (H) code and slow (L) code formed by the system shown in Figure 3.3-3. A temporal description of the composite code is given in Figure 3.3-3. There are 511 bits in the H code and 127 bits in the L code. $2T_L$, the L code period, is equal to $1022T_H$, the high code period.

During the acquisition and tracking periods, both the low frequency (L-code) and the high frequency (H-code) will be present on a time sharing basis; however, the principles can be best presented by assuming only the L-code is used.

The local range code signal, m_2, is generated by taking a local PN sequence, which is identical with $m_1(t)$ except for a time shift, and multiplying this code by a clock, F_L, which is coherent with the range VCO and has two complete cycles in one code bit period. The received signal is multiplied in a balanced modulator (correlation multiplier) with the signal $m_2(t+\tau)$. The resultant signal is:

$$(2) \quad e = m_1(t)\, m_2(t+\tau)\, \sin(w_1 t + \theta_1)$$

Figures 3.3-4a and 3.3-4b show the product of $m_1(t)$ and $m_2(t+\tau)$. With $\tau = 0$, this product is a symmetrical square wave at a frequency F_L Hz. Equation (2) is then represented by a sine wave periodically reversed in phase at a rate of F_L Hz. The output of the correlation multiplier is a suppressed carrier double sideband signal and is shown in Figure 3.3-5a.

When $\tau \neq 0$, the product of $m_1(t)\, m_2(t+\tau)$ is not correlated over the entire PN bit period. This is illustrated in Figure 3.3-4b.

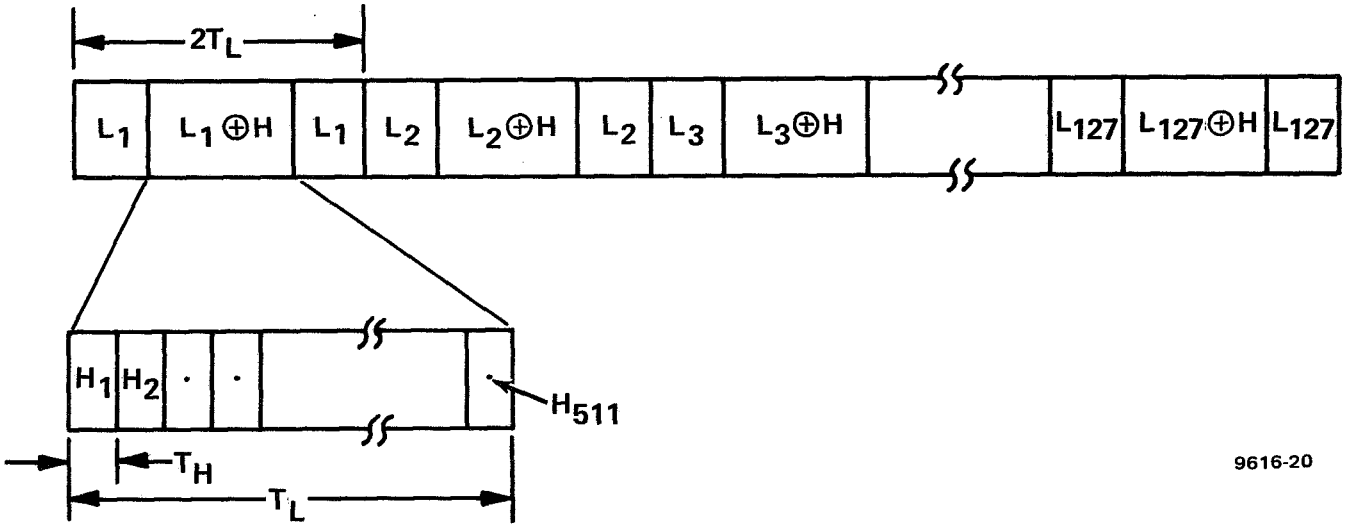

Figure 3.3-3. Composite PN Code

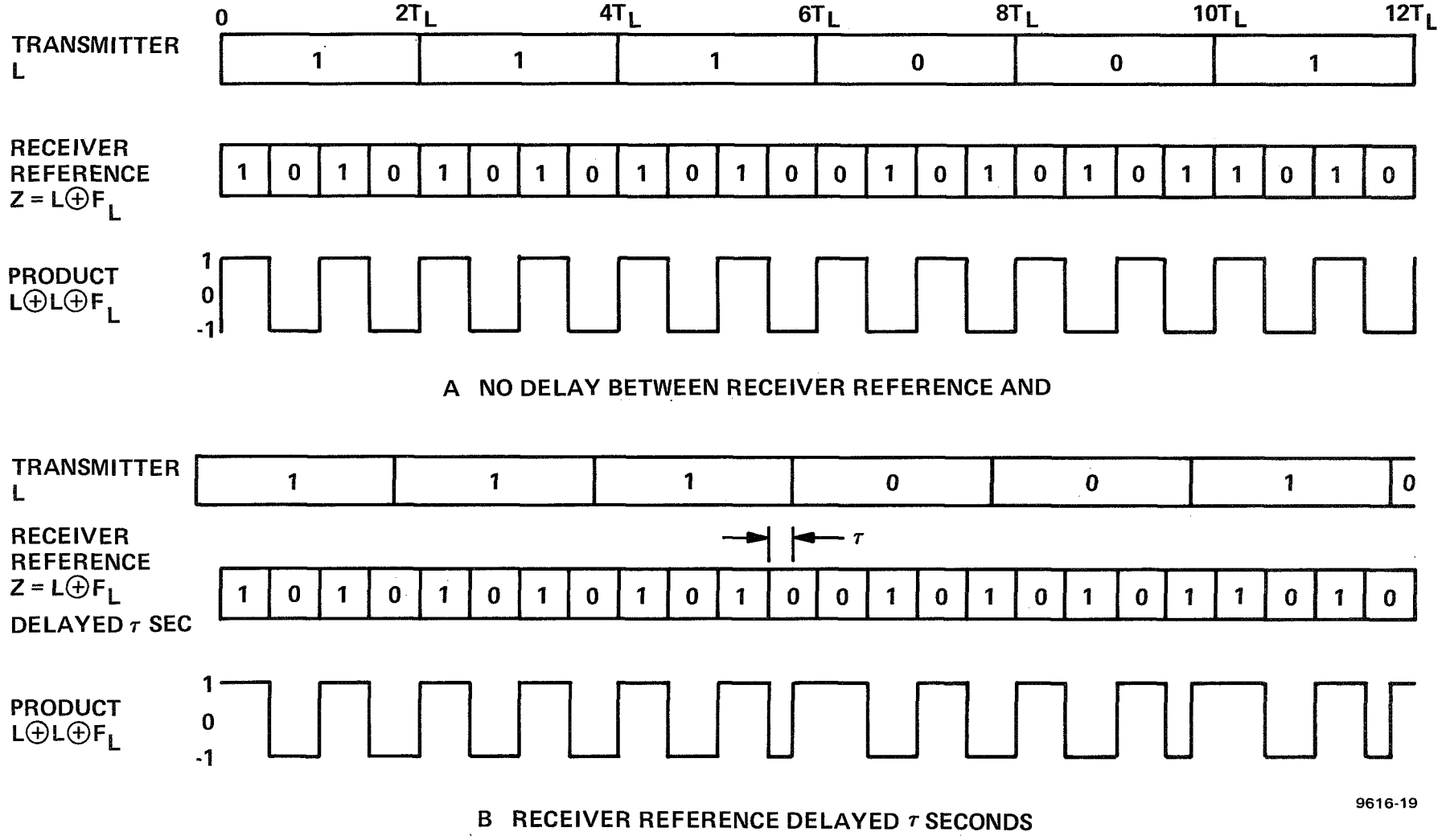

Figure 3.3-4. L Code Relationships and Output Product

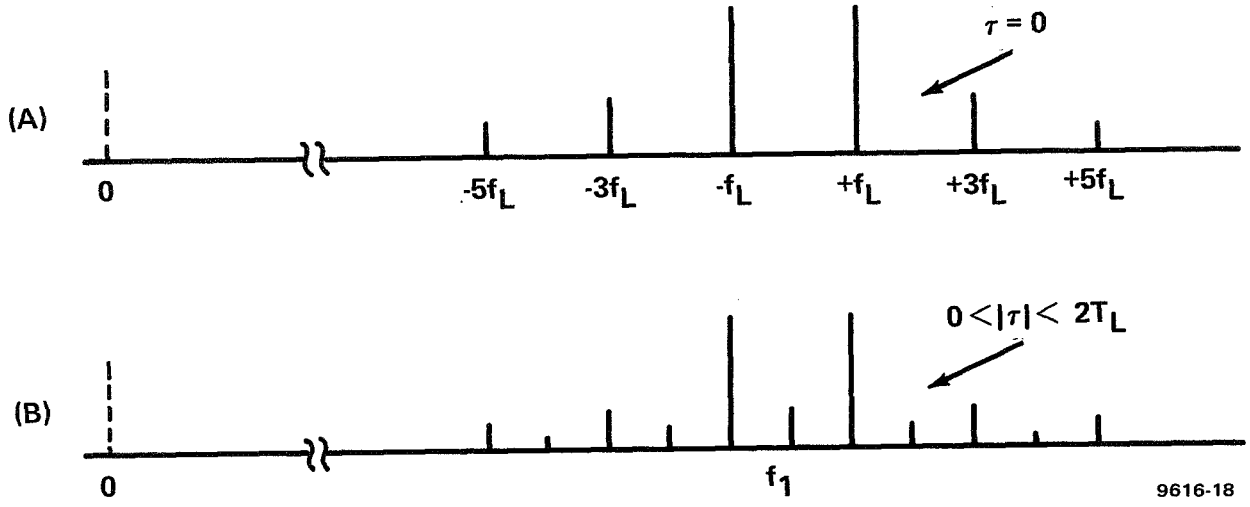

Figure 3.3-5. Spectrum of Signal at Pt. (1) of Figure 3-20

The result is an unsymmetrical square wave. Equation (2) is no longer a suppressed carrier signal and a carrier component will appear as shown in Figure 3.3-5b. The amplitude of this component is proportional to $\tau/(2T_L)$. The phase of the carrier component is in phase with the carrier phase, θ_1, for $+\tau$ delay and is out of phase, $\theta_1 = \pi$, for $-\tau$ delay.

The range loop servo system will drive the carrier component to zero; i.e., to drive the delay, τ, to zero. Variations in system gain and in the phase θ_1 are only variations in servo gain and do not contribute to the time delay of the receiver. It can be shown that such variations cause second order variations or conversely the second derivative of the parametric variations cause time delay error. This is the key to the time stability of the AROD receiver.

The ground transponders are essentially identical to the vehicle system and has the same system stability.

The output of the correlator is multiplied by the carrier VCO and filtered in a narrow band i-f amplifier. The carrier VCO adjusts its frequency until the i-f frequency equals the offset frequency f_r. The carrier VCO adjusts its frequency until the i-f frequency equals the offset frequency f_r. The carrier VCO adjusts the phase of the carrier so that the offset reference f_r is in-phase with the carrier at the coherent amplitude detector (CAD). The output spectrum of the CAD is shown in Figure 3.3-6. The d-c component is either positive or negative depending only on the delay, τ. Therefore, the balanced demodulator is the

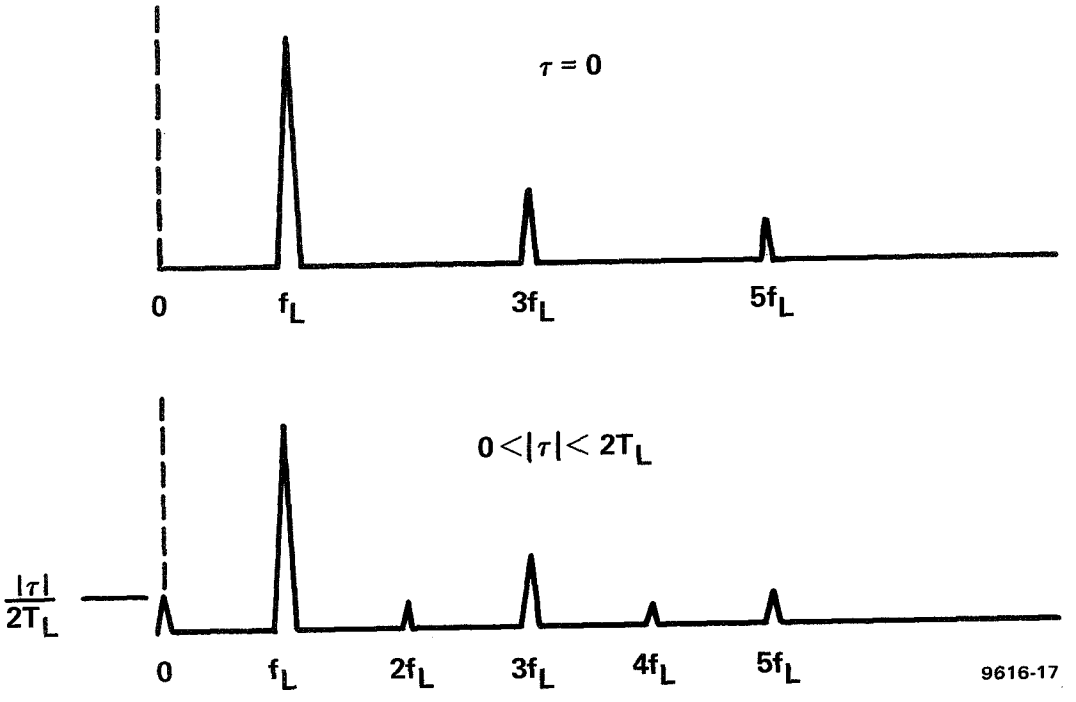

Figure 3.3-6. Spectrum of Signal at (4) for Small Error τ

correlation point for the range loop. Since the range loop is only sensitive to the amplitude of the suppressed carrier, variation in phase (time delay) in the narrow band i-f channel only effects the open loop gain and is reduced to a second order effect. This eliminates the largest contributor of tracking error which confronts most range tracking systems.

3.3.2 Time Delay Measurement

The AROD system does not measure range directly. It measures time delay of the round trip signal. This can be transformed into an equivalent range estimate. However, the transformation requires an understanding of the exact method used.

Each channel has its own range extractor. One such is shown in figure 3.3-7. Coarse range is determined by counting the number of 6.4 MHz clock pulses between the all ones state of the transmitted code and that of the received signal. Seventeen bits of coarse range can be obtained with a resolution of about 23 meters and a total unambiguous range of better than 3000 km. Fine range is extracted by comparing the phase of the transmitter reference 6.4 MHz with that of the received signal. This measurement is also made by measuring the time between positive zero crossings of the two clocks. This is done by heterodyning the clocks by a common oscillator to frequency which is 1/128 of the clock frequency and counting clock pulses for the length of time the gate is open. Seven bits of five range are therefore obtained with a resolution of 0.183 meters.

By heterodyning this way time delay is increased by 128 times. It is necessary to account for range rate in the five range measurement.

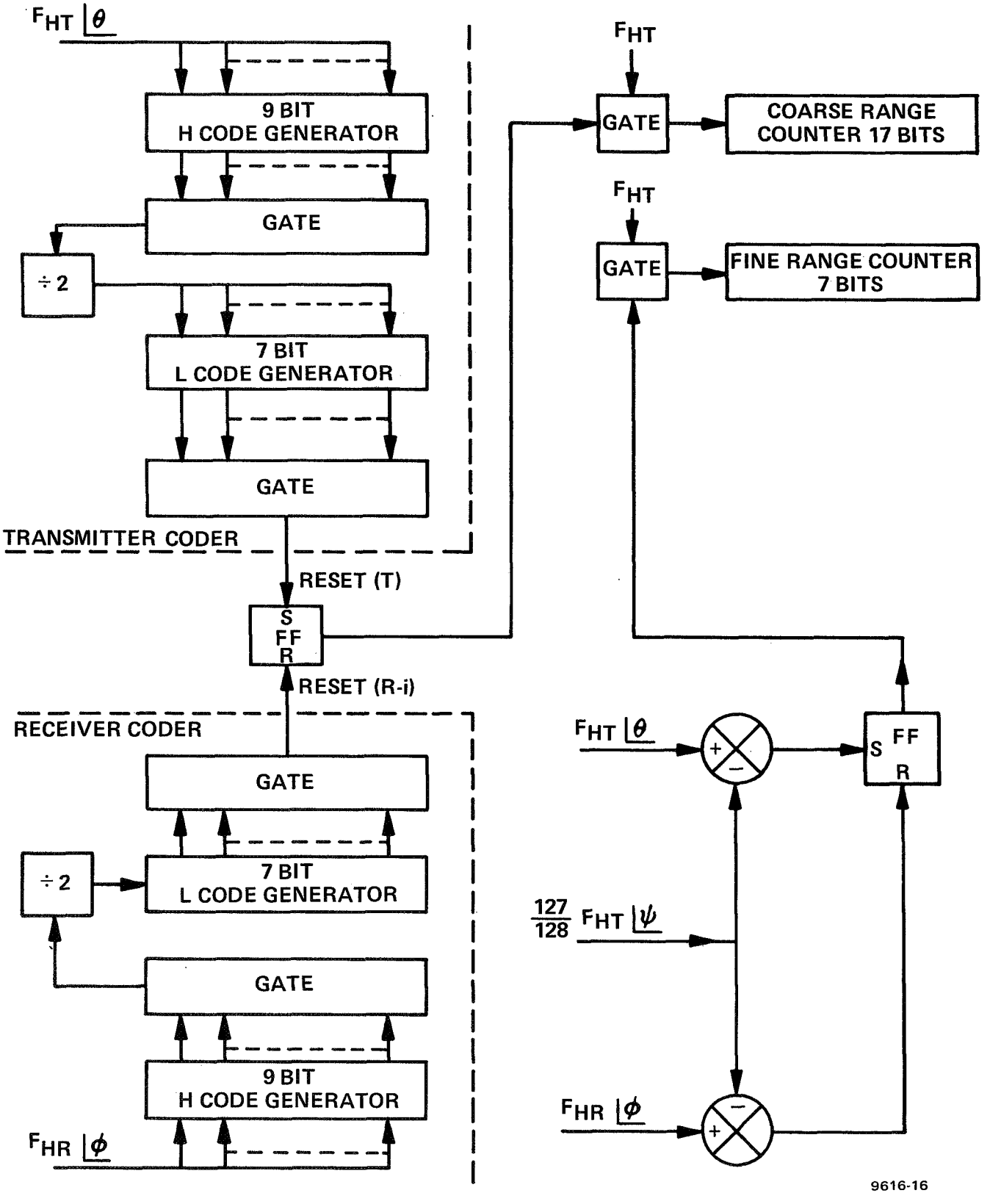

Figure 3.3-7. Functional Block Diagram of the Range Extraction Unit

Range on each channel is measured nominally four times each second.

3.3.3 Doppler Measurement

The doppler on each channel is measured by comparing the frequency of the recovered carrier against the system clock. In effect the two are heterodyned and the resultant multiplied by a factor of 16 to yield a resolution corresponding to one cycle per second in a 0.2 second. The number of cycles of doppler is counted in a fixed interval of time corresponding to 10 periods of the low code. This is approximately 0.2 seconds. The maximum doppler that can be measured corresponds to about 13,000 m/s. The maximum doppler expected in this mission corresponds to 3500 m/s or 48 kHz.

3.3.4 VHF Command and Control Downlink

The VHF link at 137 MHz is not directly used in either ranging or range rate measurement. However, it does provide several important system functions. As the satellite nears a ground station the VHF link is used to call up that station. The S-band system transmitting as well. Potentially there is a significant doppler on the S-band. In addition, the S-band system may employ a directive antenna system at the ground station. The VHF signal is received over an omni antenna, but which estimates the direction cosines for S-band antenna pointing. In addition, the VHF carrier is coherent with the S-band signal carrier. By recovering the VHF carrier an estimate of the doppler on the S-band signal is obtained. The residual doppler is all that is searched by the S-band receiver.

Finally, there is a 3000 km range uncertainty. However, a time marker is sent over the VHF link which positions the S-band PN code to within one L code bit of that received over the S-band link.

Thus, the VHF link provides antenna pointing, an estimate of doppler, and an estimate of system time. All these contribute significantly to reduction in synchronization time which requires about 3.5 seconds on the average for a complete link.

In addition, the VHF link carries commands and may be used for telemetry.

3.4 PRESENT AROD SYSTEM DESIGN AND PERFORMANCE CHARACTERISTICS

The previous sections described the AROD basic concepts and principles of operation. Here the systems constraints, design goals and overall performance characteristics are reviewed. Future sections review the measured system performance in detail. It is only intended here to give approximate results of the more important factors.

3.4.1 Original System Design Constraints

The following factors were imposed on the system:

VHF carrier frequency	138 MHz
S-band carrier downlink	2214 MHz
S-band uplink	1800 MHz
VHF antennas gains	3 db
Veh. S-band antenna	3 db linearly polarized
Ground S-band antenna	16 db circular polarized
VHF transmitter power	6 watts

Veh. S-band power	10 watts
Ground S-band power	20 watts
S-band width	<12 MHz downlink
	<20 MHz uplink
VHF bandwidth	<75 kHz
Maximum velocity	>12,000 m/s
Minimum range	>50 km

In addition, size, weight and prime power limitations were given.

3.4.2 System Design Goals

Range Accuracy	<.5 meters
Range ambiguity	>2000 km
Range resolution	<.25 meters
Range rate resolution	<.03 m/s
Range rate accuracy	<.02 m/s
Acquisition time	<2 seconds
Signal dropout	>2.5 seconds

The system was to be completely automatic and unattended. After initial alignment no calibration was to be required for a life of 2 years and maintain the performance goals. The system was to maximize the range capability and to reject multipath to a maximum degree.

3.4.3 Overall System Performance

In general, all goals were met or exceeded with three exceptions: Dropout was limited to .25 seconds, average acquisition time is 3.5 seconds, and range rate accuracy was about .05 m/s. The latter

was due to equipment and is correctable. The others were basic compromises in system design.

Range resolution is .183 meters with ambiguity greater than 3000 km. Maximum range is from 16000 to 20000 km. System threshold is -127 dbm at which point all functions essentially fail, acquisition, track, and communication. The data links are 400 bps on VHF for command and control and capable of 10000 bps for telemetry. The S-Band data link is 50 bps. Both are adequate for total system performance.

RMS range accuracy is about 1 meter at threshold and .08 m/s on range rate.

Overall range accuracy exclusive of noise is better than 0.5 meters due to all other causes.

There are three major sources of range error introduced by the AROD system. The first is the performance in the presence of noise and interference. The second is the effect of circuit variations upon range and range rate measurement. The third is the error introduced in the data extraction equipment. The noise error vs. slant range for the AROD system is presented in Figure 3.4-1. Their curves are based on the system parameters listed in 3.4.1 and 3.4.2. The modulation loop noise bandwidth (one sided) is 5 Hz and carrier loop noise bandwidth (one sided) is 200 Hz when in full track mode.

The major equipment error sources are shown in Figure 3.4-2. These error sources represent the time delay introduced by various circuits in the transmitter and receiver units. These sources were analyzed during the AROD design phase and the predicted effects on the range and range rate measurements are summarized in Table 3.4-1.

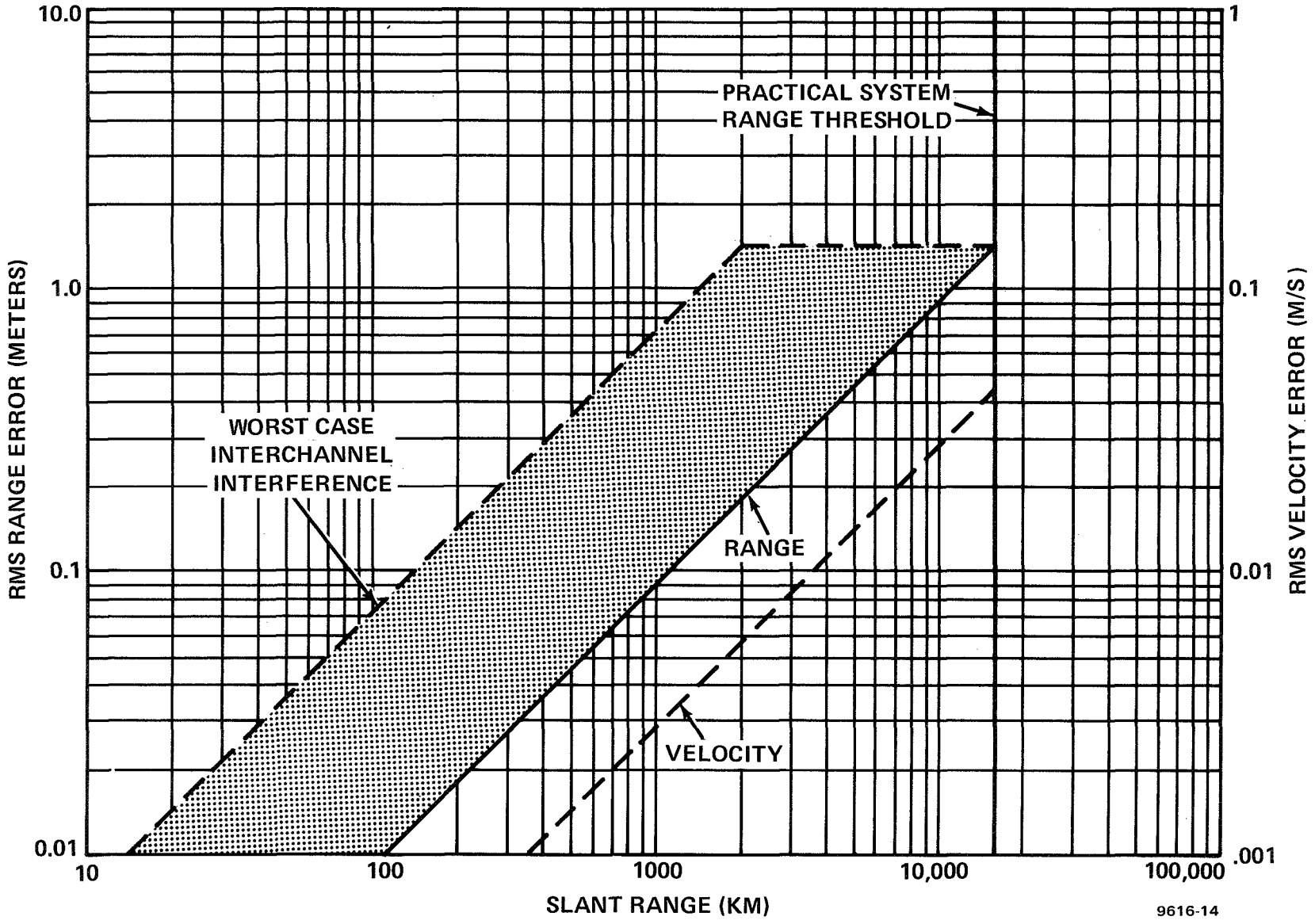

Figure 3.4-1. Noise Error vs. Range

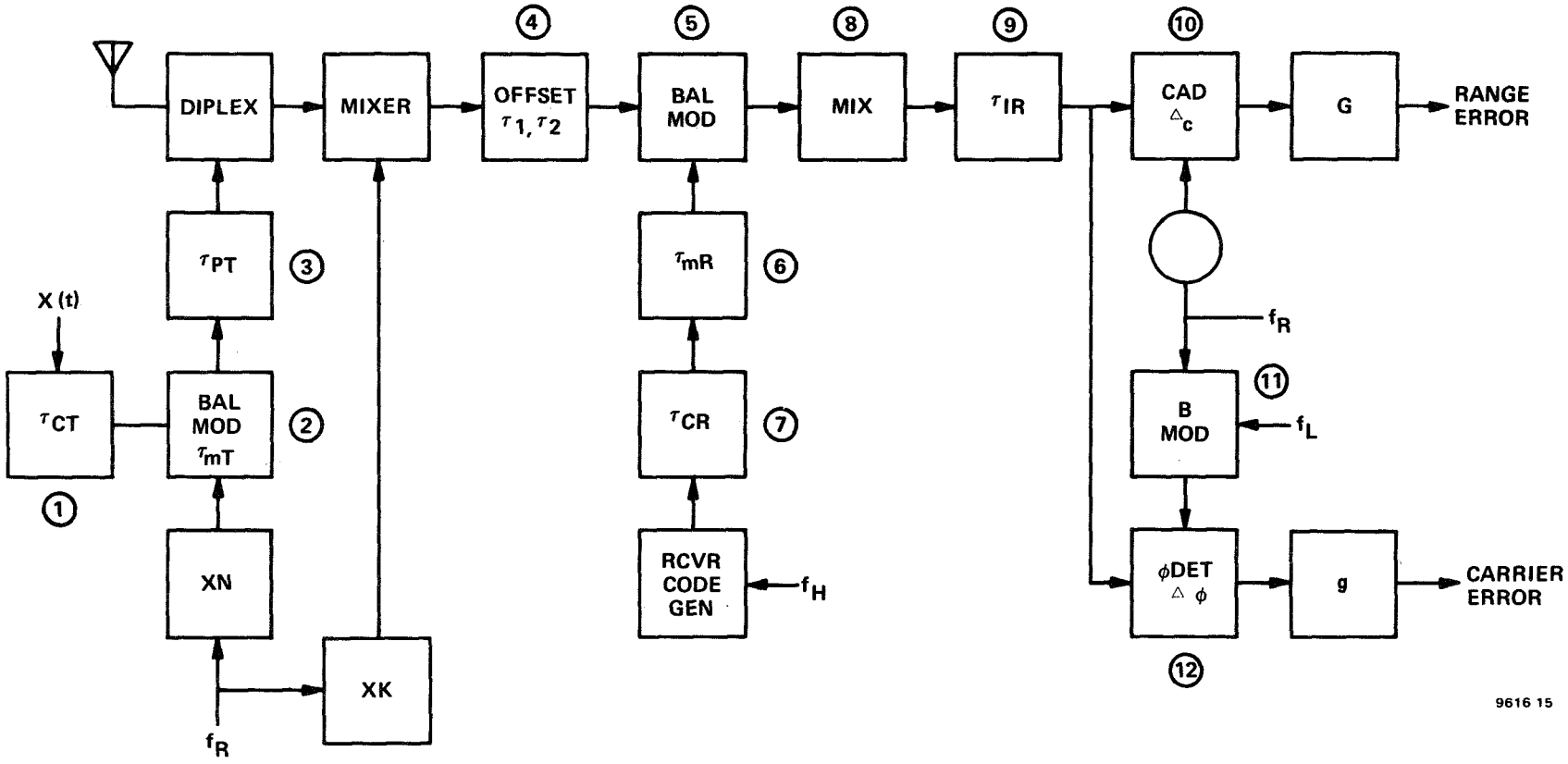

Figure 3.4-2. Equipment Error Sources

Source of Error	Range (T_H) Bits		Carrier (degrees)	
	Bias	Error	Bias	Error
①	0.064	0.0064	--	--
② a	--	--	--	--
b	--	--	0.5	0.05
c	0.0032	0.00032	--	--
d	0.064	0.0064	--	--
③	0.0064	0.00064	--	--
④ a	0.004	0.001	0	4
⑤	0.0032	0.00032	0.5	0.05
⑥	0.032	0.0032	--	--
⑦	0.064	0.0064	--	--
⑧	--	--	0.5	0.05
⑨	--	--	--	--
⑩	--	0.007	--	--
⑪	--	--	0.5	0.05
⑫	--	--	--	3.0
Sum of items 1-12	0.2408	0.03168	2.0	7.2
RMS of items 1-12	0.1155	0.0136	1.0	5.0
Sum in meters of items 1-12	5.64	0.74	--	--
RMS in meters of items 1-12	2.70	0.32	--	--

9616-28

Table 3.4-1. Summary of Bias and Error Effects

The circled numerals key the circuit to the table. This analysis showed that the expected rms range error, due to equipment variation, was 0.52 meters. Since the AROD system is completely coherent, there is no velocity error due to these sources.

In addition to the equipment errors, quantization and timing errors in the range and velocity extraction units contribute to the total overall system instrumentation error.

Vehicle Velocity Extraction Error

Two sources of error exist in the vehicle velocity extraction equipment. These are errors in the timing period T and quantization errors.

The total accumulated count in the velocity extraction counter can be represented as

$$N = T\ (2\ f_o \pm 16\ f_d)$$

where N is accumulated count

$2\ f_o$ is offset frequency (6.4 MHz)

and

$$f_d = \frac{2\ v}{C-v}\ f\ (t)$$

where v = vehicle relative velocity

C = velocity of propagation

f(T) = up link S-band carrier frequency

(1750 to 1850 MHz)

then

$$N = T\ (2\ f_o + \frac{32\ v}{C-v}\ f(T))$$

Since the time interval T is directly derived from the same reference oscillator as f_o and f(T), a change in frequency of the

reference oscillator does not result in a velocity measurement error. Considering short time variations of T due to noise on the timer clock or counter noise, the readout error becomes

$$\Delta N = \Delta T \left(2 f_o \pm \frac{32 v}{C-v} f(t)\right)$$

and at v = 12000 meters/sec.

$$f(t) = 1800 \text{ MHz}$$

$$\Delta N = \Delta T \, (6.4 + 2.3) \, 10^6$$

To maintain ΔN less than 1/4 count

$$\Delta T = 28.8 \times 10^{-9} \text{ seconds.}$$

This can readily be achieved with normal clocked digital techniques. The resulting error is thus equal to 1/4 the quantization level.

The quantization error can be determined from the following:

$$N = T \left(2 f_o \pm \frac{32 v}{C-v} f(t)\right)$$

and

$$\Delta N \approx \frac{T \, 32}{C} \, f(t) \, \Delta v_{(q)}$$

for $\Delta N = 1$

$$\Delta v_{(q)} = 0.026 \text{ meters/second.}$$

The rms quantization error is then

$$v_{(q)} \text{ rms} = \frac{v_{(q)}}{\sqrt{6}}$$

$$v_{(q)} \text{ rms} = 0.0106 \text{ meters/second}$$

From the quantization level of 0.026 m/sec., the timing error can be computed.

$$v_{(t)} = \frac{v_{(q)}}{4} = 0.0065 \text{ meters/second}$$

TABLE 3.4-2. Summary of Instrumentation Errors

Error Source	Range (meters)		Velocity $\frac{\text{meters}}{\text{sec.}}$	
	Peak	Rms	Peak	Rms
Vehicle Equipment				
a. random noise errors	0.47	0.175	0.0137	0.0056
b. processing equip. errors	0.78	0.32	--	--
c. data extraction errors	0.62	0.316	0.0325	0.0124
Transponder Station Equip.				
a. random noise error	0.47	0.175	0.0137	0.0056
b. processing equip. error	0.78	0.32	--	--
Total	3.12	0.604	0.0699	0.0148

3.5 IMPACT OF SYSTEM PARAMETER CHANGES ON THE AROD SYSTEM

Some of the AROD system parameters were dictated by external factors and may not be optimum for the survey problem. This section will consider several of these parameters and will discuss the impact of the parameter values on the equipment design and the system operation. The parameters considered are: 1) carrier frequency, 2) code frequency, and 3) antenna system.

3.5.1 Carrier Frequency

The AROD system was designed for S-band operation with the down-link in the band from 2150-2250 MHz and the up-link in the bank from 1750-1850 MHz. The system utilizes a vhf down-link at 138 MHz as a control link and acquisition aid. Because ionospheric propagation characteristics are better at higher frequencies (say 5-10 GHz), it may be desirable to increase the carrier frequency

to this region.

The important areas which are affected by such a change are:

1) acquisition

2) frequency synthesis

3) receiver front-end

4) antenna

The areas of frequency synthesis, receiver front-end and antenna would require redesign; however, the redesign would be straight forward and would not significantly alter the system characteristic. The most significant factor is carrier acquisition.

The AROD system used the Doppler frequency of the vhf down link to preset the transponder S-band receiver to within its carrier loop bandwidth. This technique can easily be extended by a factor of five so that transponder acquisition is not affected.

The up link transmissions do not contain a vhf link to provide an estimate of Doppler; therefore, the transponder measures the one way S-band Doppler with respect to a stable oscillator. The transmitted carrier is offset by the negative Doppler shift so that the signal arrives at the vehicle with zero Doppler shift except for the relative stable oscillator uncertainty of 360 Hz at 1800 MHz. A higher frequency, say 10 GHz , will have an uncertainty of 5x360 = 1800 Hz. The vehicle must acquire by searching sequentially, bit-by-bit through the low frequency code (L-code, which is 127 bits long). At each code bit shift, time must be allowed for the carrier to lock and for the code to be examined. The carrier loop bandwidth is 565 Hz (one sided) during acquisition and carrier acquisition is on the

order of 1-2 ms which is insignificant with respect to the code integration time of 20 m.s. An increase of frequency uncertainty of 1800 Hz will increase the carrier acquisition time to the order of 70 m.s., so that the code search time must be increased to the order of 90 m.s. per bit or 11.4 seconds for the entire code length. This is a maximum time. The average time would be 5.7 seconds and is acceptable for most applications. After the low-frequency code has been acquired by vehicle, the transponder will linearly sweep from zero Doppler to the full two way Doppler shift. The present time allocation is one second for this function, and would also increase to 5 seconds. The total impact of the carrier changes on acquisition time is to increase the time from 3 seconds to 11 seconds.

3.5.2 Code Rate

The AROD code is formed by combining a high speed code with a low speed code as shown in Figure 3.3.3. The high speed code operates at a rate of 6.4 MBbs and has a period equal to one half a low code bit. The low frequency code has a period of approximately 20 milliseconds and a rate of $6.4 \times 10^6 \div 1022$ or 6.25 KHz. These code rates and code periods are selected to minimize the acquisition time while providing the accuracy (high frequency rate) and unambiguous range (low-frequency period).

The geodetic survey might well use orbital altitudes of 1,000 nautical miles and require a slightly longer unambiguous range. This can be accomplished simply by lengthening the L-code generator by one bit with an increase in acquisition time of a factor of four for that portion of the cycle.

The total velocity measurement error resulting from these two effects is then

$$v_{rms} = (v_q \text{ rms}^2 + (v_t)^2)^{1/2}$$

$$v_{rms} = 0.0124 \text{ meters/second}$$

Vehicle Range Extraction Error

There are three types of errors directly associated with the range extraction equipment. These are (1) an error resulting from frequency error in the range modulation reference oscillator, (2) quantization error resulting from representing range in a digital manner, and (3) errors introduced because of the finite period required to make the range measurement.

The first source of error is a direct proportionality; that is, an error of $1/10^7$ in calibration of the range modulation reference oscillator will result in an equivalent error in any range measurement. This can be a maximum of 0.2 meter at the maximum specified range of 2000 kilometers.

Since range is quantized to 1 part in 128 of the wavelength of the 6.4-Mc range modulation clock frequency,

$$\Delta R_q = \frac{300 \times 10^6}{2 \times 6.4 \times 10^6 \times 128} = 0.183 \text{ meter}$$

The rms quantizing error is then

$$\Delta R_{q \text{ rms}} = \frac{0.183}{\sqrt{6}} = 0.0745 \text{ meter}$$

The method of range readout as described in section 3.3.2 is essentially one of measuring the phase delay experienced by a transmission from the vehicle to the transponder and return. A coarse

measurement counts the number of total clock-cycles of delay which exist and the fine measurement determines the phase delay in the clock frequency. Since the phase measurement is actually made at $\frac{6.4 \times 10^6}{128}$ Hz, the maximum period of the measurement is 20 microseconds. At maximum velocity, the Doppler appearing on the 6.4 MHz clock signal is 512 Hz/Sec. Or, in 20 microseconds, a phase change of up to 0.01024 cycle can occur. This is equivalent to 0.234 meter at maximum velocity and proportional to velocity.

Thus the range errors contributed by the readout equipment are:

1. Quantization error, $R_{q\ rms} = 0.0745$ meter
2. Clock frequency error, $R_C = 10^{-7} \times R$ meter
3. Readout velocity error, $R_v = 1.95 \times 10^{-5} \times v$ meters

Considering maximum velocity and range, the total rms error is 0.316 meter.

Measurement Error Summary

Table V-4 is a summary of the estimated system errors. The quantities listed have been evaluated at a range of 2000 kilometers and a velocity of 12,000 kilometers/second. These data illustrate that a good balance among the error sources has been achieved in that no single error source dominates.

At S-Band, this increase is on the order of 4 seconds. For a carrier frequency of 10 GHz, this increase becomes 20 seconds. This still provides a reasonable acquisition time. It is possible to combine a lower frequency code to the present modulation to reduce the acquisition time to the order of 5-10 seconds should a shorter acquisition time be required.

3.5.3 Antennas

The AROD rf link budget was calculated using an omni directional antenna at the vehicles terminal and a directional dish with approximately 16 db gain at the transponder terminal. The beeamwidth of the antenna is on the order of 26 degrees. The system has a threshold slant range of 10,000 km or 5,000 nautical miles.

The additional loss at 10 GHz, can be compensated for by an increase in antenna gain for the same antenna dimensions; however, the beamwidth will be decreased to about 5 degrees. This makes the initial antenna acquisition more difficult. The beamwidth can be broadened by restricting the operating range.

This may require an antenna pointing system on the tracking system carrier.

4.0 RADIO RANGING

There are a number of basic contributors that can influence the residual slant range error. These can be divided into those associated with the system design and equipment and those associated with the propagation path.

The former system factors, can be divided into two parts: System design factors and equipment performance factors. The latter, propagation, encompasses four factors, the velocity of light in vacuo tropospheric effects, ionospheric effects, and multipath. Each of these is discussed and evaluated in the subsequent portions of this section. The final part is a summary of effects and a range error model for use in the simulation.

The system or equipment performance is divided into two parts: design and practice. This is done because the system design includes many factors which can materially effect the ranging error unless they are accounted for and factors which do influence accuracy whose theoretical performance is designed in, but which could be changed if the goedetic survey performance requires it.

The equipment practice or performance includes those factors that contribute to residual range error, environment, aging, temperature, characteristics with which the designer must live.

4.1 AROD SYSTEM DESIGN FACTORS

There are eight design factors which influence range accuracy:

1. Transformation of time delay to an estimate of range.
2. Time delay extractor.
3. Range resolution.
4. Range rate compensation.
5. Signal-to-Noise ratio dependence.
6. Dependence on the fundamental frequency of modulation waveform.
7. Carrier frequency dependence.
8. Antenna system.

4.1.1 Transformation of Time Delay to an Estimate of Range

Time delay in a dynamic environment is not identically equivalent to range even assuming exact knowledge of propagation velocity. Figure 4.1.1-1 is a geometric picture of this problem.

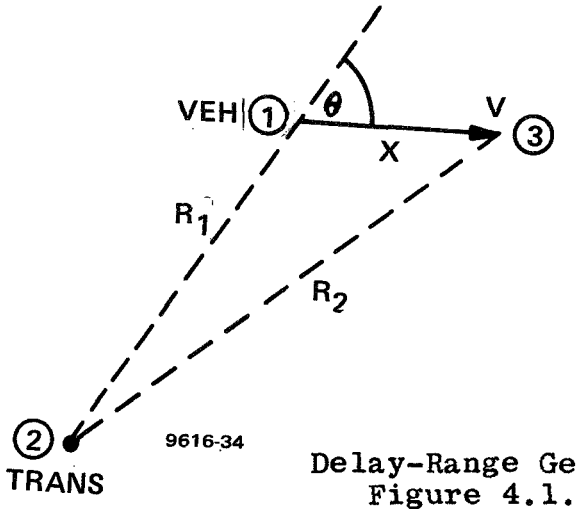

Delay-Range Geometry
Figure 4.1.1-1

Point (1) is the position the vehicle is in at the time on event is transmitted. (2) is the transponder location, and (3) the vehicle location at the time the event returns to the vehicle. $t_3 - t_1 = \tau$ the observed delay. V is vehicle velocity. C = the velocity of propagation.

$$V\tau = X$$

$$R_1 + R_s = C\tau = R_1 + \left[(R_1 + V\tau\cos\theta)^2 + (v\tau\sin\theta)^2\right]^{1/2}$$

$V\sin\theta = \overset{o}{R}_1$ or range rate at time, t_1.

$$R_1 = \frac{c\tau}{2}\quad\frac{1-(\frac{v}{c})^2}{1+\frac{v}{c}\cos\theta}$$

If the estimate of R_1 is $\hat{R}_1 = c\tau/2$ then an error, δ, occurs. If $\delta = \hat{R}_1 - R_1$

$$\delta = \frac{c\tau}{2}\,\frac{R_1}{c} + \frac{\left(\frac{v}{c}\sin\theta\right)^2}{1+\frac{v}{c}\cos\theta}\,\frac{c\tau}{2}$$

To exactly determine δ the true velocity and angle θ must be known. These can be obtained by geometric reduction but δ may be estimated using the observed $\overset{o}{R}_1$ which is directly obtained from the AROD system. The last term is then the residual. Using the values given in Appendix A,V is of order 7500 m/sec. The residual is maximized when θ = 90 degrees. R_1 is less than 10,000 km. (The correction δ could be nearly 250 meters and thus, must be made.)

The residual ε is less than .625 mm which may be ignored, and this can be considered to be residual free.

4.1.2 Time Delay Extractor (1)

Each channel of the AROD system has its own time delay (range) extractor. One such is illustrated in Figure 3.3-7. The fine range extractor presents a problem. If a resolution of $(1/128)^{th}$ of a high code bit is desired, a direct measure of delay between zero crossings of the receiver reference and the received signal involve a counting rate of 128 x 6.4 $\triangleq$ 800 MHz, which is highly undesirable.

To maintain a counting rate of 6.4 MHz the reference and received phases are translated to a frequency equal to 6.4/128 MHz. If effect this stretches the fine range time delay by a factor of 128. The maximum period of fine range measurement is (128/6.4) = 20 μ sec. The maximum Doppler is 320 Hz on the 6.4 MHz signal or a phase change of .064 cycles or .146 meters. The correction to be made is $\Delta R = 1.95 \times 10^{-5} \times 2^{N-7} \times \overset{o}{R}$ where ΔR is to be subtracted from observed range and N is the number of bits of fine range.

(In the AROD laboratory test program the correction due to the test conditions was .25 meters).

In addition to this factor, the heterodyne oscillator at 127/128 of 6.4 MHz was free running. This can lead to error. (See Figure 4.1.2.-1).

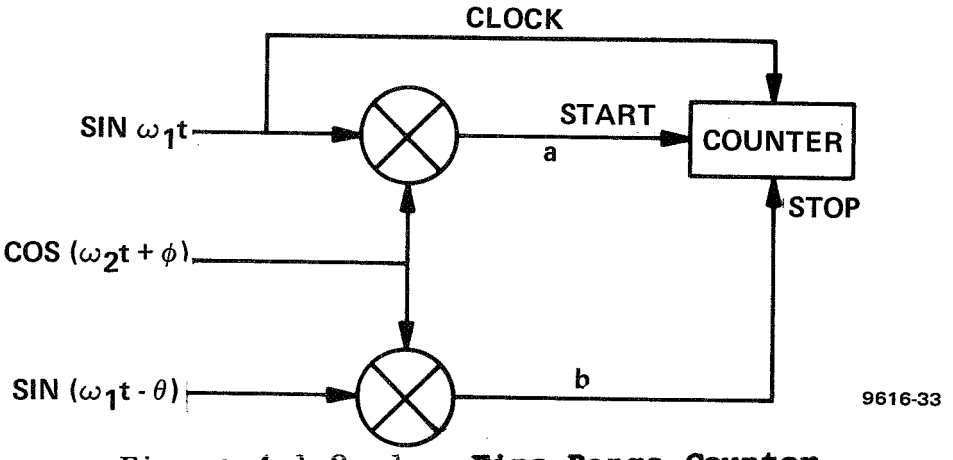

Figure 4.1.2.-1. **Fine Range Counter**

$$a = \sin \left[(w_1 = w_2)\ t - \phi\right]$$

$$b = \sin \left[(w_1 - w_2)\ t - \phi - \theta\right]$$

$w_1 - w_2 = w_o$

Start occurs when $w_o t_1 - \phi = \Pi$

Stop occurs when $w_o t_2 - \phi - \theta = \Pi$

$t_2 - t_1 = T$, $\frac{cT}{2}$ = Fine range measurement, $\hat{R}$.

$$\hat{R} = \frac{c}{2}\frac{T}{128} = \left[\frac{\Pi + \phi + \theta}{w_o} - \frac{\Pi + \phi}{w_o}\right]\frac{c}{2}\frac{1}{128} = \frac{c}{2}\frac{\theta}{w_o}\frac{1}{128}$$

Fine range resolution is 7 bits or 128 counts for 360^o or one wave length of w_1. $\theta = \frac{2R}{C} w_1$, where R is the real fine range. The error is $\hat{R} - R = \frac{1}{128}\frac{c}{2w_o}\frac{2R}{c} w_1 - R$

$$\mathcal{E} = \left(\frac{w_1}{128 w_o} - 1\right) R$$

w_o is supposed to equal $w_1/128$.

$$\mathcal{E} = \frac{-\delta}{1+\delta} R, \qquad \delta = \frac{\Delta w_o}{w_o}$$

δ is better than 10^{-5}. $R_{max.}$ for fine range is 23.4 meters. Hence, $\mathcal{E}$ = .234 mm and may be considered to be residual free.

4.1.3 Range Resolution Error (1)

The minimum resolvable element in the AROD system is 0.183 meters. With an average velocity of about 2000 m/s, the range change from measurement to measurement is 500 meters. Consequently, it is reasonable that the error is uniformly distributed across the resolution element. The rms error per measurement is therefore 7.45 cm.

The error is independent from measurement to measurement. Further reduction is possible by either increasing the modulation rate (6.4 MHz) or by obtaining greater resolution. However, this does not seem warranted at least for the geodetic survey problem. Hence, the residual, $\mathcal{E}$, equals 7.45 cm rms.

4.1.4 Range Rate Compensation (3)

The AROD system, when tracking the high code modulation for good range accuracy, uses Type I second order rate aided loops. The rate aiding is obtained from the carrier. In the transponder, the rate aiding is exact, but in the vehicle, it is good to a fraction of a percent.

In the transponder, the rate aiding means that the lead or lag to compensate is a fraction of a carrier cycle or less than about 1 mm. In the vehicle, however, rate aiding is good to the order of 3×10^{-2}.

The modulation tracking open loop gain is 4125. With a maximum doppler of 3500 m/s the error is:

$3 \times 10^{-2} \times 3500/4125 \; < \; 3$ cm and can be neglected.

This is a calculable error and could be corrected but it seems hardly worth it.

There may also be an acceleration error. This amounts to:

$$\delta = 3 \times 10^{-3} \, A/K_a$$

and $A \leq 47$ m/sec.^{2}, $K_a = 90$

$$\delta < 3 \times 10^{-3} \times 47/90 = .15 \text{ cm}$$

provided the acceleration does not last longer than 46 seconds.

4.1.5 Signal-To-Noise Ratio Dependance (1, 3)

From the AROD system design report, the mean square error in range is given by the following expression:

$$\sigma R^2 = \left(\frac{2N_o W}{A^2/2} \right) \frac{T_H^2}{\cos^2 \epsilon \left[\frac{T_L - \tau}{T_g} \right]^2} \quad \frac{16 \Pi B_R}{W} \quad \frac{C^2}{4}$$

B_R = 5Hz

W = $2\Pi \left(\frac{\Pi}{2} \right)$ 1.2×10^5 rad/sec.

T_H = $(1/6.4) \times 10^{-6}$ sec. = $.1565 \times 10^{-6}$

T_L = $511 \, T_H$ = 80×10^{-6} $\qquad$ $2 \, T_L$ = L code bit period

T_g = $1.1 \, T_L$ = 88×10^{-6}

τ = $10^{-5}/\Pi$ = 3.18×10^{-6}

C = 3×10^8

ϵ = the phase error in radians in the carrier tracking loop.

$$\overline{\delta^2} = \left(\frac{2N_oW}{A^2/2}\right) \frac{8\Pi\ B_c}{W}$$

B_c = 200 Hz

W = $2\Pi\ (\Pi/2)\ 1.2 \times 10^5$ rad/sec.

$$\frac{8\Pi Bc}{W} = \frac{800}{(\Pi/2)\ 1.2\times10^5} = .424\times10^{-2} \quad (6.26\text{-}30)$$

N.F. 8.3 db veh

9 db 1 & 2 Transponder

10 db 3 Transponder

KT(v) = -174 + 8.3 = -165.7 dbm/cps

KTB = -165.7 + 2.75 + 50 $\doteq$ -113 dbm

$$\overline{\cos^2 \epsilon} = e^{-\sigma^2/2} \doteq 1-\frac{\sigma^2}{2}$$

$$\frac{T_L - \tau}{T_g} = \frac{80 - 3.18}{88} = .873 \quad (-1.2)$$

$$\frac{CT_H}{2} = \frac{3\times10^8 \times .1565\times10^{-6}}{2} = 23.45 \text{ meters} \quad (27.4)$$

$2N_oW$ = KTB = -113 dbm on Veh

$$\frac{16\Pi B_R}{W} = \frac{2\Pi\ 8\times5}{2\Pi\ (\Pi/2)\ 1.2\times10^5} = \frac{80}{1.2\Pi}\ 10^{-5}$$

$= 2.12 \times 10^{-4}$ (3.25 - 40 = 36.75)

This is plotted as the theoretical curve in Figure 4.2.5-1.

The total signal-to-noise dependance is the effective sum of that at the transponder and that at the vehicle. The loop characteristics are the same for both. A total system transfer function is shown in Figure 4.1.5-2.

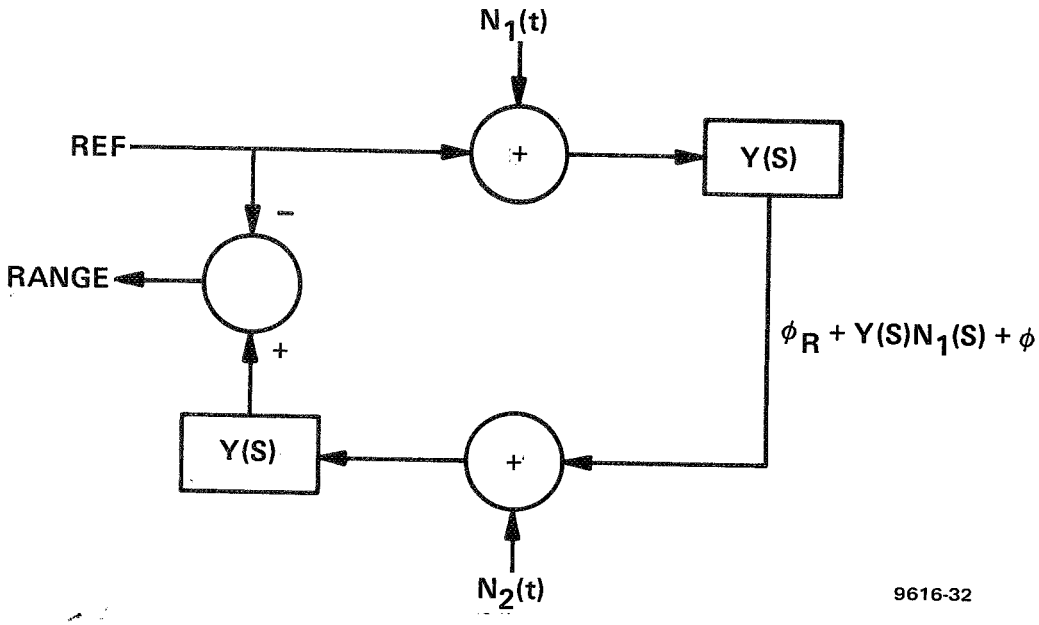

Figure 4.1.5-1
Range Loop Noise Model

$$K\hat{R} = \left[\phi + 2\phi_R + Y(s)\, n_1(s)\, E(s) + Y(s)\, n_2(s)\right] - \phi$$

$$K\varepsilon_R = \frac{1}{2} Y(s) \left[n_1(s)\, E(s) + n_2(s)\right]$$

$$E(s) = 2 - Y(s)$$

$$\overline{\varepsilon_R^2} = \frac{1}{K^2} \int \left| Y(s)\, n_2(s) + E(s)\, Y(s)\, n_1(s) \right|^2 ds$$

K is the meter/rad. conversion factor. n_1 and n_2 are independent Gaussian noises normalized by received signal level.

Y(s) = closed loop response of the receivers. (s) = 1-Y(s).

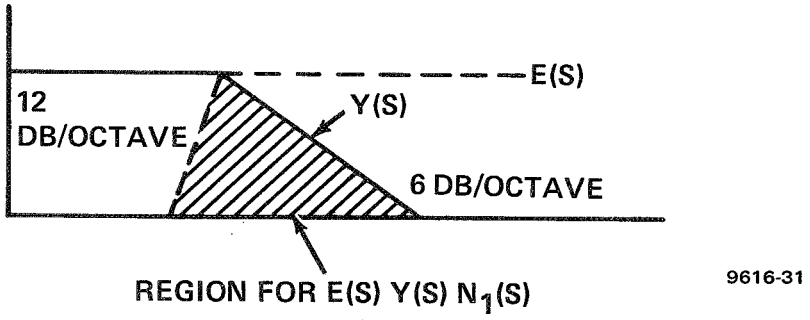

Figure 4.1.5-2
Noise Spectrum

The first term in $\overline{\varepsilon_R^2}$ is that calculated in the previous section. The second is that caused by the transponder. Clearly that contribution is small so long as the error is small compared to the wavelength.

$$Y(S) = \frac{1 + \tau S}{1 + \tau S + \frac{\tau^2}{2} S^2} = \frac{S + 1/\tau}{S^2 + \frac{2}{\tau} S + \frac{2}{\tau^2}} \cdot \frac{2}{\tau}$$

$$= \frac{S + \alpha}{(S + \alpha)^2 + \alpha^2} \quad (2\alpha), \quad \alpha = \frac{1}{\tau} = \frac{4B}{3}$$

with break frequency at α radians/sec.

$$E(S) = \frac{S^2}{(S + \alpha)^2 + \alpha^2} \quad \text{with break at } \alpha \text{ radians.}$$

$$\int_0^\infty \left| E(S)\ Y(S)^2 \right| ds \doteq \int_0^\alpha \left(\frac{S}{\alpha}^4\right) ds + \int_\alpha^\infty \left(\frac{2\alpha}{S}\right)^2 ds$$

$$= \frac{S^5}{5\alpha^4}\Big|_0^\alpha - \frac{(2\alpha)^2}{S}\Big|_\alpha^\infty$$

$$= \frac{\alpha}{5} + 4\alpha = 4.2\alpha = 4.2\left(\frac{4B}{3}\right)$$

This ratio 4.2/5 of that straight through Y(S) or a reduction of about 10% in the **rms** error measured at the transponder.

A composite assuming threshold at both terminals is plotted in Figure 4.2.5-2 as the theoretical curve.

The residuals to use are given in section 4.2.5-2.

4.1.6 Dependance on the Fundamental Frequency of Modulation

The range error equation given in the previous section (4.1.5) illustrates that the rms error is inversely proportional to the basic clock frequency (6.4 MHz), higher frequencies, lower error and vice versa.

The reason for introducing this is if higher rms accuracy is required, which is unlikely, both cost and prime power required is increased. If a higher rms is tolerable, a lower clock may be used. If it is below 3 MHz a lower power digital family can be used. The

disadvantage is reduced protection against multipath.

4.1.7 Carrier Frequency Dependance

The carrier frequency is a factor involved in obtainable range accuracy. Its influence is largely dependant upon the ionospheric propagation characterisitics which is discussed in section 4.5.1.

If range rate obtained from the carrier doppler is useful in either reducing the position error or in reducing the number of points, then a higher carrier frequency may prove desirable.

The range rate error dependance on signal-to-noise ratio is:

$$\sigma_v^2 = \left(\frac{2N_oW}{A^2/_2}\right) \frac{8\Pi B_c}{W} \frac{2}{T^2} \left(\frac{\lambda}{4\Pi}\right)^2, \quad (m/s)^2$$

which clearly illustrates the wavelength dependance. An increased carrier frequency may require a wide loop bandwidth (B_L) and either higher antenna gain or higher transmitter power at both vehicle and the transponder.

4.1.8 Antenna System

Although not really a system factor contributing directly to range error, nevertheless some consideration must be given to it.

The system described herein has a range capability of about 20,000 km (a signal level of -127 dbm) when including 5 db incidental losses. This is a margin of 6 db corresponding to a signal of -121 dbm.

Motorola did not develop an antenna in conjunction with the AROD hardware. Auburn University did some basic development work on a VHF direction finding system and incrementally phased array for the S-band system. These developments are not presently complete

and some problem could be experienced with the phased array which has a 16 db gain, circular, towards the zenith but tends to 12 db linear on the horizon. This could present a real problem. An antenna system does need to be developed.

The physical to phase center displacement of the antenna system can contribute error in range. A parabolic dish with a diameter of 1.5 feet is all that is required. The mechanical to phase center error should be at best a few % of that. Conservatively, this should never exceed 5 cm. For the error model, we shall use 5 cm as the residual. It is, of course, a function of direction of pointing and will vary throughout a pass and between passes. It must be assumed to be a fixed bias but random from site to site.

The error on the vehicle should be considerably less and negligible.

4.1.9 Summary of AROD System Design Factors

Some seven separate system design factors, which contribute to ranging accuracy are of the transformation of time delay to a range estimate, the effect of the method of time delay extraction, and range rate compensation-leave either so small or no residual when properly compensated.

Modulation frequency accuracy dependance is a function of signal to noise ratio. If it becomes desirable to change this frequency for other reasons, the rms range error versus signal-to-noise will change. Currently, it is of order $(R/R_o)^{1/2}$ meters where R is true range and R_o is maximum range or 16,000 km.

Carrier frequency dependance comes about in two ways, ionospheric propagation discussed later, and if range rate can be used for position

estimation. It does not directly contribute to ranging accuracy in the AROD system design.

Three factors contribute to residual error, range resolution, signal-to-noise ratio, and antenna system. The rms residuals are:

	ε (rms meters)	
Range Resolution	.0745	independant at .25 sec.
Signal-to-noise	$(R/16000)^{1/2}$	"
Antenna System	.05	Fixed

4.2 AROD EQUIPMENT PERFORMANCE

The previous section discussed those factors which are directly within the control of the system designer. In general, they are factors which can either be accounted for exactly or whose theoretical performance and, hence, the resulting range error residual is controllable.

This section examines the performance of the actual AROD system equipment exclusive of propagation. Where appropriate the measured performance is compared to the theoretical predicted performance.

Ten significant factors have been identified. The first seven describe the measured performance whose deviation from ideal cannot be accounted for and must be accepted as representative of what can be expected of flight equipment. (This could not be assumed if significant changes in equipment design were taken. In general, an awareness of these factors will lead to improved performance). Three other factors have been identified whose non-ideal performance has been determined from extensive testing of the AROD equipment in the lab test program.

The performance results to be reported herein, were essentially all obtained in the laboratory test program, which became a part of the overall AROD development program. A fairly extensive program extending over 9 months was conducted. The results have been documented in a report, "AROD System Test Model, Final Report, AROD Laboratory Test and Evaluation Program." (2)

An acceptance test program was conducted under the original contract. These results are also reported in the same report (2) as initial tests.

The purpose of the laboratory test program was fourfold: One, to test the system under simulated flight conditions. Two, to examine the aging characteristics of the AROD equipment, since new circuit approaches were used. Three, to identify any inadequacies in system and equipment design. Four, to correct any deficiencies where practical or to positively identify the failure and to recommend the correction necessary in flight equipment.

Approximately 1800 detailed and carefully recorded tests were made during this program plus countless others used in the evaluation of several problem areas.

The basic methods of analysis of ranging were to calculate means and variances as a function of the test parameters. When further evaluations were believed to be necessary prolonged tests were run and correlation functions of the error obtained such that the resolution was better than 10 cm. That is, if a non-random error appeared, it could be identified if its weight in the error exceeded 10 cm. Often the resolution was better than this.

Several deficiencies were identified, the most notable were related to the local oscillator phase noise of the original design, the doppler reverse to true doppler sweep circuits, and the doppler extractor. The first two were corrected. The last was not, but the problem thoroughly identified and the method of correction was determined. The correction is simple, and inconsequential in the future, but very expensive in the existing equipment.

Unfortunately, the consequence of the thorough testing for these problem areas resulted in adjusting and rearranging the test setup. This in turn meant that the periodic tests of constant range under various conditions do not represent a valid test of aging. Only secondary factors can be studied and even most of these were subject to realignment throughout the program.

As a result under the present contract, a fixed setup was established and a series of tests were given at frequent intervals to get aging comparisons. However, it must be mentioned that over 3000 hours of full system operating time have been accumulated. During this time, no failures of any kind have been incurred in any of the six units built: Vehicle equipment, three transponders, and two checkout equipments.

Operational tests were not conducted under conditions of vibrations, shock, or vacuum. No problem is expected, but certainly flight equipment must be qualified in these areas.

The seven factors that must be accepted as performance capability are:

1. Equipment Delay Calibration

2. Temperature Stability

3. Master Oscillator Stability

4. Aging Stability

5. Delay vs. Signal Level

6. Delay vs. Range Rate

7. Delay vs. Multiple Channel Operation

The three factors that effect system performance and whose effect is present in the tests, listed above, but whose effect has been identified and a method of correction identified are:

8. H code search in the Vehicle Equipment

9. Loss of coarse bit in time delay extraction

10. Range rate extraction

4.2.1 Equipment Delay Calibration

An important aspect of system accuracy is the ability to calibrate the system when installed in its operating location. This includes antenna and antenna coupling delays. This, of course, has not been done. However, the equipment has been calibrated with prime emphasis on the vehicle equipment. These calibrations of range delay in the transponders or the vehicle equipment were not used in the data reduction for other tests.

The results of the calibrations are given in Table 4.2.1-1.

TABLE 4.2.1-1 AROD Test Setup System Delays

System Component	Delay, Meters	
	Without TWTA	With TWTA
Vehicle, Chan A	50.34	53.81
Vehicle, Chan B	50.94	54.50
Vehicle, Chan C	51.17	54.69
Vehicle, Chan D	51.13	54.95
Cable, to XPDR 1	36.98	36.32
Cable, to XPDR 2	37.02	36.32
Cable, to XPDR 3	37.43	36.72
System, with XPDR 1	90.51	94.32
System, with XPDR 2	89.07	93.73
System, with XPDR 3	90.30	95.24
Transponder No. 1	2.59	3.50
Transponder No. 2	1.11	2.91
Transponder No. 3	1.94	4.02

As a part of the aging or drift tests conducted in the laboratory test program, the vehicle was checked again. The results are shown in Table 4.2.1-2.

TABLE 4.2.1-2

Final Vehicle Range Delay Data

CHANNEL	DELAY (METERS)	CHANGE (METERS)
A	51.24	.9
B	51.50	.56
C	51.40	.27
D	51.48	.35

The change is believed to be misleading, as all channels were realigned. (See Section 4.2.4). The test setup is shown in Figure 4.2.1-1.

The values given in Table 4.2.1-2 are therefore representative of the vehicle system. Alignment of the channels is done without regard for delay. The alignment is to null DC bias, set threshold levels, etc.

Table 4.2.1-3 is a summary of the vehicle receiver delays as calculated and compares this with the measured values. The difference is perhaps even closer than Table 4.2.1-3 might be expected. Nevertheless, the agreement gives credence to the validity of the system delay calibrations.

The transmitter section includes coding delay, amplifier delay, the times four multiplier, and diplexer. The receiver section includes the diplexer, IF amplifier, distribution amplifier and balanced demodulator.

TABLE 4.2.1-3
VEH RECEIVER DELAYS

EXTERNAL CABLE DELAY		31.5 n.s. Calculated
RANGE EXTRACTOR DELAY	(235 THEO)	242 n.s. Meas. ave.
INTERNAL CABLE DELAY		8 n.s. Calc.
TRANS. SECTION DELAY		36.1 n.s. Calc.
RECEIVER SECTION DELAY		32.9 n.s. Calc.
RECEIVER PHASE LEAD		- 3.6 n.s. Calc.
TOTAL:		346.9 n.s.
TOTAL MEASURED:		341.0 n.s. Meas.
DIFF.:		5.9 n.s.

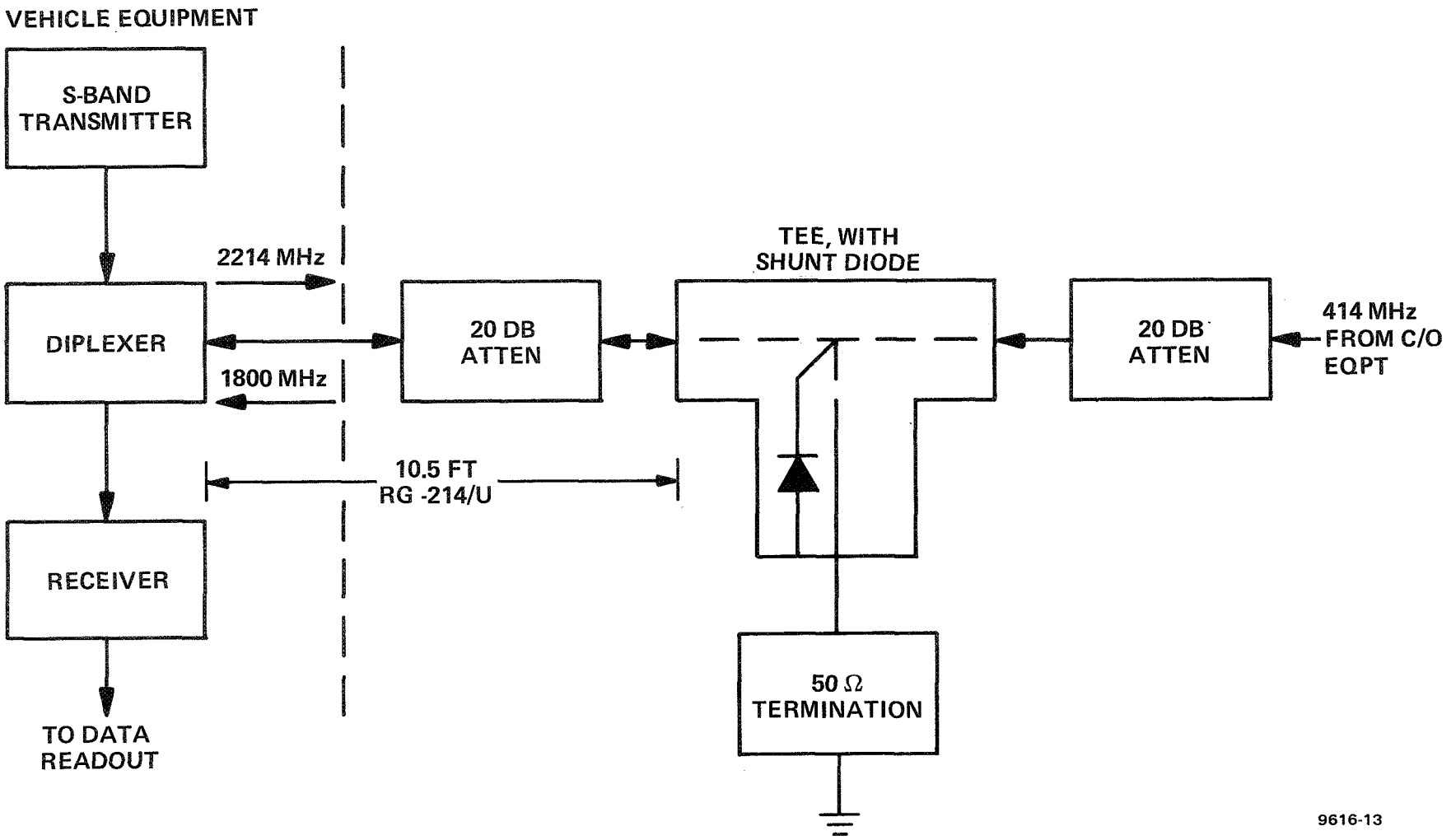

Figure 4.2.1-1. Vehicle System Delay Test SetUp

For this reason, it is believed that the equipment can be calibrated to within less than one resolution element or .183 meters. Assuming this is uniformly distributed, the rms bias error should be less than .1 meter per channel including both transponder and vehicle equipment. This is a fixed error and random from channel to channel.

4.2.2 Temperature Stability (23)

One channel of the vehicle equipment (Channel B) and one transponder (No. 1) were tested for range stability under temperature versus signal level. Figure 4.2.2-1 is a plot of the results. The $\Delta R = 0$ line is arbitrary.

The vehicle equipment was to be designed to operate on a $23^{o} \pm 2^{o}C$ cold plate. Therefore, these tests of this unit greatly exceed the expected operating temperature range.

The ground equipment was to be designed to operate over a temperature range of -24^{o} to $+71^{o}C$. As the transponders were constructed as experimental laboratory equipment, they were tested only to $+50^{o}C$.

The characteristic of the vehicle equipment as a function of signal level is due at high level to diplexer VSWR and at the low end to carrier leakage in the final IF. Both are discussed in depth in Section 4.2.5.

The variation with temperature in the transponders was traced to the crystal used in the range tracking loop. A better crystal should cure this problem; or temperature dependance of the transponders down to -115 dbm can be measured. The apparent change in range as a function of temperature can be estimated and the effect removed.

One could do this for the vehicle down to about -105 dbm where the carrier leakage begins to have effect. (This is not apparent in

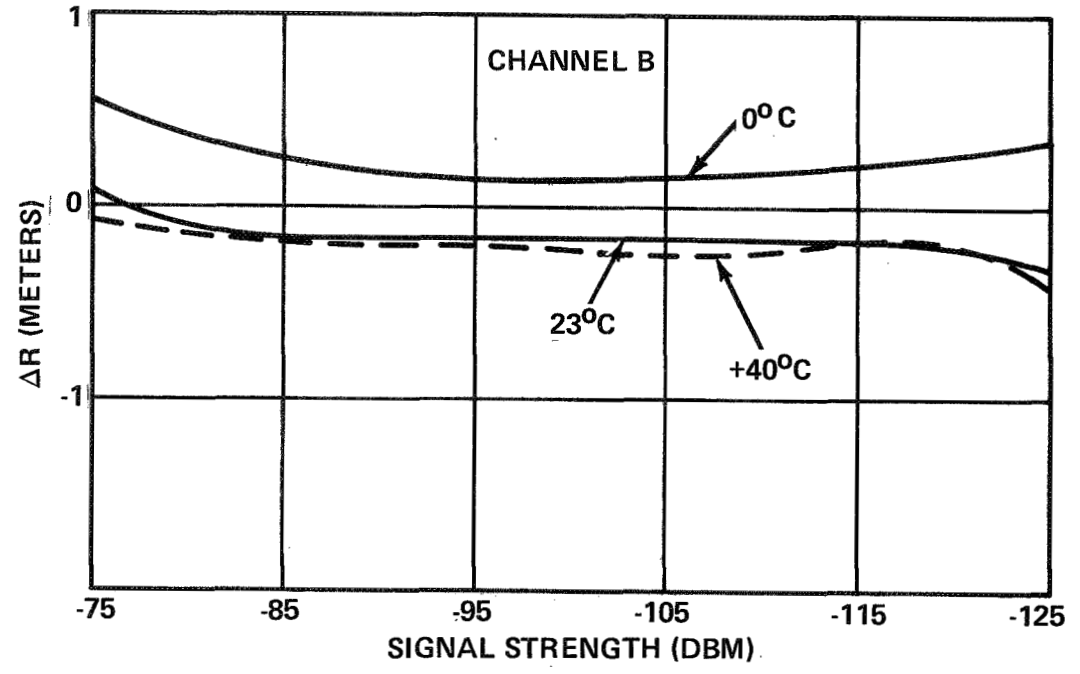

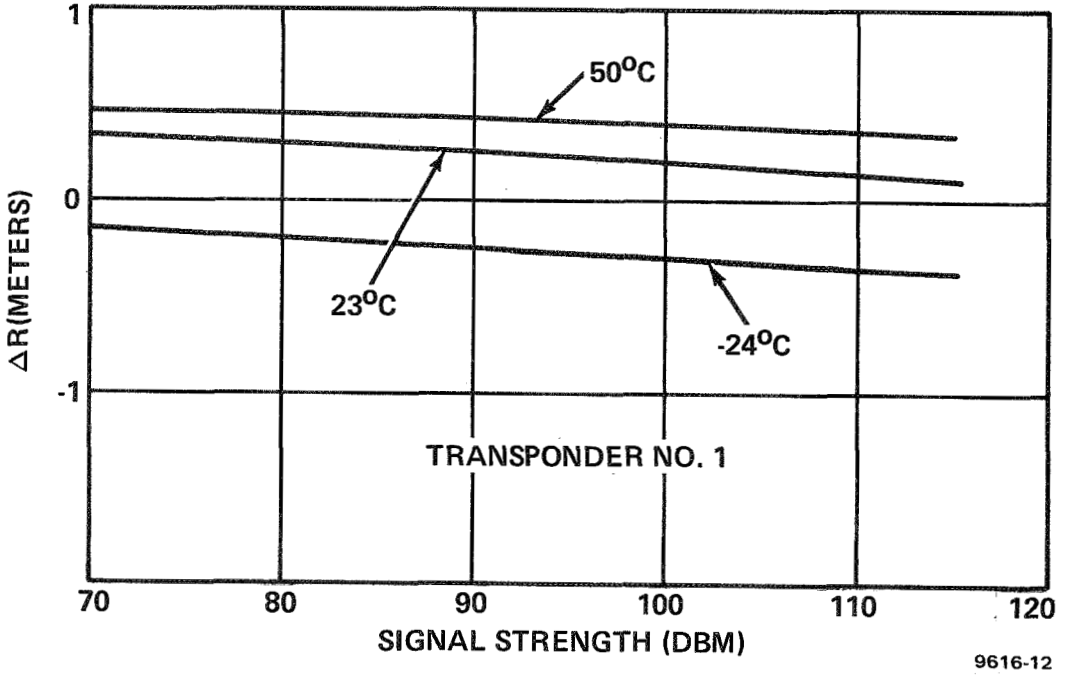

Figure 4.2.2-1. Temperature Stability

these curves, but does result at an extreme of doppler and temperature). Below this point doppler, temperature, and signal level interact to cause variation up to 1 meter that cannot be considered to be predictable.

To these levels, it is assumed that the corrected given temperature is predictable to .1 or .2 meters. The uncertainty should last for the length of a pass and probably be independant from pass to pass.

4.2.3 Master Oscillator Stability

The master oscillator stability was specified to be one part in 10^7. A temperature test on the delivered unit proved that its stability from 0 to 55°C was within the required $1:10^{-7}$.

The effect of the oscillator is to make a range error in direct proportion to the oscillator stability. The maximum range is expected to be less than 10,000 km (Appendix A). Hence, the oscillator stability effect is $\frac{R}{2} \times 10^{-7}$ meters. By measuring the temperature and using the frequency vs. temperature calibration curve, this should be removable by a factor of 10 or more. However, at this juncture this is hypothesis only and will not be used in the error model.

Long term drift of the oscillator is, of course, also important. In the tests after one month of operation, the oscillator had drifted 1.5 parts in 10^7. It was reset to the correct value. Subsequent tests at intervals over a year and half show that it has remained well within $1:10^7$. The drift, therefore, after stabilization has had an rms value of $1/\sqrt{6 \times 10^7}$ or less rms.

Multiple passes over a period of several days are not exptected to result in a material change. Whatever the error, it should be considered constant throughout a mission.

Short term stability could also be important. Direct measurements were made of the master oscillator short term stability. However, any effect that it might have is also included in the rms range error measurements as a function of signal level. The dependance upon short term stability cannot be isolated except that it, and the basic tracking loop noise set the minimum rms error attainable. This is discussed in the results in Section 4.2.5.

We shall use for residual the result for master oscillator stability = $(10^{-7}/\ 6)$ R, meters rms considered to be constant throughout a mission.

4.2.4 Aging Stability

For the reasons given previously, the tests of the AROD system to measure aging characteristics during the laboratory test program were generally invalid although the observed changes were relatively small. As a result a fixed test setup was used throughout this program and periodic tests were made of range accuracy. Some seven sets were run over a period of seven months. The first and last sets were composed of some 96 separate tests. In between the sets included some 36 tests.

The final set was intended to duplicate the initial set and to test nearly all conditions. Unfortunately, difficulty was experienced with the data recordings. Many of the last set of tests were lost. Paper tape recordings were also used. These indicated no difficulty with the AROD equipment. Consequently, it was not thought worthwhile to retake the data.

The mean range measurement varied over the tests a maximum peak-to-peak of less than .5 meters on any range. A more typical value was .25 meters peak-to-peak.

Threshold held to about a db or well within the absolute calibration accuracy. Range variance was consistant with previous data. In short there was nothing to indicate that the AROD equipment is operating other than as designed. It continues to be within specifications.

The system as a whole has nearly 4000 failure free operating hours over a three-year period.

4.2.5 Delay vs. Signal Level

There are several ways in which the observed time delay can be effected by signal level. Figure 4.2.5-1 is a graph of the standard deviation of range error as a function of signal level. Each channel of the vehicle system was operated with transponder No. 1. The signal level into the vehicle was varied, but that into the transponder was held constant at -80 dbm.

The theoretical curve is the calculated curve assuming noise in the vehicle receiver only. The values at the margin are the standard deviations at -70 dbm.

Much of the discrepancy at strong signal has been identified as the H code search circuit. This is discussed in Section 4.2.8.

Figure 4.2.5-2 is a plot of mean range taken from the same data. Table 4.2.5-1 is this data given in tabular form.

From Figure 4.2.5-2 a number of things can be noted. There is a significant shift in the mean range as a function of signal level. The shift as a function of range rate is predictable and discussed in Section 4.2.6 and also in 4.1.2.

The effect below -110 dbm has been identified as carrier leakage in the IF's. Since the range tracking loop operates on residual carrier, any stray carrier will cause "bias." The effect is definitely a function of signal strength and phasing of desired and stray carrier.

Channel C was characteristically the worst throughout the tests. A prototype or engineering model unit was substituted for the carrier tracking loop (CTL) and modulation tracking loop (MTL) and the same tests run. The prototype CTL was known to have little or carrier

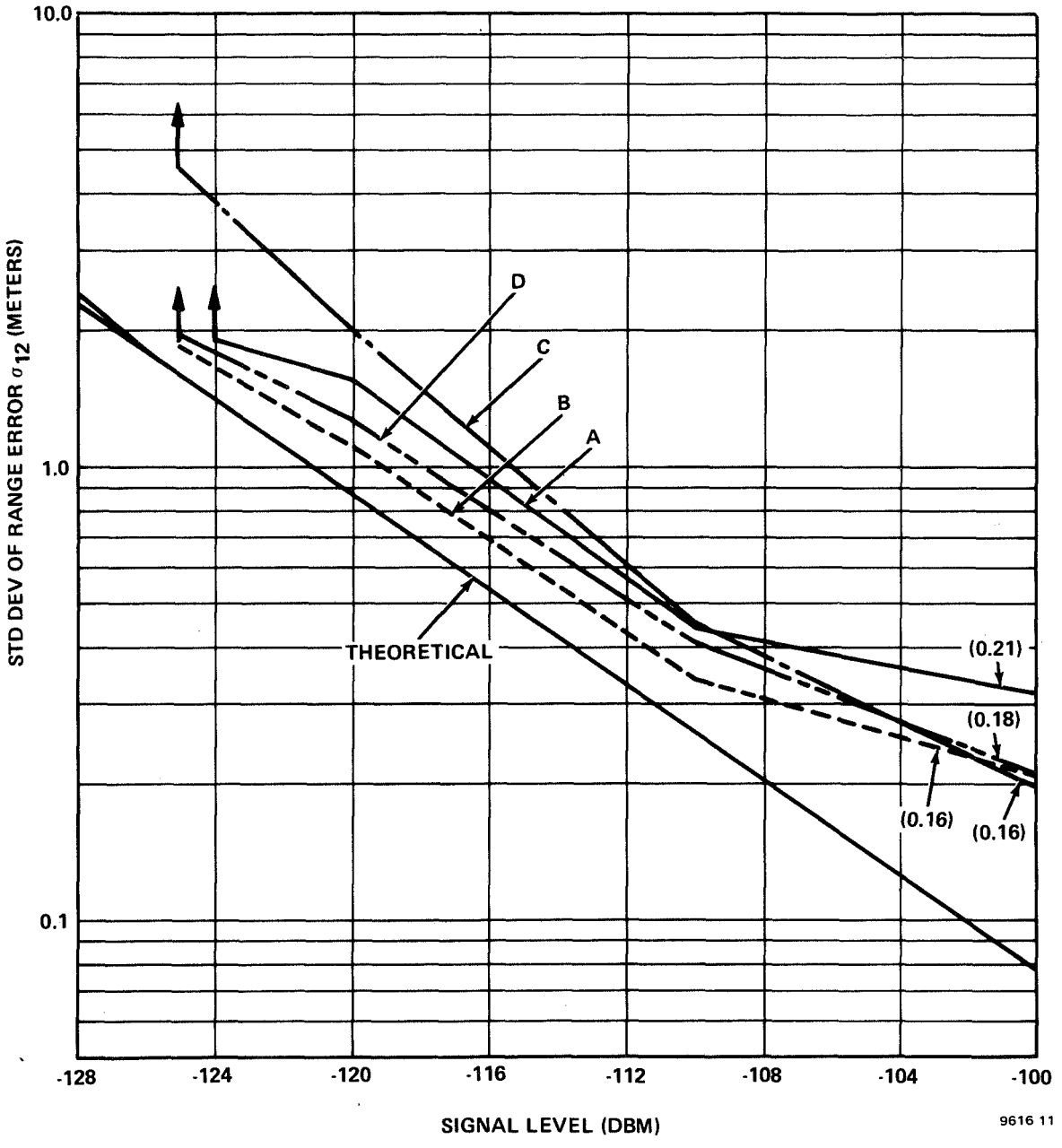

Figure 4.2.5-1
Range Noise vs. Signal Level

leakage. When using the prototype CTL and either MTL, the variation as a function of signal level was less than 0.1 meters not including the predictable effects of doppler. One such curve (0 doppler) is shown in Figure 4.2.5-2 translated from 88.75 meters for clarity.

It should be noted that the effect differs from channel to channel. It certainly is not a predictable error.

The effect above -80 dbm is somewhat more difficult to explain. Perhaps it can be done better by analyzing the transponders first.

Figure 4.2.5-3 is a graph of the performance of each transponder holding the vehicle channel B at -80 dbm. Table 4.2.5-2 is a tabular list of this data. The same low level variations can be noted and it is again carrier leakage, this time in the transponder. Note that there is no high signal level effect.

When these tests were started a quick calibration of the transponders revealed a very pronounced effect with signal level. This was traced to VSWR at the diplexer to cable interface. This was corrected and the result is shown in Figure 4.2.5-3.

It is known that the vehicle VSWR was bad, but could not be simply corrected. As a result, it was left alone and this is believed to be the cause of high level mean shift. This is certainly a correctable error.

The tests previously described were tests on the individual units. Tests were then run varying the signal level to both the transponder and the vehicle. This is shown in Figure 4.2.5-4 and Table 4.2.5-3.

The same general characteristics at high and low signal levels

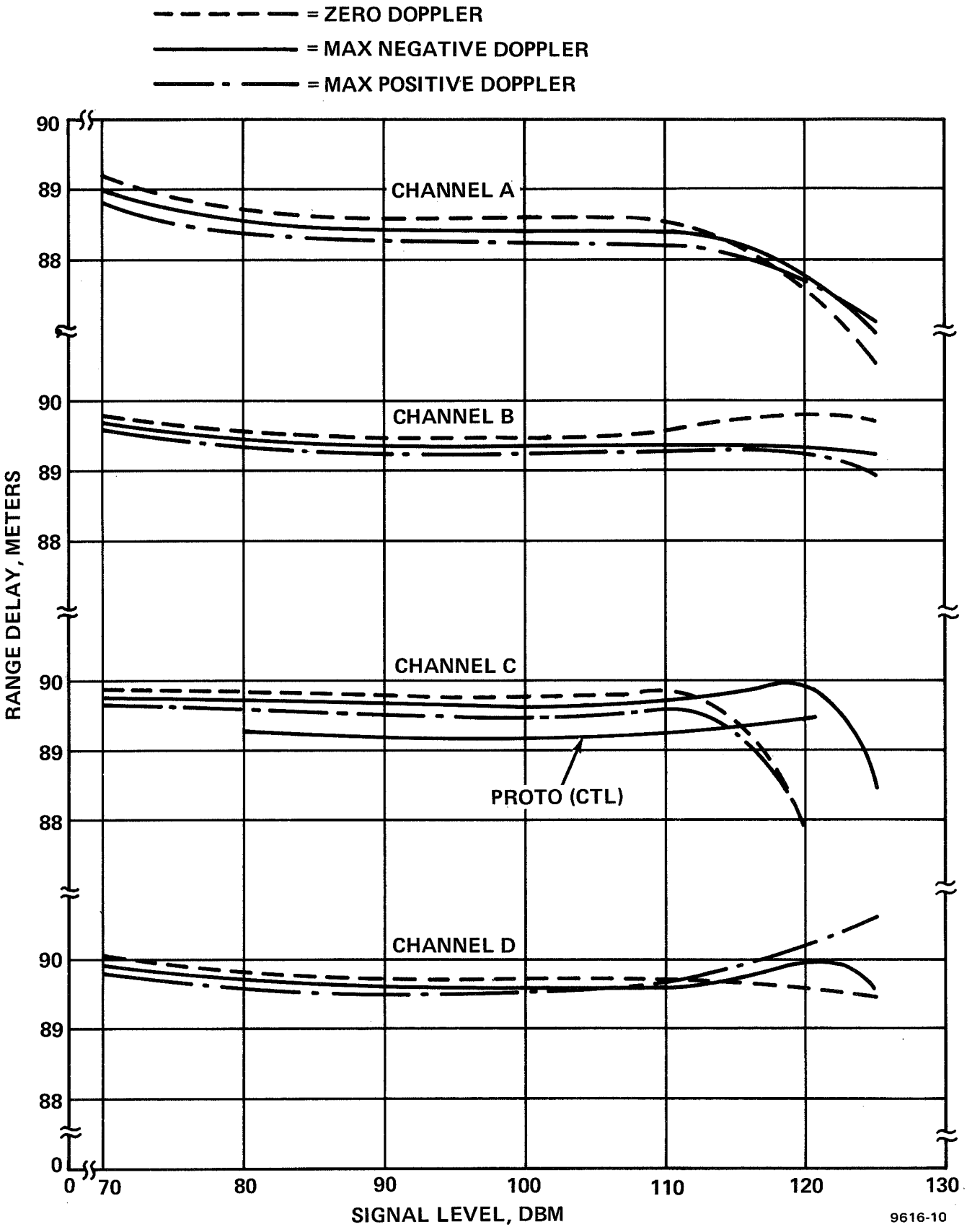

Figure 4.2.5-2
Range Delay vs. Signal Level

CHANNEL	DOPPLER	RANGE, METERS																					Δ
		-70 DBM			-80 DBM			-90 DBM			-100 DBM			-110 DBM			-120 DBM			-125 DBM			
		R	σ	C.F.	R	σ	C.F.	R	σ	C.F.	R	σ	C.F.	R	σ	C.F.	R	σ	C.F.	R	σ	C.F.	
A	–	89.13	0.25	.037	88.71	0.27	.041	88.62	0.28	.047	88.58	0.31	.047	88.54	.43	.065	87.57	1.07	0.161	-124 86.60	1.84	0.278	2.53
	O	88.96	0.21	.031	88.53	0.27	.041	88.46	0.28	.043	88.45	0.32	.049	88.41	0.44	.067	87.83	1.56	0.234	-124 86.97	1.91	0.287	1.99
	+	88.81	0.20	.030	88.37	0.27	.041	88.28	0.27	.040	88.23	0.27	.041	88.18	0.43	.065	87.75	0.94	0.141	-124 87.08	1.51	0.207	1.73
B	–	89.76	0.18	.027	89.51	0.19	.026	89.44	0.19	.029	89.43	0.22	.033	89.49	0.38	.059	89.79	1.08	0.17	89.69	1.90	0.316	0.33
	O	89.66	0.16	.025	89.39	0.22	.030	89.35	0.19	.028	89.32	0.21	.031	89.33	0.34	.051	89.36	1.10	0.17	89.20	1.86	0.285	0.46
	+	89.59	0.18	.027	89.33	0.18	.028	89.25	0.20	.028	89.24	0.19	.030	89.29	0.37	.058	89.33	1.27	0.20	89.02	2.16	0.30	0.57
C	–	89.87	0.16	.022	89.79	0.17	.026	89.74	0.19	.029	89.76	0.22	.032	89.77	0.61	.094	-118 87.91	1.74	0.27				1.96
	O	89.78	0.16	.025	89.68	0.16	.027	89.63	0.17	.026	89.61	0.20	.031	89.80	0.45	.069	90.02	1.99	0.28	-124 88.36	4.58	0.93	1.66
	+	89.70	0.16	.022	89.58	0.16	.024	89.53	0.18	.032	89.47	0.37	.056	89.58	0.93	0.143	88.05	2.61	0.40				1.65
D	–	90.01	0.38	.049	89.78	0.35	.054	89.69	0.20	.035	89.68	0.31	.043	89.69	0.41	.062	89.48	1.48	0.23	-124 89.44	1.81	0.23	0.57
	O	89.89	0.18	.027	89.67	0.18	.025	89.65	0.31	.048	89.61	0.21	.027	89.59	0.41	.057	90.03	1.26	0.164	89.63	1.90	0.267	0.44
	+	89.83	0.29	.045	89.60	0.20	.030	89.56	0.18	.025	89.55	0.20	.031	89.66	0.43	.067	90.25	1.41	0.280	90.61	2.31	0.491	1.06

9616 24

Table 4.2.5-1
Range Delay and Standard Deviation vs. Signal Level

XPNDR	DOPPLER	SIGNAL LEVEL, DBM										
		-70		-90		-110		-120		-125		
		R	σ	R	σ	R	σ	R	σ	R	σ	Δ
1 FILE #18	–	89.22	0.18	89.18	0.18	89.09	0.35	88.02	1.03	87.46	1.34	1.76
	0	89.01	0.18	89.00	0.20	88.78	0.29	87.68	0.66	86.61	1.26	2.40
	+	89.17	0.19	89.13	0.17	88.97	0.28	87.99	0.93	86.92	1.38	2.25
2 FILE #27	–	88.66	0.17	88.65	0.18	88.80	0.52	89.14	1.66	90.52	2.87	1.86
	0	88.55	0.19	88.51	0.18	88.51	0.26	88.80	0.56	89.08	1.05	0.53
	+	88.47	1.04*	88.32	0.18	88.44	0.45	88.44	1.71	88.38	2.68	0.15
3 FILE #19	–	89.28	0.19	89.20	0.22	89.13	0.29	89.01	0.88	89.23	1.31	0.27
	0	89.06	0.17	89.00	0.18	89.05	0.25	88.22	0.72	88.06	1.15	1.00
	+	88.97	0.17	88.91	0.17	89.15	0.26	89.81	0.85	88.67	1.39	1.14

* LOST LOCK MOMENTARILY

9616-25

Table 4.2.5-2

Transponder Range Delay Versus Signal Level
and Doppler Condition. Doppler = ±512 Hz at 12 MHz (12,000 M/S)
Using Vehicle Channel B at -80 dbm

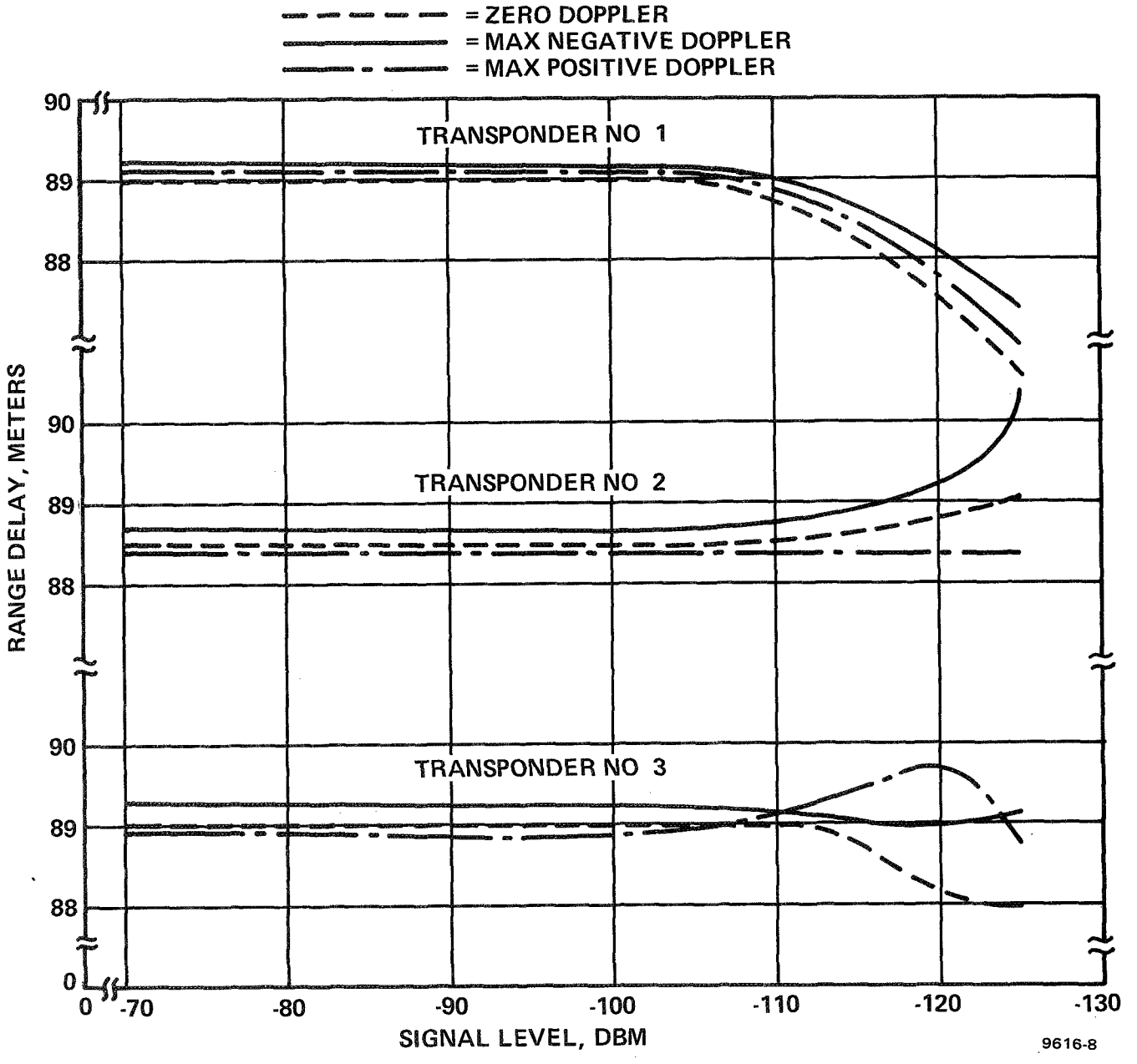

Figure 4.2.5-3
Transponder Delay

XPNDR	SIGNAL LEVEL, DBM AND RANGE, METERS														
	-70		-80		-90		-100		-110		-120		-125		
	R	σ C F	R	σ C F	R	σ C F	R	σ C F	R	σ C F	R	σ C F	R	σ C F	Δ
1	88.28	0.17 .024	87.93	0.20 .031	87.90	0.19 .029	87.75	0.20 .030	87.85	0.29 .045	87.49	0.81 .105	86.10	1.75 .246	2.18
2	88.44	0.18 .028	88.04	0.18 .027	87.98	0.18 .027	87.98	0.19 .030	88.00	0.35 .054	88.32	1.23 .189	87.96	2.50 .440	0.48
3	89.89	0.15 .023	89.68	0.31 .048	89.59	0.19 .032	89.49	0.20 .030	89.48	0.38 .054	89.43	0.82 .126	89.00	1.51 .233	0.89

9616-29

Table 4.2.5-3. System Range Delay Zero Velocity (0 Doppler) Condition Using Vehicle Channel B.

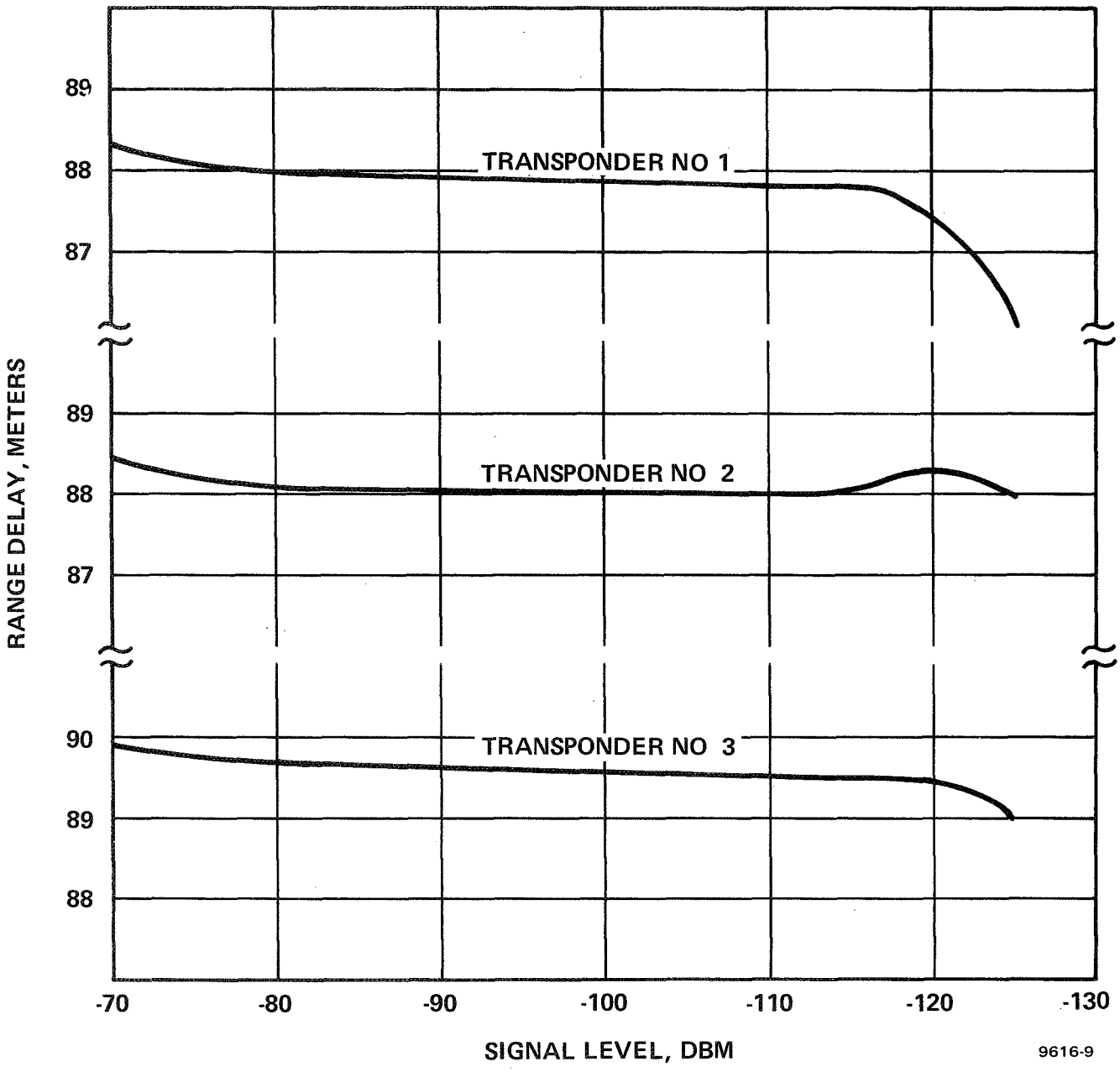

Figure 4.2.5-4. System Range Delay Variation with Signal Level Common Path Attenuation using Vehicle Channel B. Zero Doppler

can be observed. A comparison of these curves (Transponder No. 1 and Vehicle Channel B) illustrates the problem encountered in the so-called aging tests as discussed in Section 4.2.4. New test set-ups and new alignment procedures were instituted in the time span covered by these tests. As a result, these tests show a mean shift in range.

It should also be noted that the full system signal level tests show less rms range error than vehicle channel only. This is believed to be a consequence of calibration of signal level and noise which has an absolute uncertainty of about 2 db.

For the range error model the following is assumed. The variance due to noise is R/R_o, $(\text{meters})^2$ where R_o is 16,000 km and R is true range. These are independant from channel-to-channel and from measurement to measurement at 0.25 second intervals. In addition, a 0.5 meter standard deviation will be assumed as a range error at any range.

4.2.6 Delay vs. Range Rate

The system was tested for range accuracy vs. range rate. The tests were generally limited to range as a function of plus or minus maximum range rate and zero range rate. The data presented in Section 4.2.5 represents raw data transformed from time delay to range using the value of propagation velocity equal to 2.9 m/s and a frequency of 6.4 MHz. No corrections as outlined in Section 4.1.2 and 4.1.4 were included. The curves given in Section 4.2.5 illustrate a dependance upon range rate. The mean range error as a function of range rate is consistant with the theoretical factors

previously evaluated (4.1.2). There is no statistical significance at the 90% level to indicate that the observed effect is other than as predicted theoretically.

Therefore, no residual error is attributed to this factor.

4.2.7 Delay vs. Multichannel Operation

The previous measurements were all single channel tests. Multichannel tests were conducted to determine the degree of data degradation with adjacent channels in operation. Tests were conducted with one, two, and three interfering signals both with and without Doppler.

Tests were conducted with signal level variations from -80 dbm to threshold. Data readouts were taken on both range and velocity. The test channel for both range and velocity data utilized common path attenuation: that is, both terminals were adjusted to the same signal level.

The two-channel tests were conducted with channel A locked to the checkout equipment at a signal level of -80 dbm and with +10 Hz of Doppler at 12.8 MHz (a velocity of about 120 m/s). Range data was taken with channel B vehicle receiver and No. 3 transponder, and was repeated using channel C and D vehicle receivers. A summary of this range data is presented in Table 4.2.7-1. The threshold of -105 dbm is typical with strong signal adjacent channel occupancy. The system design threshold to multichannel operation was about 27 db, one channel relative to another. This was found to be about right. The range data for all three 2-channel tests is plotted in Figure 4.2.7-1. The curves indicate that the coherent leakage effect

CHANNEL TESTED	-80 DBM		-85 DBM		-90 DBM		-95 DBM		-100 DBM		-105 DBM	
	R	σ C.F	R	σ C.F.	R	σ C.F.	R	σ C.F.	R	σ C.F.	R	σ C.F.
B	89.50	0.17 .030	89.47	0.20 .031	89.46	0.28 .043	89.48	0.29 .044	89.68	0.50 .077	89.84	0.52 .079
C	89.86	0.18 .031	89.87	0.17 .026	89.85	0.18 .028	89.88	0.20 .031	89.92	0.30 .047	90.23	0.56 .086
D	89.93	0.19 .029	89.91	0.20 .030	89.90	0.19 .029	89.94	0.21 .032	90.04	0.27 .042	90.58	0.60 .092

9616-26

Table 4.2.7-1. System Range Data Two-Channel Tests

TEST CONDITIONS	-80 DBM		-85 DBM		-90 DBM		-95 DBM		-100 DBM		-105 DBM		-110 DBM	
	R	σ C.F.	R	σ C.F.	R	σ C.F.	R	σ C.F.	R	σ C.F.	R	σ C.F.	R	σ C.F.
CH A &C @ -80 DBM TO C/O	89.80	0.23 .029	89.80	0.21 .035	89.81	0.25 .038	89.94	0.41 .063	90.43	0.79 .122	90.67	0.77 .137	89.77	0.16 .025
CH A @ -80 DBM TO C/O CH C TO XPNDR #2	89.69	0.17 .026	89.68	0.18 .028	89.65	0.21 .032	89.79	0.26 .040	90.08	0.31 .048	90.11	0.61 .094	89.83	0.22 .034
CH A&C @ -80 DBM TO C/O CH D TO XPNDR #2	89.75	0.20 .030	89.72	0.21 .032	89.74	0.30 .046	89.94	0.33 .050	90.34	0.71 .109				

9616 27

Table 4.2.7-2. System Range Data Multi-Channel Tests

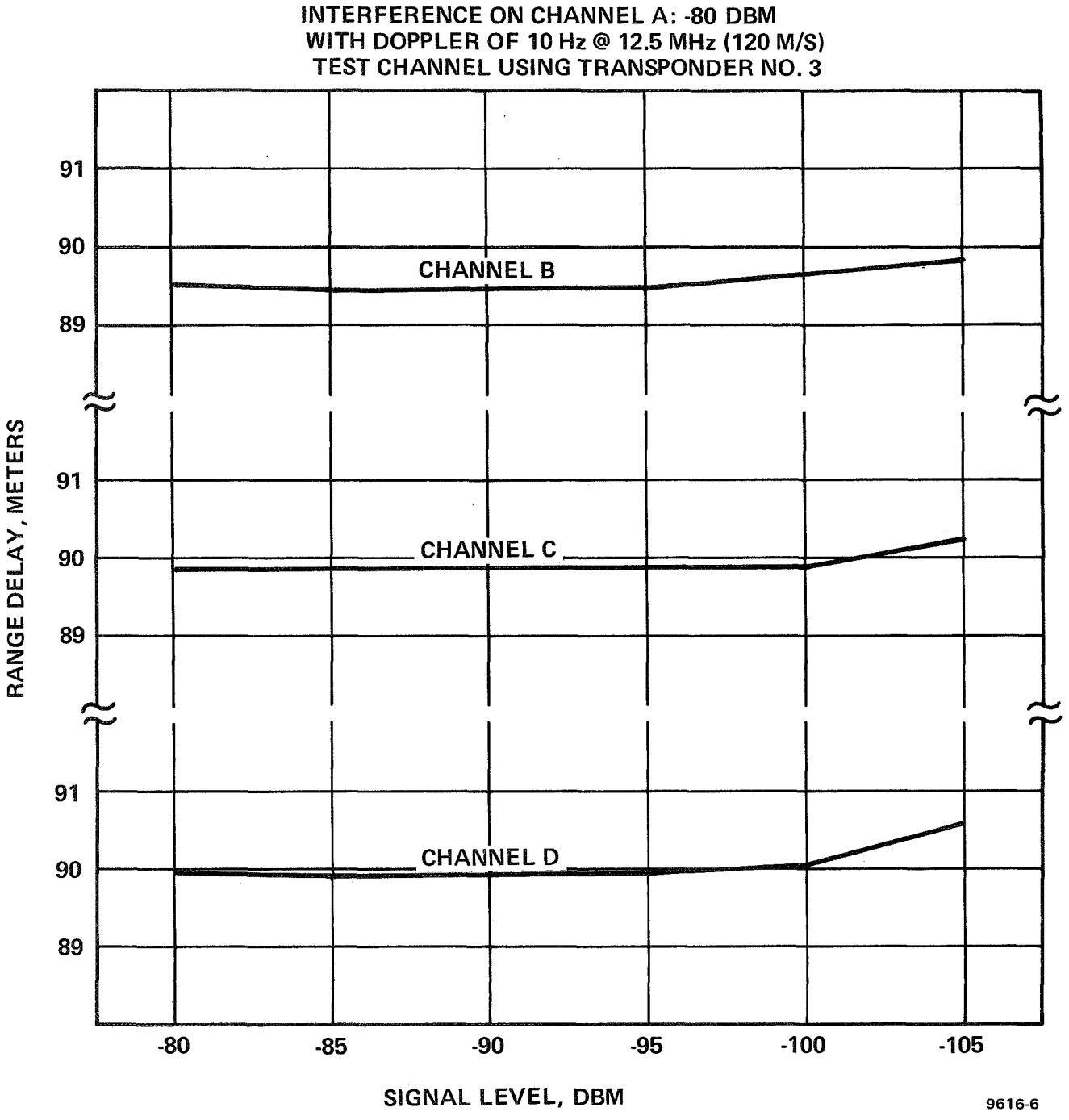

Figure 4.2.7-1. System Range Data
Multi-Channel Tests

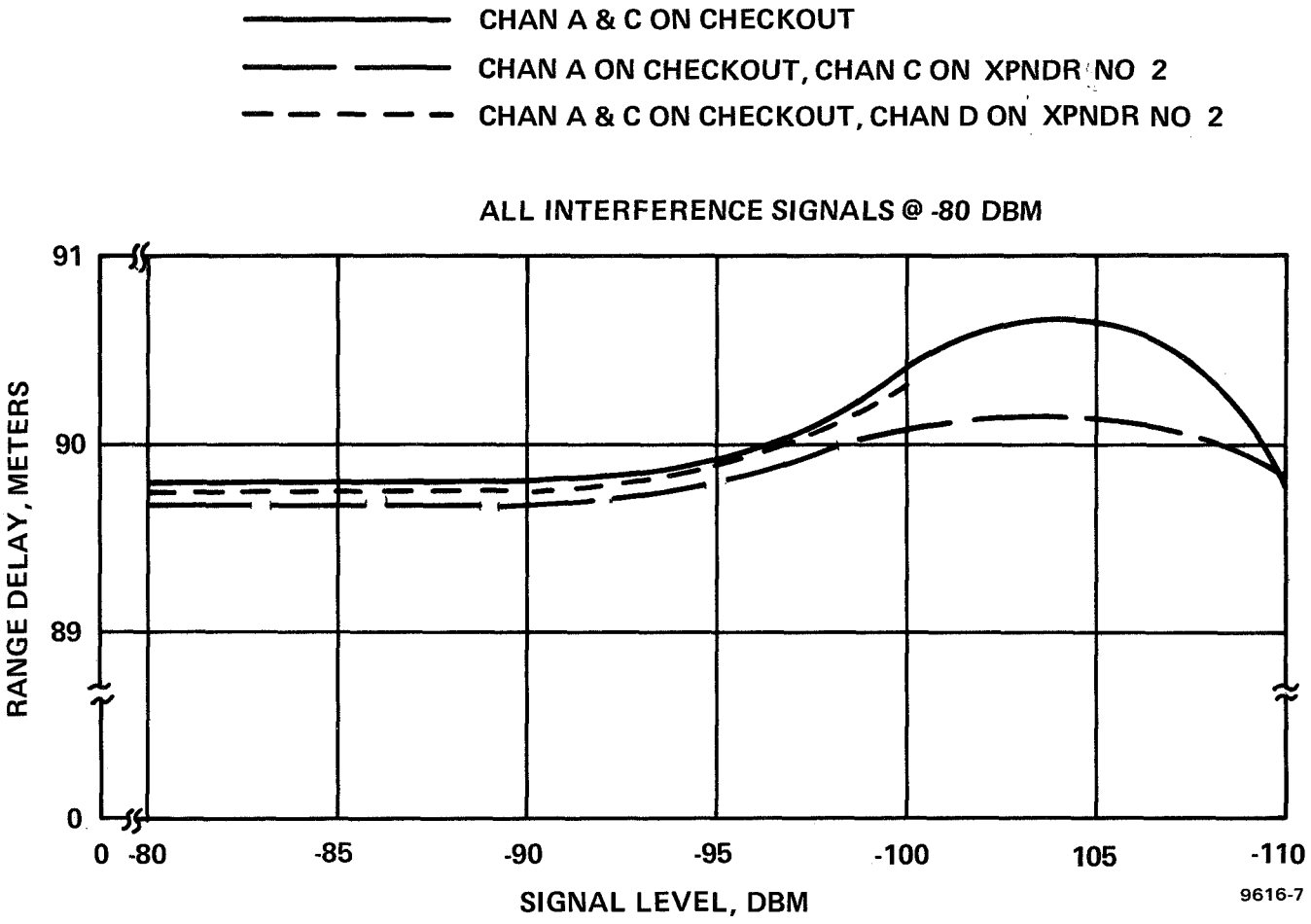

Figure 4.2.7-2. System Range Delay
Multi-Channel Tests
Data on Vehicle Chan. B - Transponder No. 3

contributes very little, since the threshold here is much higher. All data points are within ± 0.25 meter with channels B and C showing a much smaller spread.

Range data with interference from two and three channels were obtained with three additional tests of channel B - Transponder No. 3:

1. With interference from checkout channels A and C.

   Channel A: -80 dbm, +120 m/s velocity
   Channel C: -80 dbm, -120 m/s velocity

2. With interference from checkout channel A and Transponder No. 2 on channel C.

   Channel A: -80 dbm, +120 m/s velocity
   Channel C: -80 dbm, 0 velocity

3. With interference from checkout channels A and C and Transponder No. 2 on channel D.

   Channel A: -80 dbm, +120 m/s velocity
   Channel C: -80 dbm, -120 m/s velocity
   Channel D: -80 dbm, 0 velocity

The results of these tests are summarized in Table 4.2.7-2. The data are plotted on Figure 4.2.7-2 with a somewhat expanded scale. All three curves fall within a ± 0.5 meter range.

4.2.8 H-Code Search In The Vehicle Equipment

During the laboratory test program it became apparent through an analysis of the autocorrelation functions of the range error data that there was a periodic component present. This was traced to the H-Code search signal in the vehicle equipment.

The theoretical effect of leaving this search signal on during track was less than 3 cm. The effect, however, was demonstrated to be much greater. The means by which this signal contributed to an error much larger than expected is unknown.

A test was run with it shut off. At -90 dbm the total rms error was .29 meters. With the H-Code search signal shut off it was only .12 meters. Further analysis revealed that as the signal was reduced the error source increased although not as rapidly as the error due to a decreasing signal-to-noise ratio.

The transponders do not have this problem as the H-Code search is shut off during track. It is quite apparent that this problem can be eliminated in future flight equipment.

4.2.9 Loss of Coarse Bit In Time Delay Extraction

Approximately one time in a thousand the range error exhibited an error in excess of one coarse bit or 23.4 meters. The data reduction program used rejected all errors greater than 13 meters, but counted all such rejections and tabulated them. Theory rejected them so they were not included in the mean and variance analysis.

This problem was traced to an ambiguity problem between the fine and coarse range extractor. An experiment was conducted which demonstrated that when certain phase relationships existed, this sudden jump could be expected.

A specific cure was not found. However, by using the range rate information such jumps can be rejected. The range rate error is constrained to less than 0.1 m/sec. The time between range measurements is 0.25 sec. so that the expected range error is no more than .025 meters from measurement to measurement. If the change exceeds some value such as 13 meters, the response can be rejected or reliably replaced by one coarse bit added or subtracted appropriately.

No residual should result from this effect. In final flight equipment, this problem will be resolved.

4.2.10 Range Rate Extraction

Although not directly related to range accuracy the possibility of using range rate to improve position accuracy, the performance of

the system to obtain an accurate measure of range rate could be important.

Several problems in range rate extraction were uncovered during the test program. First, the local oscillator frequency, derived coherently from the reference oscillator, was derived using a phase locked loop whose bandwidth was too narrow. This meant that the local oscillator did not follow the phase of the reference accurately enough. This injected a phase error into the recovered carrier which approximately doubled the range rate rms error.

This problem was corrected by redesign of the frequency synthesizer. A new one was built and put into the equipment.

A second problem arose. As reported in Section 3 the doppler beat note (plus an offset frequency) was multiplied by 16 to obtain the necessary range rate resolution.

The last product by 2 was to be done by sampling the phase at the beginning and the end of the measurement interval. Through a logic error, only the beginning was sampled. As a result, one bit of resolution was effectively lost.

This problem was identified and a breadboard doppler extractor built to demonstrate the proper logic. It was not incorporated in the final equipment, however. Re-layout of modules and mother-boards was not considered worthwhile.

The net effect of these two corrections was to bring the rms range rate error to within a value of about 1.5 of the calculated rms value as a function of signal to noise.

No residual range error results from this problem.

4.3 VELOCITY OF LIGHT IN VACUO

The uncertainty in the velocity of light in vacuo is a constant scaling factor in all range measurements. This assumes that the unit of measurement, the meter for example, is defined by means other than using the definition of the velocity of light as a reference.

In a geodetic survey, if the reference stations, from which the survey is extended, are surveyed within their network by a radio ranging system using trilateration, then the velocity of light is assumed to be perfect or invariant and the meter is defined thereby. In this case, using a fixed velocity of light simply expands or contracts the linear range between all locations of the geometry uniformly and proportional to each range itself.

The following is abstracted from ASLAKSON. (21) A value of 299,766 km/sec., the Berge statistical value was assumed prior to 1944. Subsequent measures disclosed about a 17 km/sec. error. In 1949 the Air Force adopted 299,793.1 as the standard for all HIRAN measurements.

A statistical average of measurements from 1944 through 1955 is 299,792.4 km/sec. Measurements of atomic constants by Dumand and Cohen, 299,792.9 km/sec, and Beardon and Thoursen, 299,792.8 km/sec, confirm this average.

The Air Force standard appears to be consistant with these and differs by one part in a million. Hence, for this study use

$$c = 299{,}793.1 \text{ km/sec.}$$

with a standard error of $10^{-6}R$ common to all range measurements.

4.4 TROPOSPHERIC EFFECTS

A dominating factor in radio ranging is that of the index of refraction of the Troposphere. Fortunately, a large portion of its effect can be accounted for leaving only a small residual error.

Two effects are the result of propagating through the Troposphere. One, the path is actually curved from transmitter to receiver. Thus, the distance traveled is longer than the slant range. Two, the radio wave undergoes a retardation through the medium.

The ability to correct for these factors depends to some extent upon the information available and its quality.

Before suggesting methods of correction, it will give a brief review of the theory.

In order to utilize the potential accuracy of the system design concepts it is mandatory that corrections be made to the time difference data for conditions influencing the propagation time through the atmosphere. The basic quantities measured by the system are time difference and frequency shift. Both of these quantities are influenced by the refractive index variation of the atmosphere. In the case of the time difference measurement the effective propagation velocity of the r.f. wave between the ground and vehicle portions of the system must be known to convert the time difference measured to a physical distance. In the case of the frequency shift the bending of the wave by the inhomogeneous refractive index causes the angle of arrival of the wave at the point of measurement to be different than the geometrical angle associated with the chord connecting the vehicle and the ground station. Both of these errors in measurement

are significant in view of the design objectives of the AROD system. It is the purpose of this section to investigate means of correcting the measured quantities for the effects of the refractive index of the atmosphere.

A considerable effort has been expended by various investigators over the past several years to produce a quantitative description of the atmosphere. Notably, the National Bureau of Standards has developed models for the refractive index of the troposphere and has also developed direct methods of relating both ray bending and range measurement errors in terms of measurable parameters of the atmosphere. It is clear that either approach cannot account for the statistical variations of the refractive index which occur in local areas along the path of propagation, but it has also been shown that the residual error due to these local variations is of the order of a few percent of the total error. The significant result of the investigation to date is that better than 90 percent of the effects of the atmosphere can be accounted for by a knowledge of the refractive index at the surface (on the ground). This, in effect, says that by measuring the index of refraction at each of the AROD ground stations and transmitting that data to the vehicle, corrections can be made, in real time, to the measured time difference and doppler frequency to produce position and velocity data.

4.4.1 Ray Bending

The path that a wave follows in traversing an inhomogeneous medium is determined by the rate of change of the refractive index at each height. The refractive index is given as a first approximation

by $n = 1 + N_s e^{-\frac{r-r_o}{H}}$

where N_s is the value of refractive index at the surface ($r = r_o$)

H is an effective correlation height ($\sim$7 km)

r is the distance from the center of a spherical earth.

The geometry of the problem is shown in Figure 4.4.1-1

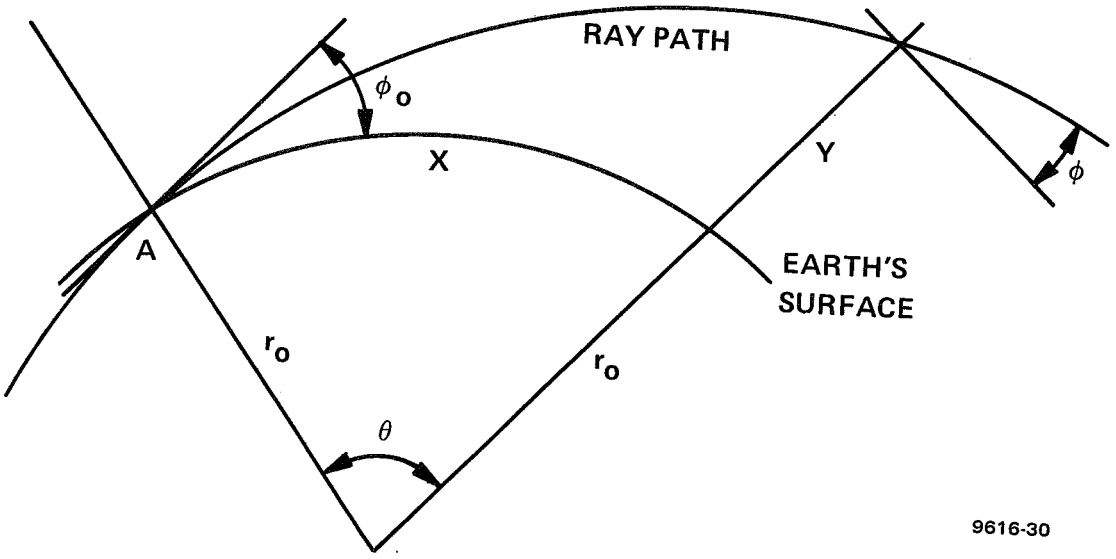

Figure 4.4.1-1

Ray Path Geometry

From Snell's law of refraction

$$\tan \phi d\phi = \frac{dr}{r} + \frac{dn}{n}$$

For the assumed exponential model of the atmosphere

$$\frac{dn}{n} = -\frac{N_s}{H} \frac{e^{-\frac{r-r_o}{H}}}{1 + N_s e^{-\frac{r-r_o}{H}}} dr.$$

From the spherical geometry,

$$dr = r d\theta \tan \phi$$

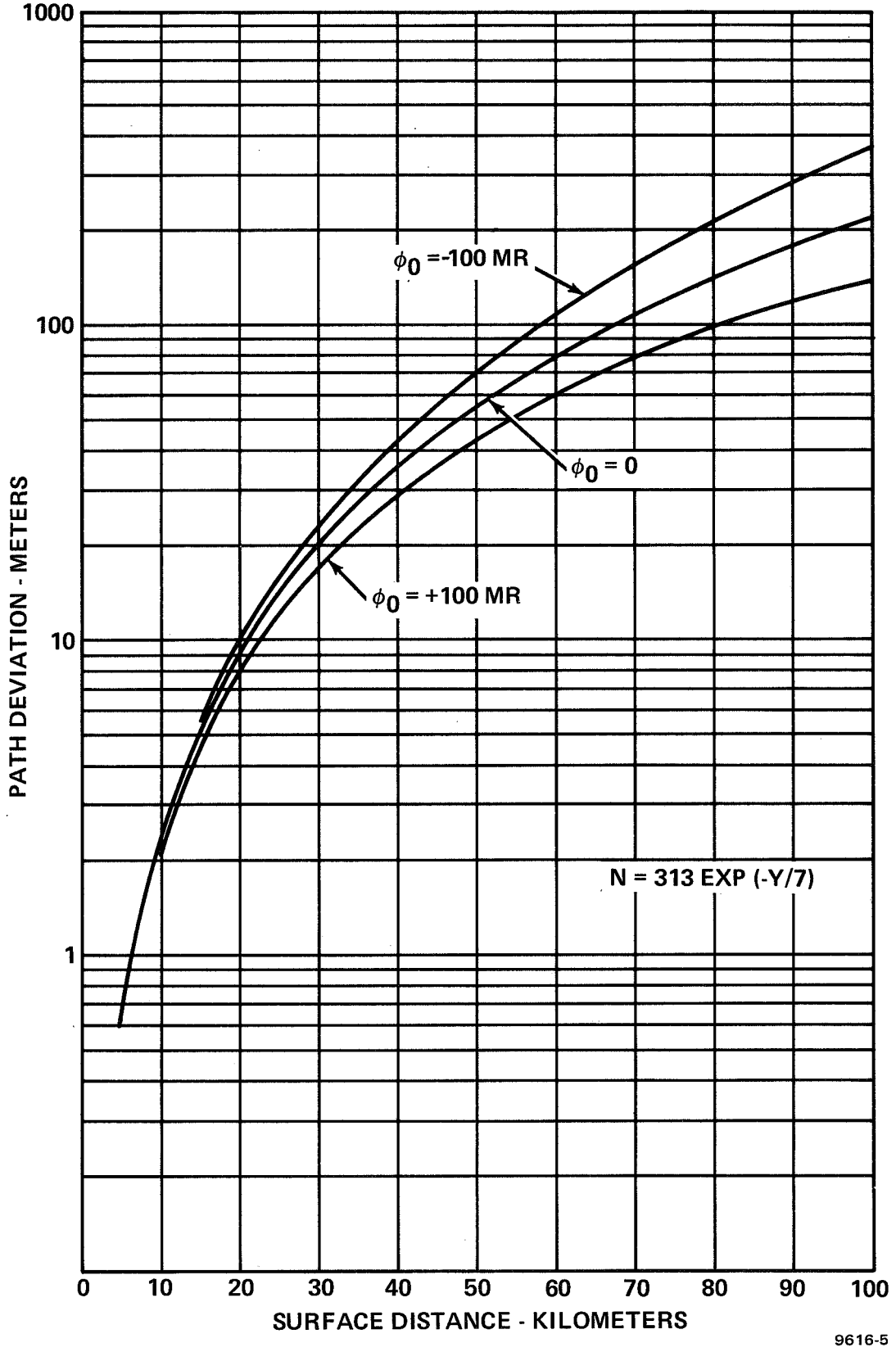

Figure 4.4.1-2
Path Deviation vs. Distance

Therefore

$$d\phi = r d\theta \left[\frac{1}{r} - \frac{N_s}{H} \frac{e^{\frac{r-r_o}{H}}}{1 + N_s e^{-\frac{r-r_o}{H}}} \right]$$

Making the substitutions

$$x = r_o \theta$$

and

$$y = r - r_o,$$

gives

$$dy = \tan \phi \, dx.$$

and

$$d\phi = \left[\frac{1}{y + r_o} - \frac{N_s}{H} \frac{e^{-y/H}}{1 + N_s e^{-y/H}} \right] dx.$$

Using numerical integration procedures the path $y = f(x)$ was computed. The equation of a straight line from point A with a departure angle ϕ_o is given by

$$y_L = 2r_o \frac{\sin(x)/2r_o)\sin(\phi_o + x/2r_o)}{\cos(\phi_o + x/r_o)}$$

The deviation of the path of propagation from a straight line is then $y_L - y$. Figure 4.4.1-2 shows a plot of $y_L - y$ as a function of distance along the earth's surface, x, for three values of ϕ_o. It can be seen from Figure 4.4.1-2 that typical deviations from a straight line are in the order of 100 to 300 meters at distances of 100 km from the ground station. In view of the nearly straight path of propagation it seems plausible to assume that the path is a straight line.

Since the wave actually travels over the curved path between the ground and vehicle stations the distance of travel will be longer than a straight line path would indicate. In order to assure that the path of propagation is not appreciably longer than the chord connecting the end points of the path a numerical integration of the two paths lengths was made for a typical atmosphere at various elevation angles and ranges corresponding to the conditions expected in the line crossing flight case. The geometry of the problem is the same as that indicated in Figure 4.4.1-1. The results of the computation are shown in Figure 4.4.1-3. From Figure 4.4.1-3 it can be seen that the path length errors are less than 0.1 meters out to 70 km for all elevation angles between $\pm$ 100 milliradians. The larger errors at negative values of ϕ_o occur because the refractive index becomes larger as the wave is sent downward from the ground station.

The same data was extrapolated for propagation paths entirely through the troposphere. This is contained in Table 4.4.1-1. (10)

$N \simeq 320$

ϕ_o deg.	ϕ_o mr	ΔR_g meters	ΔR_N meters	ΔR_e meters	σ
0	0	10	100	110	
1.15	20	2.5	62.5	65	.815
2.9	50	0.7	38.1	38.8	.57
5.73	100	0.14	22.26	22.4	.38
11.5	200	0.02	11.9	11.9	.22
28.7	500	0.001	5.01	5.01	.08
90	$\pi/2 \times 10^3$	0.0	2.41	2.41	.04

Table 4.4.1-1
Tropospheric Effects

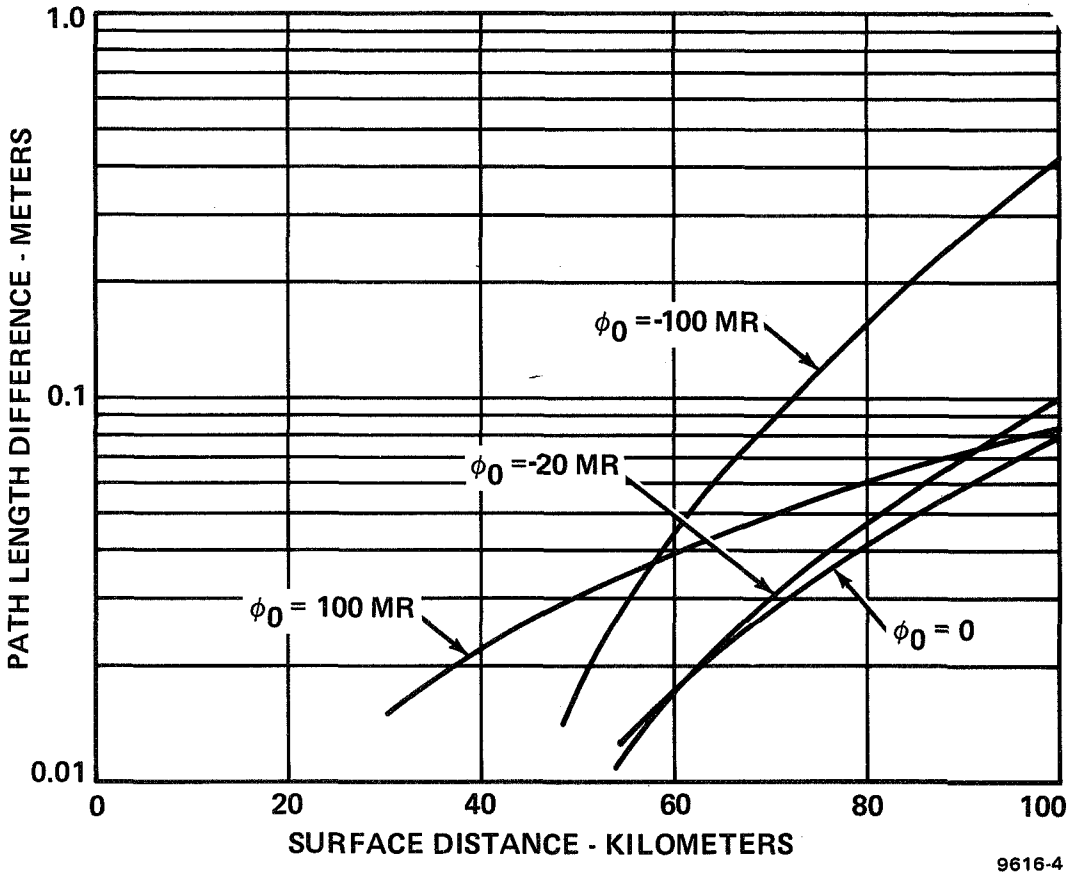

Figure 4.4.1-3
Path Length Difference

ΔRg = Geometrical increase in range

ΔR_N = Retardation factor

ΔR_e = Total apparent increase in range

The values of ΔRg are always small compared to ΔR_N. This is particularly true at $6^o$and above. It may be neglected.

4.4.2 Retardation Effect

In the previous section, Table 4.4.1-1 indicates that the wave retardation effect is the principle source of cause of difference between apparent slant range and true slant range. Clearly this is the case for launch angles of 6^o or more.

In the region of the radio spectrum of interest the index of refraction of the troposphere is indepentant of the frequency employed. The index of refraction is (14)

$$\eta = 77.6 \frac{P_d}{T} + 72 \frac{e}{T} + 3.75 \times 10^5 \frac{e}{T^2}$$

where η is the index of refraction

P_d is the pressure of dry air in mb

e is the partial pressure of the water vapor in mb

and T is absolute temperature in degrees Kelvin each measured in the local volume of interest.

The apparent range to a target is

$$R_e = \int_{h_1}^{h_2} \frac{\eta \, dh}{\sin \theta}$$

where h_1 is the station altitude, h_2 is the satellite altitude, η the index of refraction at altitude h_1 and θ is the angle from the

horizontal at altitude h. $R_e - R = \Delta R_e$.

This equation cannot be solved explicitly without knowledge of $\eta(h)$ and $\theta(h)$. A variety of methods have been used. One is to assume a model of $\eta(h)$, usually exponential. Another is to use a "standard" atmosphere. Another is numerical integration using radio sonde data and the relationship of θ and η given in the previous section. Finally, a statistical regression has been used between ΔR_e and various parameters at the station location.

The difference, ΔR_e, can be written as: (1)

$$\Delta R_e = \int_{h_1}^{h_2} \frac{N(h) \times 10^{-6} dh}{\sin \theta} + \int_{h_1}^{h_2} \csc. \theta_2 (h) dh - R$$

$N(h) = (\eta - 1) \times 10^6$

θ_2 is the angle at altitude h.

h_1 and h_2 are as before.

The last two terms are the difference in distance between the curved path and the slant range previously shown to be small. The first term is the retardation effect. This term is often written as

$$\csc(\theta_o) \int_{h_1}^{h_2} N(h) \times 10^{-6} \, dh$$

and is used for launch angles above about 6^o. When this is done the integral $\int N(h)\, dh \times 10^{-6}$ is called I(h) and is the retardation vertically over the station.

In principle if one knows the index of refraction profile overhead, can one estimate ΔR_e. This expression blows up for $\theta = 90^o$ when in reality ΔR_e does not.

These equations are a model of the tropospheric effect. Among

other factors, it assumes that the atmosphere is uniformly stratifid over a spherical earth. Departure from these conditions results in a variation in ΔR_e. It is the ability to estimate accurately the total behavior that is important.

4.4.3 Methods of Estimating ΔR_e

As noted above a number of methods of estimating ΔR_e have been used. These can be lumped into four basic types.

1. Measure the profile index of refraction along the propagation path and use ray tracing.
2. Use a model troposphere and either predicted or measured parameters. Wilmanns' approach is of this type (16).
3. Measure the effect of significant factors on ΔR_e directly during the time of measurement. (17, 18)
4. Use linear regression of surface parameters against observed ΔR_e. (15, 19, 20)

The first method given above is the classical method and is used in somewhat modified form in aerial survey. The details and problems therein are thoroughly covered in the Shoran (Hiran) Manual by Aslakson. (21) What is used is a modified standard atmosphere sometimes known as the Air Force model. The technique does not depend strongly on a model. In effect it measures the index of refraction along the path. The difficulties are entailed in transfer horizontally from the points where the profile was measured.

In general this method is potentially the best as almost no assumptions are required except the basic physical laws, Snellius's Law among others. These are pretty well established as are the factors

that define the index of refraction in terms of temperature and pressure. Indeed using refractometers only Snellius's law is required.

To a certain extent methods 2 and 4 rely on this technique. The problem is the complexity and cost of acquiring the data. In principle refraction must be measured along the path throughout the trosposphere when ranging is being performed. This is both impractical, if not impossible, and certainly costly at best.

The second method (No. 2) is fairly common. A number of techniques of the same general nature are used. One, a standard atmosphere which is essentially the mean of all measured radiosonde tropospheric profiles. This is sometimes refined for the lcoal area.

The same profiles have been fit with one and two exponential models. Basically, $N_{(H)} = N_s e^{\frac{-h - h_s}{H}}$, when N_s is the surface index and H is a characteristic height, usually 7 to 9 km. Tables of H as a function of N_s, the surface index of refraction in N units, and as a function of location on the earth may be obtained. h_s is the height above mean sea level. By using the model, some assumptions about small angles and homogeneity of the lateral layers of air, the influence of refraction on R_e is "almost integrable". Wilmann has used simplifie versions to reliably calculate ΔR_e. This technique has been used for reduction of SECOR data. (16)

At angles above 6^o the accuracy is quite good, of order one meter or less. One simply measures N_s and the appropriate H. Unfortunately this is a function of ΔN the change in N in the first kilometer. An alternative is to estimate N_s and H, or their equivalents, from the observed data.

The success of this method is still dependant upon the model and is only as good as the model. It can also be overly weighted by poor propagation conditions such as low angle effects.

The third method (No. 3) is an attempt to strike directly at the cause. It attempts to measure the actual refractivity of the atmosphere. It is true that the refractive effects are independant of carrier frequency in the radio frequency spectrum. However, in the K band the water vapor causes absorption.

By measuring the energy absorbed a direct measure of equivalent water vapor content can be obtained. This can be used to estimate the vapor pressure sensitive terms of η. The refractivity is most sensitive to this parameter. By using a dry model, generally quite stable, and a measurement for the wet term the total refractivity can be reliably estimated.

The difficulties are manifest. First, a K band source and receiver are required both very well calibrated as the sensitivity to a db is strong. The added satellite power and weight is probably not warranted.

Method 4 has been reserved for last. It is believed to be the most satisfactory for the geodetic survey problem, being a compromise betweèn accuracy and complexity. Furthermore, there is real hope that its performance can be improved by further analysis of existing data. This effort may well be worth the while if radio ranging is to be used for geodetic survey since it is applicable to any radio system, either ranging or doppler.

The basic material is reported in references 15, 19, 20 and 22.

For want of a better term, this has been called a statistical approach to range adjustment. A number of radiosonde profiles were obtained. From these, using standard ray tracing methods and assuming a uniformaly stratified troposphere, the adjustment in observed range ΔR_e was obtained. These values were then used in linear regression against surface index of refraction and ehight of station above mean sea level.

$$\Delta R_e = A(h_1 R) + B(h_1 R)N_s + C(h_1 R)h_s$$

where A, B, and C are functions of geometry only. R is apparent range and h is height of receiver above mean sea level. N_s is surface refractivity and h_s is station height. If one terminal is above the atmosphere then $R_e = A(\phi) + B(\phi) N_s + C(\phi) h_s$ when ϕ is the apparent launch angle at the ground station. In general A, B, C have the form $D(\phi) = \dfrac{2 d_1}{\sin\phi + (\sin^2\phi + d_2 \cos^2\phi)^{1/2}}$

These coefficients were fitted to this polynormal with the following results:

$D(\phi)$	d_1	d_2
A	1.4751	.004684
B	.002923	.002949
C	-.1559	.005295

Table 4.4.2-1
Correction Coefficients

Two sets of data were used to derive the D (ϕ). First, 13 standard meteorological stations throughout the U.S. were selected. 6 profiles were chosen from each to represent 6 different propagation conditions. A total of 77 such profiles were obtained. (One station failed to have one of one type).

In addition to the method described above, a third parameter was used, ΔN, the change in refractivity in one kilometer above the station. However, this was dropped as being too difficult to measure in the field.

The second set was 84 profiles chosen at random at the Cape Canaveral meteorological site. Two other factors were used here ΔN and ΔN_o. The last is the change in the first 40 meters above the surface.

The data from the former is used as being representative of the conditions of the simulation. The data from the latter gives rise to the hope that for certain stations in a geodetic survey set local profiles can be used.

Table 4.4.3-2 is a summary of the constants, the mean correction and the observed standard deviation of the final error. ΔR_e is the mean correction. A, B, and C as before. SE, is the standard error using only N_s. SE_2 is the standard error using both N_s and h_s.

The same approach works for any R and h, but only that above 70 km is retained for this problem.

There are two basic reasons for advocating the use of this method. The method is no more complicated than Wilmann's and is to some extent less dependant upon a model, i.e., its inherent accuracy should

therefore be greater. A polynomial fit to N_s might be tried. But of possibly more advantage is the same approach using a wet and dry term regression. The basic raw data is still available for this and may reduce the error further by perhaps a factor of 2 or 3.

Residual Error Profiles

(Table 4.4.3-2)

70 Profiles

h = 700 N_s (Units) h_s(km)

R(km)	$\Delta\overline{R}_e$(m)	A	B	C	SE_1	SE_2	$\sim\phi$(mr)
700	2.39	1.4751	.002923	-.1559	.075	.042	
1000	3.44	2.116	.004193	-.2237	.108	.062	770
1250	4.32	2.658	.00527	-.2809	.136	.076	
1500	5.21	3.208	.00636	-.3389	.164	.091	
1750	6.12	3.769	.00748	-.3981	.193	.107	
2000	7.06	4.342	.00862	-.4585	.222	.123	342
2500	9.00	5.534	.01101	-.5838	.282	.156	
3000	11.07	6.801	.01356	-.7168	.346	.192	
3500	13.31	8.165	.01632	-.8593	.414	.229	
4000	15.75	9.648	.01935	-1.01378	.488	.269	144
4500	18.45	11.280	.02272	-1.18274	.569	.313	
5000	21.46	13.090	.02652	-1.36916	.659	.362	
5500	24.86	15.119	.03087	-1.57647	.758	.416	
6000	28.76	17.407	.03591	-1.80834	.870	.478	70
6500	33.25	20.003	.04186	-2.06878	.997	.549	
7000	38.48	22.953	.04901	-2.36151	1.142	.634	
7500	44.65	26.305	.05778	-2.68928	1.308	.736	
8000	51.97	30.086	.06878	-3.05289	1.500	.860	17.4
9000	71.40	38.856	.10153	-3.86966	1.967	1.203	

4.4.4 Random Temporal Component

One aspect of the effect of the tropospheric index of refraction not contained in the above is the random temporal component. The relative power spectrum of the range variations and index of refraction have been measured at Maine, Hawaii, and Boulder, Colorado. (24) A typical range variation spectrum is proportioned to $f^{-2.4}$ with a power density of 10^{-6} $(cm)^2$/cycle per second at 1 Hz. Total daily variation is therefore: $(\Delta R)^2 = 10^{-6} \int_{10^{-5}}^{\infty} f^{-2.4}\, df = 4\ (cm)^2$ or a .02 meter standard deviation. The spectrum is known to be proportional to range. These measurements were made over a nearly horizontal path of 15 km.

Two factors alter this conclusion for geodetic survey. For propagation above several degrees the path through the important layers of the atmosphere is from 70 to 90 kilometers. Hence, at worst the standard deviation will be no more than .06 meters. Also this path generally passes through a more stable atmosphere so one would expect that this could be reduced.

A comparison with the residuals given in Table 4.4.4-1 illustrates that this effect is 10 to 20 percent of the "model" errors. One might hope to be able someday to reduce the residuals to the random error.

4.4.5 Errors Associated with the Horizontal Gradient of Refraction Index.

The preceding investigations assumed that over the distances between the ground station and the vehicle the index of refraction at the surface was constant. This is, of course, not true. The horizontal variations of index of refraction will then add to the uncertainties in the determination of the mean index of refraction over the propagation path.

Unfortunately, there is very little information in the literature to indicate the statistics of the variations with horizontal displacement. In an effort to get some feel for this source of error a set of data taken during flight test of the Drone Navigation, Guidance and Control System in 1963-64 was analyzed. The data taken were values of the surface value of refractivity, N_s, at two stations separated horizontally by 160 km and vertically by 0.62 km. These stations were the ground transponder sites for HIRAN electronic surveying equipment located on mountain tops along the Mogollon Rim in Central Arizona. A set of 24 pairs of N_s values were taken which represented the average N_s over a 2-3 hour period at each of the two stations. The data were taken during the months of October 1963 through January 1964.

The data from the lower of the two stations were used to predict the refractivity at the higher station. The result of this prediction is typified by a mean error of -2.8 N units and a standard deviation of 6.8 N units. This, in effect, says that the prediction of the index of refraction from a point 160 km (100 statute miles) horizontally displaced and .62 km (2021 ft.) vertically displaced was accomplished with an error of about 3 parts per million mean and 7 ppm standard deviation. If this procedure had been used to correct range data the errors would have corresponded to 0.45 m mean and 1.1 m standard deviation. The correlation coefficient between the refractivity at the two locations was 0.71. The use of the model atmosphere to predict refractivity at a point 100 miles away accounts only for the mean and that part of the variability which is correlated. In this case since the standard deviations were 7.2 at the low elevation and 9.6 N units at the remote high elevation. The standard deviation of the difference of the index of refraction at the

two locations is 6.8 N units. The equality between the standard deviation of the error of correction and the standard deviation of the difference of index of refraction at the two locations indicates that only the mean can be corrected accurately at a remote location, the variability is correlated only to the degree the two points are correlat with each other.

To define the effect of the horizontal gradient on the mean index of refraction consider the following simplified model of the atmosphere.

$$N(h) = N_s(0) + \triangle Nh + N_s(x).$$

where N(h) is the refractive index at altitude h above the surface at any distance x from a reference point (a ground station for example).

$N_s(x)$ is the variation of the actual index from a value predicted by using the surface value at x = 0.

i.e. $N_s(x) = N(h,x) - N(h,0)$

The quantity $N_s(x)$ is assumed to be a random variable. For the simplifi case let the path of propagation be defined by a straight line whose equation is: h = mx.

The mean index of refraction is then

$$\overline{N} = \frac{1}{M} \int_0^M \left[N_s(0) + \triangle N(mx) \right] dx + \frac{1}{M} \int_0^M N_s(x)dx$$

or

$$\overline{N} = N_s(0) + \triangle N \frac{mM}{2} + \frac{1}{M} \int_0^M N_s(x)dx.$$

Taking the expected value of both sides gives:

$$E\left[\overline{N}\right] = N_s(0) + \triangle N \frac{mM}{2} + E\left[N_s\right]$$

assuming $N_s(x)$ is a stationary random process.

The variance of $\bar{N}$ may also be computed as

$$\sigma^2_{\bar{N}} = E\left[\bar{N} - E(\bar{N})\right]^2 .$$

Then

$$\sigma^2_{\bar{N}} = \frac{1}{M^2}\int_0^M dx_1 \int_0^M dx_2\, E\left\{N_s(x_1)N_s(x_L)\right\}$$

assuming that $E\left[N_s\right] = 0$.

Since,

$$N_s(x) = N(\mu + x) - N(\mu)$$

Where $N(\mu)$ is the index of refraction at a point, μ,

$$\sigma^2_{\bar{n}} = \frac{1}{M^2}\int_0^M dx_1 \int_0^M dx_2\, E\left[\left[N(\mu + x_1) - N(\mu)\right] \cdot \left[N(\mu + x_2) - N(\mu)\right]\right]$$

Expanding the product under the integral gives,

$$\sigma^2_{\bar{n}} = \frac{1}{M^2}\int_0^M dx_1 \int_0^M dx_2\, E\Big\{N(\mu + x_1)N(\mu + x_2) - N(\mu)N(\mu + x_2) - N(\mu)N(\mu + x_1) + N^2(\mu)\Big\} .$$

Taking the indicated expected values given,

$$\sigma^2_{\bar{n}} = \frac{1}{M^2}\int_0^M dx_1 \int_0^M dx_2 \left[\phi_N(x_1 - x_2) - \phi_N(x_2) - \phi_N(x_1) + \phi_N(0)\right]$$

where $\phi_N(\mu)$ is the autocorrelation function of the index of refraction, $N(\mu)$.

The expression for $\sigma^2_{\bar{n}}$ may be simplified to

$$\sigma^2_{\bar{n}} = \frac{2}{M^2}\int_0^M (M - \mu)\phi_N(\mu)d\mu - \frac{2}{M}\int_0^M \phi_N(\mu)d\mu + \phi_N(0)$$

The autocorrelation function, $\phi_N(\mu)$, is not known precisely. It may be assumed that the function is a simple exponential of the form,

$$\phi_N(\mu) = \sigma^2 \quad e^{-\frac{\mu}{D}}$$

Where σ^2 is the variance of the index of refraction (at the surface)

D is the correlation distance

For the investigation reported earlier, σ is about 6 N units and D about 470 km.

Substituting the value for $\phi_N(\mu)$ into the expression for $\sigma^2_{\bar{n}}$ and carrying out the indicated integration gives

$$\sigma^2_{\bar{n}} = 2\sigma^2 \left\{ \frac{1}{2} + \frac{D}{M} e^{-\frac{M}{D}} + \frac{D^2}{M^2} \left(e^{-\frac{M}{D}} - 1 \right) \right\} .$$

For $M \ll D$

$$\sigma^2_{\bar{n}} \doteq \sigma^2 \frac{M}{D}$$

or

$$\sigma_{\bar{n}} = \frac{M}{D}$$

The standard deviation of the mean index of refraction is then of the order of 3 N units at 100 km or 0.3 meters because of the horizontal variability of the index of refraction.

This computation of the effects of horizontal variations in the index of refraction is necessarily a rather rough estimate of what may actually occur. The lack of data on this particular subject has precluded any better estimate.

4.5 IONOSPHERIC PROPAGATION EFFECTS

The ionosphere, like the troposphere, causes the received signal to have a delay other than that of free space. This factor must be accounted for to minimize the potential range error. Likewise, the imperfect corrections achievable lead to residual error.

Unlike the troposphere, the ionospheric effects are significantly dependant upon the carrier frequency. The theoretical effects have been thoroughly studied. An excellent review of the theory is contained in Lawrence, et al. (25) An excellent analysis of the effects upon ranging is contained in reference 26 and also in the AD HOC Committee on Propagation final report. (17)

The theory, although complex, is quite well understood. However, far less is known about the detail characteristics of the parameters that cause the ranging variations. As a result, it has been variously estimated that the residual error will be of order 20 to 30 percent of the mean correction to be applied. This can be compared with the ability to correct tropospheric effects to the order of one percent which is the result of far better knowledge of the statistics of the tropospheric parameters. This is not to fault the researchers in the study of the ionosphere. It is a far more difficult and costly problem with more parameters to consider.

The ionospheric dominant factor in a ranging system is the variation in phase velocity (and group velocity) from that of free space. The ionosphere causes several other phenomena such as ray bending, wedge refraction, frequency change, differential phase, Faraday rotations and absorption. As can be shown none of these have

an effect upon ranging. With the exception of ray bending, see Table 6-3, Page 6-55 of Reference 26.

4.5.1 Ionospheric Index of Refraction

At frequencies above the critical frequency, the real part of the index of refraction is given by the Appleton-Hartree formula:

$$\eta^2 = 1 - \frac{X}{1-1/2\left[\frac{YT^2}{1-X}\right] \pm \left[1/4\,\frac{YT^4}{1-X^2} + Y_L^2\right]}$$

$X = W_N^2/W^2$

$Y_T = W_T/W$

$Y_L = W_L/W$

W = Carrier frequency (r/s)

$W_N = \sqrt{\frac{N_e\, e^2}{\varepsilon_o M}}$ the plasma frequency

$W_T = W_H \sin\theta$

$W_L = W_H \cos\theta$

N_e = density of free electrons

e = charge of an electron

ε_o = electric permittivity of free space

M = electron mass

$W_H = \mu_o$ He/M gyro frequency of an electron

θ = angle between wave normal and geomagnetic field

μ_o = magnetic permittivity of free space'

H = geomagnetic field intensity

The plus and minus signs in η apply to the ordinary and extraordinary waves respectively.

If one substitutes magnitudes into this expression, it is readily shown that at 2 GHz:

$$\eta \doteq \sqrt{1-X} \doteq 1 - \frac{1}{2} \frac{e^2 N_e}{\varepsilon_o M W^2} \doteq 1 - \frac{40.3 N_e}{f^2}$$

$e = 1.6 \times 10^{-19}$ coulomb

$M = 9.08 \times 10^{-31}$ kilograms

$\varepsilon_o = 8.854 \times 10^{-12}$ farad/meter

A typical daytime value for η at 2 GHz is -25 N units at the peak density of the ionosphere. This is far less than that for the typical troposphere.

The index of refraction is therefore dominated by the electron density and the square of the carrier frequency. It should be noted that the index of refraction is less than one. Hence, the phase velocity is greater than the free space velocity of light. The group velocity is less than the velocity of light, of course. $v_g v_p \doteq c^2$ at microwave frequencies.

The index of refraction at any point in the ionosphere is a function of the electron density. Characteristic profiles of N_e are given in Figure 4.5.1-1. Therefore, η is a definite function of altitude. Indeed N_e is a function of altitude, latitude, solar year, solar sun spot cycle, and time of day. Hence, so is η. It is also a function of ionospheric storm activity. It is the variation in these parameters that cause the residual error in ionospheric effects after correction. To adjust the observed range in principle the total profile along the

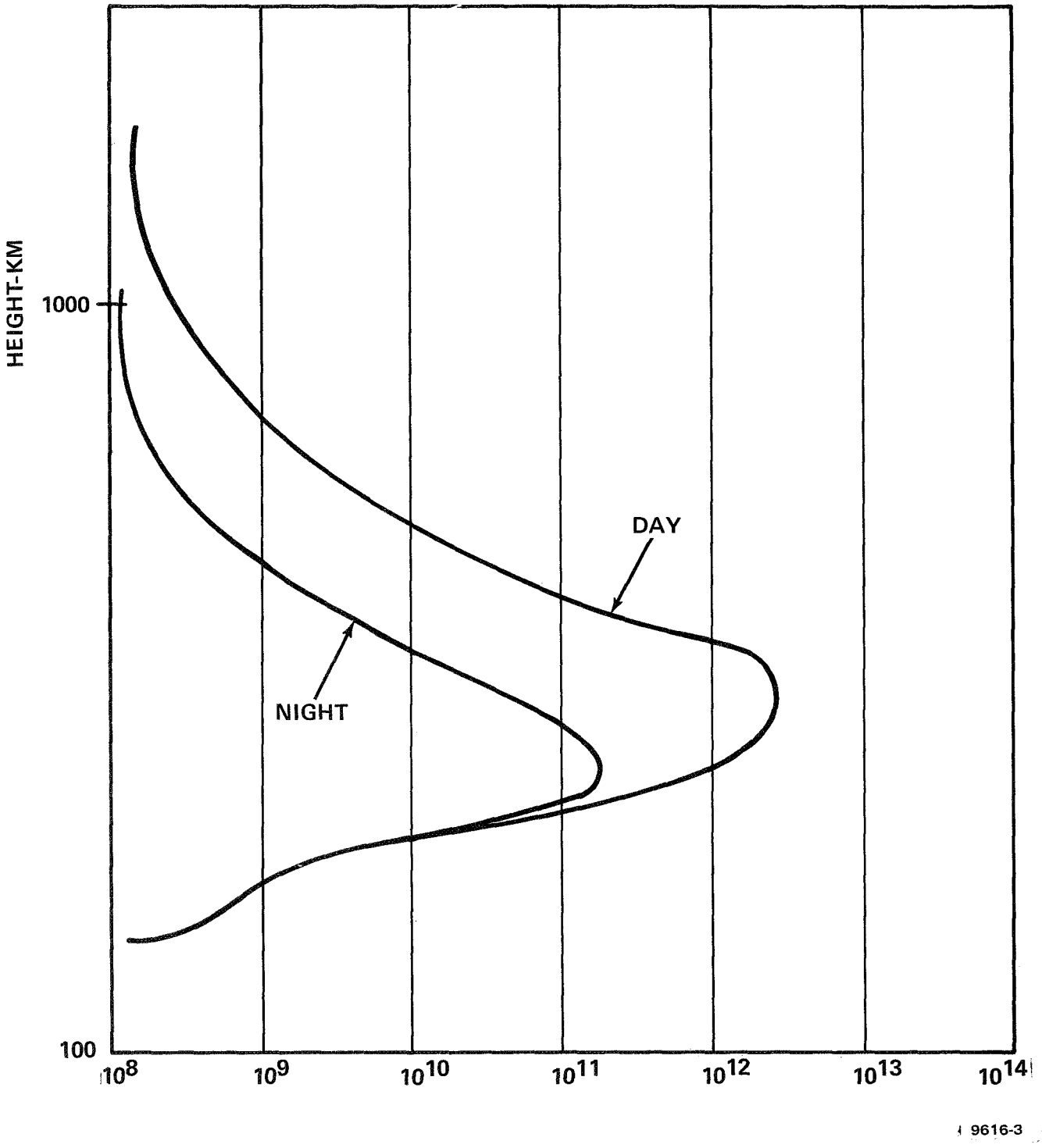

Figure 4.5.1-1. Characteristic Profiles

propagation path must be known. The information that must be known can only be estimated.

A number of models have been postulated for the electron density of the ionosphere. Perhaps the most widely used is the Chapman model which uses a parabolic fit of the data. This has been found to underestimate the top side electron density rather seriously. The upper side appears to be fitted better by a hyperbolic secant function.

4.5.2 Effect on Range Measurement

A number of approaches to estimating the effect on a range measurement have been made. (17, 25, 27) In general these were designed to estimate the magnitude of affect and were not designed for actual computational measurement adjustment.

The influence on a range measurement depends upon the method of measurement. If cycle counting of the carrier is used, then the phase velocity is the correct adjustment. If the measurement is made on modulation then the group velocity should be used. As is shown in reference 25, the adjustments for each method are equal in magnitude but of opposite sign. It is conceivable that by measuring using both methods the effect could be cancelled out. The problem is the initial constant in the cycle counting method which is really the integral of doppler.

The apparent path length through the ionosphere is:

$$(1) \qquad L = \int \eta \, ds$$

where the integral is taken along the ray path. The increment in the path ΔL, is:

$$(2) \qquad \Delta L = \int (\eta - 1) \, ds = \frac{b}{W^2} \int N_e \, ds$$

Most approaches then take the integral along the straight line path thereby ignoring the ray bending at S-Band and above. The validity of this is illustrated by the results of Wilmann's work described in reference 16. The results of this approach have been compared to actual ray tracing using Snell's Law. Even at launch angles as low as 1^{o} the error is only .5 to 1%.

Through a thin shell of the ionosphere:

$$(3) \quad \Delta L_i = \frac{10^{-6}}{W^2} \int_{h_i}^{h_{i+1}} N_e(h) \, \mathrm{cse}\, \phi \, dh$$

where h is measured perpendicular to the shell. ϕ is the angle between the ray and the tangent to the shell.

Assuming a straight line through the shell this can be written as:

$$(5) \quad L = \frac{b}{W^2} \int_{h_b}^{h} \frac{N_e(h) \, dh}{\left[1 - \left(\frac{a}{a+h}\right)^2 \cos^2\theta\right]} \quad 1/2$$

An obliquity factor (26) is defined:

$$(6) \quad Q = \frac{b}{W^2 N_T} \int_{h_b}^{h} \frac{N_e(h) \, dh}{\left[1 - \left(\frac{a}{a+h}\right)^2 \cos^2\theta\right]} \quad 1/2$$

and

$$(7) \quad \Delta L = \frac{b \, N_T \, Q}{W^2}$$

where N_T is the total electron content in a vertical column whose cross section is one square meter.

Reference 26 then estimates the variability of ΔL due to variations in N_T and Q. The gross estimate agreed to by others (17) is that the estimates of $N_T Q$ are no better than 30% of the applied correction.

At low elevation angles ΔL is of order 10 meters in the daytime at 2 AGHz (17). Hence, the rms range error would be 3 meters.

4.5.3 Methods of Range Adjustment

There are five basic methods of adjusting range. One, use a carrier sufficiently high to such that L is negligible. For example, a nominal worst case at X-Band would be only .4 meters. Two, measure the ionospheric profile along the ray path and ray trace. Operationally this is not feasible except for rare scientific ventures. Three, hypothesize a model, such as the Chapman model and estimate the significant parameters such as the height of maximum intensity, the width of the ionosphere, and so forth. Much of this must come from indirect estimates using spot number predictions, etc. It is the inability to adequately estimate these factors that results in the 30% estimate error. Four, devise a system to estimate L directly. This is done in TRANSIT and SECOR. Five, devise an adequate estimate as in three and estimate the proper parameters from redundant data measurements. This is the technique proposed by Wilmann (16).

In method four, it is apparent that ΔL is a function of frequency. The ionosphere is the only frequency dependant cause of change in the range. By measuring the range on two, or more, frequencies, it is theoretically possible to estimate ΔL directly from the observed difference. This assumes that the path is the same for both.

The correction to be applied to the higher frequency is $\frac{Rh - Re}{k^2 - 1} = \Delta L_h$ where the subscript refers to measurements at the high and low carrier frequencies (16). R is the raw range measurement. k is the ratio of the high frequency to the low frequency.

Two problems arise. First, the carrier frequencies should be chosen such that the ΔL on each dominates all error sources on both channels. This means VHF or low VHF carriers and ΔL is therefore large. Two, ray bending is not an important contributor to ΔL, but does influence the actual path taken. Since ray bending is also frequency dependant the paths might well differ enough that there is significant loss in correlation between paths and a significant error may be introduced.

Experience on the two frequency SECOR indicates that a comparison of this method and method five indicates that it does not appear to be an improvement.

Method five, or Wilmann's recommended approach for GEOS-A satellite data is outlined below and is detailed in reference 16. He starts with the Chapman model which is:

$$(8)\quad N_e(h) = N_m\, e^{1/2\,(1-x-e^{-x})}$$

$$(9)\quad X = \frac{h - h_m}{H}$$

where N_m is the maximum electron density, h_m is the height of the maximum, H a scale height. When substituted into equation 5 a closed form of integration is not possible. He replaced this by the simple polynomial $1 - \frac{x^2}{c^2}$. When this is done the integration leads to:

$$(10)\quad \Delta L = \frac{2\beta}{\sin\theta_i + \left[\sin^2\theta_i + \alpha\cos^2\theta_i\right]}^{1/2}$$

$$(11)\quad \cos\theta_i = \frac{a}{a + h_m - 3H}\cos\theta$$

$$(12)\quad \beta = 2H\,\frac{80.5\,N_m}{f^2}$$

$$(13)\quad \alpha = \frac{25H}{3\,(a + h_m - 3H)}$$

The factor β is the retardation at the zenith. α represents the ratio of zenithal to horizontal refraction.

In data reduction estimates of N_m, h_m and H are assumed for initial processing. Subsequent processing adjusts or estimates α and β as unknown just as the station locations.

This method has been demonstrated to work well in SECOR data reduction. The residuals in the SECOR data reduction varied. They were 1.4 meters rms for a nighttime pass and 2.7 and 4.0 meters rms for typical daytime passes. It was recommended therefore, that only nighttime passes be used for geodetic survey.

There is a twofold reason for this. First, the total effect of the ionosphere is typically 10 times greater than at night. One expects the error to be proportional to the magnitude of the effect. Second, during the daytime the ionosphere is actually the sum of several layers although dominated by the F_2 layer. At night, a single F layer predominates. One would expect the model to better fit the nighttime ionosphere.

Recalling that the effect is inversely proportional to the square of the frequency, the effect on AROD should be approximately one twenty-fifth that on SECOR. Hence, this restriction may be unnecessary.

The range residuals were found to be correlated. It was suggested that these effects were ionospherically induced. If so this leads to the conclusion that the ionosphere is generally the dominant factor in the error.

4.6 THE EFFECT OF MULTIPATH ON RANGE ACCURACY

A very important factor than can contribute to error in range measurement is multipath. Generally when present other than as scatter, the effect is intolerable for the accuracies desired for geodetic survey.

Subsequent subsections evaluate the effect of specific levels of multipath, the potential causes, and means of combating the problem.

Multipath is difficult if not impossible to predict. Certain measures can be taken to minimize the likelihood of multipath. The AROD system rejects multipath to the maximum possible extent given the allowable radiated bandwidths. The ability to reject multipath given a system of maximum performance against white gaussian noise is directly related to maximum use of signal bandwidth. However, beyond this the system is susceptible to the problem.

4.6.1 Effect Upon Range Measurement

The basic AROD detection system is illustrated functionally in Figure 4.6.1-1. $\tilde{\tau}$ represents the delay of a secondary path. A represents its relative strength compared to the desired "line-of-sight" signal. In general in the geodetic survey problem all multipath signals will be delayed with respect to the desired signal.

A mathematical analysis was made considering only a single secondary path.

Let the signal at point (1) in Figure 4.6.1 be:

(1) $p(t) \sin w_o t$

$p(t)$ is a pseudonoise signal with bit period T.

$$w_o = \frac{2\pi N}{T}$$

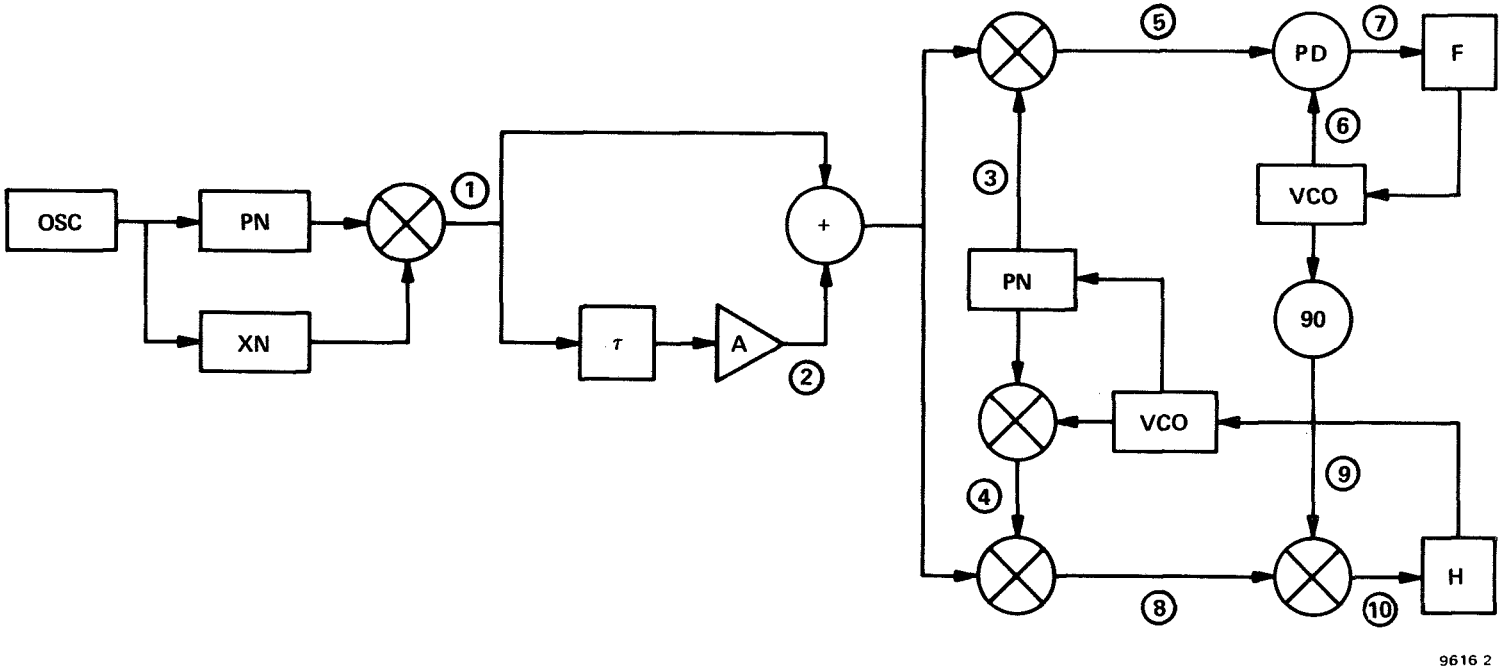

Figure 4.6.1-1. Multipath Model

(2) $A\ p(t-\tau)\ \sin w_o\ (t-\tau)$

where it is assumed that non line-of-sight paths are always delayed with respect to the direct or desired path. A is the relative magnitude, normally less than one, and τ is the delay in seconds.

(3) $p(t-\tau_o)$ the carrier reference pseudonoise. τ_o is the reference delay from the range tracker.

(4) $p(t-\tau_o)\ \mathrm{Sin}\ 2\pi\ \frac{(t-\tau_o)}{T}$ the ranging reference pseudonoise which is PN with a Manchester code.

Sin (x) is a square wave whose fundamental is 1/T Hz.

(5) $p(t)\ p(t-\tau_o)\ \sin w_o t + A\ p(t-\tau)\ p(t-\tau_o)\ \sin w_o(t-\tau)$

(6) $2\cos(w_o t-\theta)$ the carrier loop reference whose quiescent phase is θ as a result of tracking the received signal.

(7) $p(t)\ p(t-\tau_o)\ \sin\theta + A\ p(t-\tau)\ p(t-\tau_o)\ \sin(\theta - w_o\tau) = e_7$

The action of the loop is to average over this signal and drive e_7 to zero. Hence, this is:

$$\phi_p(-\tau_o)\ \sin\theta + A\,\phi_p\ (\tau-\tau_o)\ \sin\ (\theta - w_o\tau) = \overline{e_7}$$

θ will assume the value such that $\overline{e_7}$ is zero. ϕ_p is the autocorrelation function of p(t).

$$\phi_p\ (x) = 1 - \frac{|x|}{T}\ ,\quad T > |x|$$

$$= o,\ \text{elsewhere}$$

If A = 0, no multipath, $\theta = 0$ as is expected.

The condition of interest is that $A<1$ if $\tau_o < T$. For $\tau_o > T$ and proper acquisition then $\phi_p\ (\tau-\tau_o)$ can be made zero. The only influence of the multipath is to add trivially to the noise.

The delayed signal-to-desired signal power ratio, $\tau_o > T$, is reduced by about 40 db in the carrier tracking loop. For any reasonable A this effect is negligible.

For $\tau_o < T$ and $A > 1$ the delayed path will capture the signal in the carrier loop and probably in the range loop. If this happens, all bets are off and the measurements should not be made. This condition should be identified.

For the case where $A < 1$ and $\tau < T$, $w_o T = 2\pi N$ radians, N is of order 300. Hence, $w_o \tau$ can assume any value from 0 to 2π with equal probability.

In the modulation or range tracking loop

$$(8)\quad p(t)\, p(t - \tau_o)\, \text{Sin}\, 2\pi \frac{(t - \tau_o)}{T} \sin w_o t + A\, p(t - \tau)\, p(t - \tau_o)\, \text{Sin}\, 2\pi \frac{(t - \tau_o)}{T} \sin w_o (t - \tau_o)$$

$$(9)\quad 2 \sin (w_o t - \theta)$$

$$(10)\quad p(t)\, p(t - \tau_o)\, \text{Sin}\, 2\pi \frac{(t - \tau_o)}{T} \cos \theta + A\, p(t - \tau)\, p(t - \tau_o)\, \text{Sin}\, 2\pi \frac{(t - \tau_o)}{T} \cos(\theta - w_o \tau)$$

The range loop averages as in the carrier loop. However, the average is the cross-correlation function of the PN and the PN reference. The cross correlation has the characteristic shown on the next page.

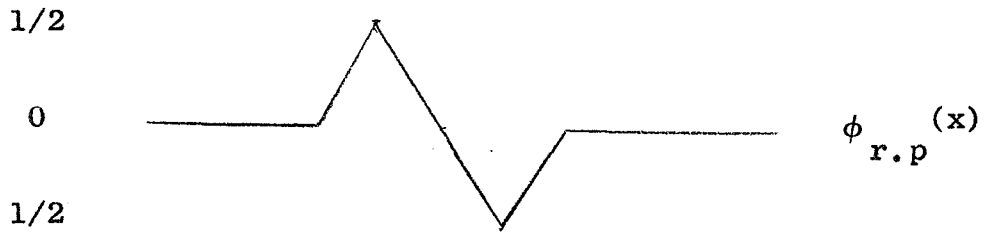

so that the signal when averaged can be represented by

$$\phi_{rp}(-\tau_o)\cos\theta + A\,\phi_{rp}(\tau-\tau_o)\cos(\theta - w_o\tau) = e_{10}$$

The loops, carrier and ranging, will operate to simultaneously drive e_7 and e_{10} to zero by adopting appropriate τ_o and θ. In the range loop if A is zero, τ_o goes to zero as is desired. The nulls will be when $\theta \sim 0$ and $\tau_o \sim 0$ not at π and T as these latter two constitute out of lock cases, which can be identified by the agc system.

There are two non-linear equations to be solved. These are:

$$\phi_p(-\tau_o)\sin\theta + A\,\phi_p(\tau-\tau_o)\sin(\theta - w_o\tau) = 0$$

and

$$\phi_{rp}(-\tau_o)\cos\theta + A\,\phi_{rp}(\tau-\tau_o)\cos(\theta - w_o\tau) = 0$$

$$\phi_p(x) = 1 - \frac{|x|}{T}, \quad |x| < T$$

$$= 0, \text{ elsewhere}$$

$$\phi_{rp}(x) = 0, \quad |x| > T$$

$$= -\frac{x}{T}, \quad -\frac{T}{2} < x < T/2$$

$$= 1 + \frac{x}{T}, \quad -T < x < -T/2$$

$$= 1 - \frac{x}{T}, \quad \frac{T}{2} < x < T$$

τ = path delay with respect to the desired signal

A = relative amplitude of secondary path

τ_e = modulation tracking error

θ = carrier tracking error

These equations were solved for various conditions and the worst case obtained. With A and τ normalized (A ranges from .1 to .9 and $\frac{\tau}{T}$ ranges also from .1 to .9) for various angles $\theta_o = w_o \tau$, the following table illustrates the result.

Table 4.6.1-1

Worst Case Multipath Effects

A	τ	θ_o	τ_o	θ	E_f Range Error (Meters)
.1	.5	180	-.05	0	-1.2
.2	.4	180	-.1	0	-2.3
.3	.4	180	-.14	0	-3.3
.4	.7	180	-.20	0	-4.7
.5	.3	180	-.23	0	-5.4
.6	.2	180	-.30	0	-7.0
.7	.2	180	-.33	0	-7.8
.8	.1	180	-.40	0	-9.4
.9	.1	180	-.43	0	-10.0

The magnitude of error (τ_o) varies to about 10% of this maximum over the full range of conditions for each value of A. Each tenth

of τ_o is equal to 2.34 meters.

For the values given, there is another of equal magnitude, but of opposite sign.

In general this indicates the undesirability of multipath. It is not readily detectable and should be avoided.

4.6.2 Causes of Multipath

There are two prime causes of multipath, reflections from the ground in the general vicinity of the ground antennas and from an inhomogenous propagation path, often called ducting. The latter is generally of little consequence in the type of problem considered here for two reasons. One, the reflected path is seriously attenuated as evidenced by tropospheric propagation attenuations and two, because it generally occurs only at grazing angle type of paths which are to be avoided in this problem because of other reasons. (11, 12)

Reflections from the surface in the vicinity of the ground antennas is a potentially serious problem. The geometry problem is illustrated in Figure 4.6.2-1. A flat earth may be considered as we are only interested in reflections near the antenna.

The delay, τ, is a function of geometry. The relative amplitude, A, is a function of the reflection coefficient at the point of reflection.

The delay is $(r_2 + x - r_1)/c$.

$$(r_2 + x)^2 = r_1^2 + (2h)^2 - 2\,(2h)\, r_1 \cos\left(\frac{\pi}{2} + \theta\right)$$

$$r_2 + x - r_1 = r_1 \left\{ \left[1 + \left(\frac{2h}{r_1}\right)^2 + \frac{4h}{r_1} \sin\theta \right]^{1/2} - 1 \right\}$$

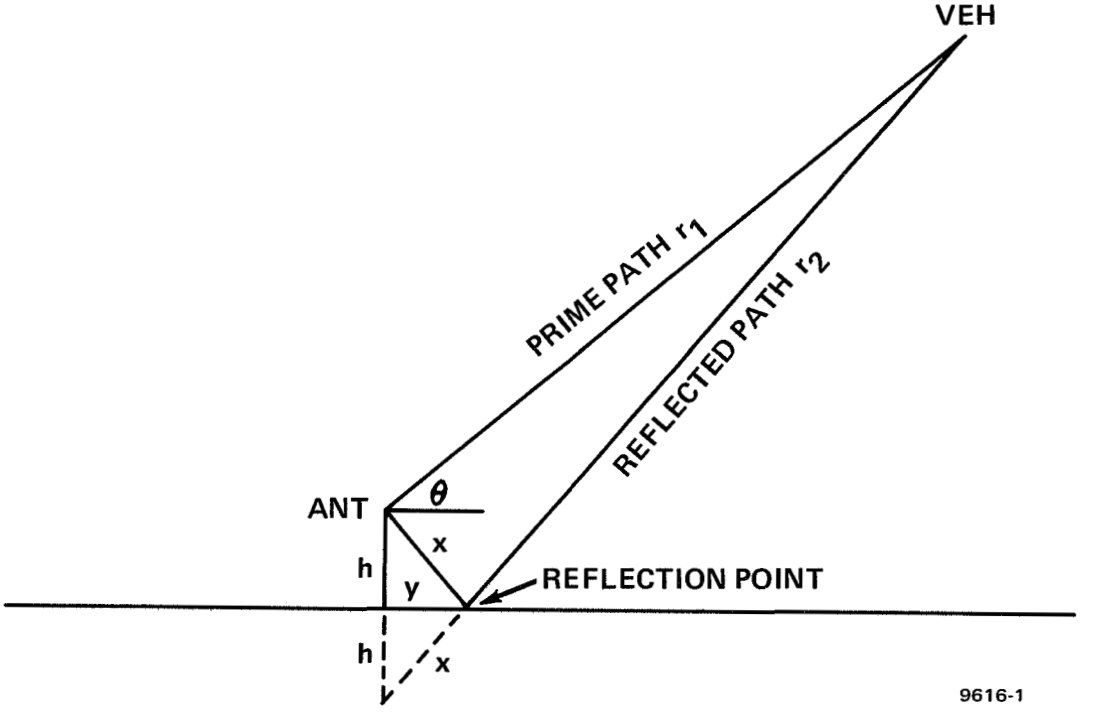

Figure 4.6.2-1
Multipath Reflection Model

But $r_1 \gg 2h$ and therefore $\tau \doteq \frac{2h}{c} \sin\theta$. Most of the interest lies in values of θ = greater than 5 or 6 degrees. To prohibit multipath $\tau >$ 157 n.s. or one bit period of the H code. Therefore, $h >$ 90 meters a rather impractical number,

$$y \doteq h \cos\theta, \quad r_1 \sin\theta \gg h$$

so that under the assumption $y < 10\ h$.

The theory of reciprocity holds so that any effect upon the vehicle may also occur at the transponder. Two factors effect this. The observed effect is a function of τ and in combination $w_o\tau$, the carrier phase.

$$w_o\tau = \frac{4\pi h}{\lambda} \sin\theta$$

Since the downlink S-Band carrier differs by 400 MHz from the uplink there is a phase difference which means sometimes a serious effect is caused at one end and not the other, vice versa, and sometimes both.

Another effect is the reflection coefficient. Linear polarization is used on the vehicle and circular on the ground.

The specular reflection coefficient is (8)

$$R_H = \frac{\sin\theta - \sqrt{\varepsilon_c - \cos^2\theta}}{\sin\theta + \sqrt{\varepsilon_c - \cos^2\theta}}, \text{ horizontal}$$

$$R_V = \frac{\varepsilon_c \sin\theta - \sqrt{\varepsilon_c - \cos^2\theta}}{\varepsilon_c \sin\theta + \sqrt{\varepsilon_c - \cos^2\theta}}, \text{ vertical}$$

where $\varepsilon_c = \varepsilon_r - j\varepsilon_i$ the complex dielectric constant and $\varepsilon_i \doteq 60\sigma\lambda$ at these frequencies. σ varies from about .002 to 5 mhos/meter and λ = 13.6 cm downlink and 16.6 cm on the uplink. The frequency

dependance is small.

The reflection coefficients at angles above 6 degrees and outside of the pseudo-Brewsters angle approach about 0.7. This is further reduced by the dilution factor caused by the curvature of the earth. This is unimportant at angles of 6^{o} or more.

The model used to derive this reflection coefficient assumes a smooth surface. It is not, of course. The effect of surface roughness is to transform a portion of the reflected energy into scatter. (13) The portion of specular energy is proportional to $e^{-\phi^2}$ where $\phi = \frac{4\pi\sigma}{\lambda} \sin\theta$ where σ is the rms roughness in the vertical in the same dimensions as the wavelength. (9)

The rest of the energy is transformed into scatter. The portion scattered in the forward direction is generally very small and of no consequence to the multipath problem.

Other sources are incidental, aircraft in the field of view, etc. Remote reflections are of no importance since the delay will be large compared to 157 n.s.

4.6.3 Corrections for Multipath

If multipath is present to an extent that significant error can arise, it is uncorrectable. All that can be done is to attempt to avoid it. Proper antenna sighting will help. In addition relatively cheap radiation absorbing materials can be used to reduce the possibility of multipath. Avoiding low angle propagation also helps. Finally, since surface roughness causes the reflected energy to be scattered, thereby essentially removing the problem, high carrier frequencies can help.

The roughness is also a function of the launch angle. For a given terrain overhead propagation is maximally rough. Unfortunately, this is also the region where absorbing materials can best be used.

There is one other thing that can be done. In some cases the presence of multipath can be identified. Although this will not permit calculating the effect, at least one can throw the suspect data out.

The presence of multipath can be identified by observing the agc voltage. The signal strength should monotonically increase from just above the horizon to the zenith and then decrease monotonically again. The expected signal level variation can be calculated and subtracted from the observed. Periodic or oscillating components in the residual is a good indication of multipath.

Strong multipath is usually quite obvious. Variations down to about 1 db can be observed. This corresponds to a second path which is about 10% in magnitude of that of the desired path. At the 10% level the maximum error is of order 1 meter which is getting into a tolerable region.

The present AROD system does monitor the agc voltages as test points but not as telemetry data. Also a better agc system would be required for multipath identification. Newer high quality agc circuits have been developed since AROD was constructed. So that in flight equipment, this could be incorporated fairly simply.

Any multipath that is present would be independant from one range to another. It will have a generally cyclic behavior with a period of about 1 second or longer.

Table 4.6.1-1 illustrates the undesirability of multipath. To a large part, through proper antenna sighting and liberal use of absorbing material multipath can be avoided.

As a result no contribution to the range error model is included for multipath. In actual practice the raw data should be searched to identify the presence of multipath.

4.7 RANGE ERROR MODEL

A necessary input to the geometry and data processing study is a model of range measurement error. A total of some 35 different potential sources of error were investigated. The great majority of these have been shown to contribute negligible error or the effects can be removed exactly by proper data reduction.

A range error model for radio ranging systems was developed in previous studies.[16] A generalized model was initially used:

$$\Delta R = \alpha_o + \alpha_1 R + \alpha_2 \dot{R} + \alpha_3 f(t - t_o) + \alpha_4 f_2(E) + \alpha_5 f_3(E) + \Delta\Delta R$$

ΔR = Systematic error in the observed range, R.

$\dot{R}$ = Range rate

$t-t_o$ = Time relative to start of a pass

E = Elevation angle

$\Delta\Delta R$ = Residual (unmodeled) systematic error

and where

α_o = Zero set or calibration error

α_1 = Range scaling error

α_2 = Inter-station timing bias

α_3 = First order phase drift

α_4 = Error in tropospheric refraction coefficient

α_5 = Error in ionospheric refraction coefficient

All forms of error were believed to fit one or another of these terms. A review of the error sources eliminated most of these terms. An elementary error model was used in the final simulations. The

error model was:

$$a_{1ij} + a_{2ij} R_{i_d}(t) + V_{ij}(t)$$

where a_{1ij} is the systematic unknown bias on the $i^{\underline{th}}$ tracker and the $j^{\underline{th}}$ pass. a_{2ij} is the scaling error due largely to uncertainty of the velocity of light and $V_{ij}(t)$ is a random error of zero mean.

A systematic uncertainty of 1 meter rms and a scale error of one part in 10^6 was used. A random error of 0.5 meters rms was assumed. All of these were considered conservative from the results obtained on AROD. No ranges were used unless the elevation exceeded 20^o. A 1000 km altitude satellite orbit was used.

Up to four ranges were used simultaneously but only the closest stations were interrogated.

5.0 AROD GEODETIC POSITION ACCURACY

The processing of tracking data for the purpose of estimating geodetic parameters such as tracking station coordinates, involves the use of several program algorithms. The usual practice is to first edit the raw observations in order to remove "bad" points and to apply any known corrections to the data. The edited set of measurements are then utilized as the data base for the estimation algorithm. Such an algorithm makes use of an overdetermined set of observations which are functionally related to the parameters to be estimated and calculates values for these parameters, which are "best" in some sense, usually that of least squares or minimum variance.

In a simulation exercise so-called tracking data must somehow be generated. A program designed for this purpose utilizes knowledge of nominal spacecraft orbits and location of hypothetical tracking stations to calculate a set of "true" spacecraft observations. The addition of random and systematic errors to the latter set of calculated observations produces a data set very much like that which is likely to arise in a real life tracking situation. The estimation program, without having exact knowledge of tracking station locations, spacecraft orbits, or the systematic errors, utilizes the corrupted data set to compute the best estimates of all parameters of interest together with their error statistics.

The results obtained from such a simulation may be evaluated by comparing the calculated parameter values with the a priori values used in the process of generating the observations. To the extent that disagreements exist, they should be within the range of expected parameter error statistics provided that the error model postulated in the estimation algorithm matches the one used in the generation of the data. Such a design provides a convenient way for analyzing the effect of modeling errors on the recovered parameters. This is particularly helpful when analyzing the propagation of errors in the postulated gravity field acting on the spacecraft.

The mathematical model associated with the algorithm used in generating AROD slant range data is given below.

Let

$$\bar{X}(t) = \left[X_1(t),\ X_2(t),\ X_3(t),\ \dot{X}_1(t),\ \dot{X}_2(t),\ \dot{X}_3(t)\right]^T$$

represent spacecraft position and velocity coordinates at time t in an inertial Cartesian coordinate system whose origin is at the center of the earth. The X_1X_2 axes lie in the earth's equatorial plane, the X_1 axis is directed towards the equinox of date, the X_3 axis is positive through the north pole and the X_2 axis is in a direction to complete a right-handed coordinate system.

Similarly, let

$$\bar{E}(t) = \left[E_1(t),\ E_2(t),\ E_3(t),\ \dot{E}_1(t),\ \dot{E}_2(t),\ \dot{E}_3(t)\right]^T$$

represent spacecraft position and velocity coordinates in a right-handed rotating (earth-fixed) earth-centered Cartesian coordinate system. The $E_1 E_2$ axes lie in the earth's equatorial plane, E_1 axis is directed towards the prime meridian at Greenwich and the E_3 axis is positive towards the north pole.

These two coordinate systems are related by means of the linear transformation

$$\bar{E}(t) = \begin{bmatrix} A & 0 \\ \dot{A} & A \end{bmatrix} \bar{X}(t),$$

where A and $\dot{A}$ are 3x3 orthogonal matrices of the form

$$A = \begin{bmatrix} \cos\theta & \sin\theta & 0 \\ -\sin\theta & \cos\theta & 0 \\ 0 & 0 & 1 \end{bmatrix} ; \dot{A} = -\omega \begin{bmatrix} \sin\theta & -\cos\theta & 0 \\ \cos\theta & \sin\theta & 0 \\ 0 & 0 & 0 \end{bmatrix},$$

ω represents the constant rotation rate of the earth and θ is the angle from the vernal equinox to the Greenwich meridian at time t.

Each spacecraft orbit, or arc, is defined by means of a given set of six initial conditions representing its position and velocity coordinates at some epoch t_0 . Spacecraft positions and velocities at arbitrary time t are obtained by a process of numerical integration of the differential equations of motion, namely,

$$\ddot{X}_K = \frac{\partial V}{\partial X_K}, \qquad K = 1, 2, 3,$$

where V is the potential function associated with the earth's gravity

field. In the present simulation algorithm, the potential function V is expressed in terms of spherical harmonic series expansion, which may include any combination of terms through seventh degree and order.

The slant range $R_{ij}(t)$, from the ith tracker during the jth arc at time t, is calculated by

$$R_{ij}(t) = \sqrt{E_{ij}(t) - E_1^i)^2 + (E_{2j}(t) - E_2^i)^2 + (E_{3j} - E_3^i)^2},$$

where E_1^i, E_2^i, E_3^i represent the given geocentric Cartesian coordinates of the ith tracking station, and $E_{1j}(t)$, $E_{2j}(t)$, $E_{3j}(t)$ are the generated spacecraft coordinates on the jth arc at time t. For each tracker, separate arc dependent systematic bias, scale, and random noise errors are added to the calculated slant range values to yield,

$$R_{ij}^{o}(t) = R_{ij}(t) + B_{ij} + S_{ij} \cdot R_{ij}(t) + \eta_{ij}(t),$$

where

B_{ij} = constant bias

S_{ij} = scale and

$\eta_{ij}(t)$ = random noise with zero mean and constant variance.

Thus, $R_{ij}^{o}(t)$ represents the set of simulated slant range data from which estimates of all parameters of interest are calculated.

In using the program, one specifies the location of all tracking stations, the type of measurements (slant range), minimum elevation

angle, systematic and random errors to be included in the generated data along with the initial conditions for nominal spacecraft orbits and a description of the earth's gravity field. Any number of satellite or spacecraft arcs may be generated. The output appears in the form of a data type containing the simulated tracking data for the arc and station specified. From this point on, it is treated as real tracking data which has undergone editing.

The purpose of the estimation program is to utilize multi-arc satellite tracking data, along with other a priori parameter information to obtain improved estimates and statistics associated with these estimates for selected parameters. These parameters include the satellite state vector(s) at some epoch, tracking station error model coefficients, and tracking station survey errors. The estimation is optimal in the general sense of weighted least squares. As is customary for such nonlinear problems, the observational equations are linearized about some nominal values and the estimation process is then based on the existence of linear relationships between measurement deviations (difference between observed and computed measurements) and the state vector deviations (from the nominal). For all practical cases, any errors introduced by the linearization procedure are overcome by iterating on the solution.

A distinctive feature of the program is the use of a precision trajectory integration technique which is particularly valuable for long arc integrations. This technique employs a power series solution to the equations of motion and the associated variational

equations. Recursive relations are used to generate power series coefficients up to order 20.

Another characteristic of the program is the application of a matrix partitioning algorithm in solving the estimation problem. Frequently, the parameter vector being estimated contains subvectors, each of which are related to distinct groups of observations. The resulting zero entries in the linearized observational equations lead to a specialized patterned structure of the normal equations. The net result is the feasibility of estimating much larger parameter vectors than would otherwise be possible with a given computer memory.

The program itself is made of three major sections. The trajectory integration section is used for the purpose of integrating the differential equations of satellite motion and thus providing a satellite state vector at any desired time to match the time of an observation. This section of the program also generates the power series solution for the variational equations.

The second major part of the program is the computation of the measurements (tracking data) and their partial derivatives with respect to the components of the parameter vector to be estimated. It is this section which generates the linearized observational equations for the third major section, which is the estimation process itself. Here, measurement discrepancies, along with the pertinent partial derivatives, are utilized in the formation of the normal equations and their solution. The existence of serial

correlation in the data is detected and may be accounted for by means of an autoregressive feedback process.

A complete description of this program is given in reference [1] and is clearly outside the scope of the present study; thus only a brief outline on the utilization of slant range data, as it pertains to the present simulation exercise, will be given.

This relationship between the true slant range from the ith AROD site to the spacecraft at time t during the jth arc is

$$R_{ij}(t) = \sqrt{(E_{1j}(t) - E_1^i)^2 + (E_{2j}(t) - E_2^i)^2 + (E_{3j}(t) - E_3^i)^2} ,$$

where all of the above quantities retain their previous definitions. Let the actual observation be related to the true range by

$$\underset{\text{observed range}}{R^o_{ij}(t)} = \underset{\text{true range}}{R_{ij}(t)} + \underset{\text{systematic error}}{\Delta R_{ij}(t)} + \underset{\text{random error}}{V_{ij}(t)} .$$

Let it be further assumed that the systematic error is defined by a two parameter linear error model of the form

$$\Delta R_{ij}(t) = a_{1ij} + a_{2ij} \cdot R_{ij}(t),$$

where a_{1ij} and a_{2ij} represent unknown bias and scale parameters for the ith tracker and which remain constant during the jth arc.

Other parameters which may be considered as unknown are the set of six initial conditions for the arc and the survey coordinates of the tracker. Inasmuch as the observational model is nonlinear, it

will be convenient to replace it by its linearized equivalent. This is accomplished by expanding the observational equation in a Taylor series about some nominal parameter values and retaining terms through first order. The linearized equation is given by:

$$\delta R_{ij}(t) = \sum_{K=1}^{3}\left\{\left(\frac{\partial R_{ij}(t)}{\partial \ell_{Kj}}\right)\delta \ell_{Kj} + \left(\frac{\partial R_{ij}(t)}{\partial X_{iK}}\right)\delta X_{iK} + \left(\frac{\partial R_{ij}(t)}{\partial X_{iK}}\right)\delta X_{iK}\right\} + \delta a_{1ij} + R_{ij}(t) \cdot \delta a_{2ij},$$

where

i	= arc,
j	= station,
t	= time of observation,
δR	= measurement discrepancy (observed minus computed),
$\delta \ell_1$	= east component of survey error (longitude),
$\delta \ell_2$	= north component of survey error (latitude),
$\delta \ell_3$	= vertical component of survey error,
$\delta X_K^\circ, (K=1,2,3)$	= error in position of coordinates of initial conditions at epoch,
$\delta X_K^\circ, (K=1,2,3)$	= error in velocity coordinates of initial conditions at epoch,
δa_1	= bias error parameter, and
δa_2	= scale error parameter.

The details of the actual calculations of all partial derivatives appear in reference [1] and all partial derivaties are evaluated at the nominal parameter values.

In a more compact matrix notation, the above may be written as

$$\delta R_j = \hat{B}_j \hat{\delta} + \dot{B}_j \dot{\delta}_j + V_j \ ,$$

where

- δR_j is the vector of discrepancies for all observations belonging to arc j,
- $\hat{\delta}$ is the vector of corrections to all station survey errors (totally stable parameters),
- $\dot{\delta}_j$ is the vector of corrections to the initial epoch conditions, bias, and scale parameters associated with the jth arc (arc stable parameters),
- $\hat{B}_j$ is the matrix of partial derivatives associated with the totally stable (station survey) parameters,
- $\dot{B}_j$ is the matrix of partial derivatives associated with the arc stable parameters, and
- V_j is the vector of random errors for arc j.

For multiple arcs, the above system of observational equations may be represented more compactly by

$$\delta R = B\delta + V \ ,$$

where

$$\delta R = (\delta R_1, \delta R_2 \ldots \delta R_N)^T$$

$$B = \begin{bmatrix} \hat{B}_1 & \dot{B}_1 & & & \\ \hat{B}_2 & & \dot{B}_2 & & \\ \cdot & & & \cdot & \\ \cdot & & & & \cdot \\ \cdot & & & & \\ \cdot & & & & \\ \hat{B}_N & & & & \dot{B}_N \end{bmatrix}$$

$$\delta = (\hat{\delta}_1 \dot{\delta}_1, \ldots \dot{\delta}_N)^T$$

$$V = (V_1 V_1, \ldots V_N)^T.$$

The minimum variance estimate for the vector of parameters is obtained by solving the system of normal equations

$$(B^T WB + P_o^{-1})\ \delta = B^T W\ \delta R,$$

where

W = inverse covariance matrix of the observational noise vector V and

P_o = covariance matrix associated with the a priori values of δ.

Finally, the covariance matrix associated with this estimate is given by

$$(B^T WB + P_o^{-1})^{-1}.$$

5.1 SIMULATION DESIGN

A set of four geometrical AROD tracking station configurations were selected as the basis of all simulations. This choice was based on the availability of previously evaluated tracking system characteristics such as geodetic SECOR and the NASA North American Optical Network. The simulated tracking geometries were:

a. North American Optical Tracking Net of 14 stations (Figure 1)
b. A network of four quads (nine stations) (Figures 2, 3, and 4)
c. Large quad (Figures 6 and 7)
d. Small quad (Figure 5).

A total of 16 separate cases utilizing the above tracking stations' geometries were performed as summarized in Table A . These consisted of one simulation characteristic of the Optical Net and is referred to as Case NET-1; eight simulations associated with the four quad geometry (Cases FQ-1 through FQ-8); six simulations associated with the large quad geometry (LQ-1 through LQ-6); and one simulation associated with the small quad (SQ-1).

Since the AROD system is capable of utilizing simultaneous range observations from no more than four stations at a time, it was necessary to develop a special station selection algorithm for those simulations involving more than four tracking stations. The algorithm was designed to select from among all participating trackers those four having minimum slant range to the spacecraft.

A new station may be selected and an old one discarded within any five second time interval.

All simulated slant range data were generated according to the algorithm described in the previous section and were thus corrupted with bias, scale, and random errors. Insofar as tropospheric and ionospheric refraction errors are concerned, we have taken the position that, through proper modelling (reference [3]), these errors can be almost totally eliminated. Any residual refraction errors are accounted for, or are lumped with the range bias by making the latter slightly larger than expected for the AROD system. Throughout the simulations, the selected geopotential model was varied in order to study the effects of such model errors on AROD's geodetic accuracy.

While AROD is capable of providing data at a rate of four observations per second, most of the simulations were performed at much lower rates. A typical sampling rate is one observation every 50 seconds. One practical reason for a much lower than nominal sampling rate was to minimize the required computer time. In addition, it was felt that the higher data rates introduce serial correlation and the observations cannot be considered as independent. On the other hand, at a rate of one observation every 50 seconds, there is very little doubt that the data will tend to be independent. The choice of a lower than nominal data rate, all else being constant, also results in more conservative final parameter error estimates. Should one have evidence that observations at a higher rate are

still independent, all of our results are still valid since they may be scaled as a function of the ratio between the data rates under consideration.

The AROD system, in its role as a geodetic tool, possesses certain advantages over the existing SECOR system (reference [3]) quite apart from its higher performance characteristics. Interstation timing errors are completely eliminated by simultaneously interrogating all four ground trackers from the satellite. SECOR, on the other hand, as the name itself implies, is a sequential processor with one of the ground stations acting as the master to start the sequential satellite interrogation process, one station at a time. An even more important advantage of the AROD system lies in its ability to provide a dynamic inflight selection of any four ground trackers out of a set of 64. Thus, one is no longer limited, as in the case of SECOR, to repetitive single quad reductions.

This latter distinctive feature of the AROD system has been considered in these computer simulations for all cases where more than four stations participate in a tracking exercise. The results obtained for the North American survey are especially valuable as a direct comparison with results from optical trackers (reference [4]).

5.1.1 Range Error Model

The following linear slant range error model was considered

$$\delta R_{ij}(t) = \sum_{K=1}^{3} \hat{b}_{ijK}(t) \cdot \delta \ell_{Kj} + \sum_{K=1}^{6} \dot{b}_{ijK}(t)\ \delta X_{iK} + \delta a_{1ij} + R_{ij}(t) \cdot \delta a_{2ij} + \eta_{ij}(t)$$

where

i = arc number,

j = station number,

t = time of observation,

δR = measurement discrepancy (observed minus computed),

$\delta \ell_{1j}$ = east component of unknown survey error, station j,

$\delta \ell_{2j}$ = north component of unknown survey error, station j,

$\delta \ell_{3j}$ = vertical component of unknown survey error, station j,

δX_{Kj} = unknown correction to orbit initial conditions, arc i,

δa_{1ij} = unknown range bias associated with station j on ith arc,

δa_{2ij} = unknown range scaling coefficient associated with station j on ith arc, and

η_{ij} = random noise, zero mean, and constant variance.

A priori information in the form of an approximate value and its associated uncertainty was assumed to be available for each of the unknown parameters. The uncertainties range all the way from zero (totally constrained) to infinite (totally unconstrained). For example, all orbit initial conditions were always taken as totally unconstrained. Survey errors were constrained only to the extent demanded by the need to avoid indeterminancy. Inasmuch as range

observations lack directional information, a unique solution to all station survey parameters does not exist. It is, therefore, necessary to constrain the origin and orientation of the tracking network. This requires the fixing, or constraining, of six survey parameters; three to fix the origin and three to define the orientation. We accomplish this by defining one of the tracking stations as the origin and holding its coordinates fixed, and by constraining the height of a second station and the local tangent east and north coordinates of a third station. All other station coordinates are assumed to be completely unknown.

For bias and scale error parameters, we have selected nominal a priori uncertainties of one meter and one part per 10^6, respectively. For the additive random range noise, a nominal value of .5 meter RMS was assumed. These are quite conservative when compared to the design specifications of the AROD system, especially when considering the much lower than nominal data sampling rate utilized in the simulation exercise. A summary of the conditions underlining each of the 16 simulation runs appears in Table A .

5.1.2 Analysis of Survey Errors for the Optical Net

The complete tracking configuration for Case NET-1 representing the simulation for the optical network is illustrated in Figure (1). The actual distribution of the observations relative to the 38 short arcs and 16 tracking stations is tabulated in Table B. The special station selection algorithm was exercised in generating all of the slant range data. Only those observations above ten degrees in elevation were utilized in the reduction.

The estimation algorithm was provided with approximate starting values for all of the parameters to be estimated. Typically, the approximations for station coordinates are within a few tens of meters of the nominal values. Orbit initial conditions were approximated within thousands of meters for position and within a few meters/second for velocity coordinates. Bias and scale parameters were approximated with one meter and one part per 10^6 of the nominal values respectively.

The final estimates after convergence (four iterations) for all station surveys are listed in Table I . The entries in the second column represent the differences between the estimated station coordinates and the corresponding nominal values used in generating the observations. Those station coordinates which were held fixed (to insure determinancy), are identified by the letter "C" in this column. The third column in the table lists the ratio of the standard deviation associated with the estimate to the standard deviation

associated with the random observation noise. The actual error estimate for each station coordinate is obtained by multiplying each corresponding entry by the value of the random observational noise standard deviation. Thus, the effect of a change in the observation noise on station coordinate error estimates is easy to determine without having to repeat the entire simulation. In this particular case, the value used was .5 meters, and thus survey uncertainties (one standard deviation) are seen to range from a minimum value of .2 meters to a maximum of 1.4 meters. The latter is associated with the height of the tracking station at Puerto Rico (PUR). The fact that the recovery for this station, as well as the other fringe stations such as Mojave (MOJ), Bermuda (BER), and Jamaica (JAM), is relatively weak is not surprising. As can be seen from Figure (1), the tracking geometry is less favorable for these stations. The distribution of observations for this tracking geometry, as given in Table ^{B}, also shows that there are less observations from these stations in comparison to the other stations. It should be noted that all estimated corrections to the nominal values are within the corresponding expected errors. While not listed, the same also applies to all other error model parameters.

The above results compare very favorably with previous results obtained from optical trackers (reference [4]). There, based on essentially the same tracking geometry, a total of 4000, right ascension and declination, observations were used. The resultant survey uncertainties ranged from 2.5 to 6.5 meters as compared with a range of only .2 to 1.4 meters for the case of AROD. Taking into

account the conservatively low data rate of one observation every 50 seconds, and the assumed values for bias and scale errors utilized in this simulation, there seems to be no doubt that the AROD system should be capable of even better performance under similar real tracking situations.

5.1.3 Analysis of Four Quad Survey Errors

The two separate four quad tracking configurations labeled "Tracking Geometry B" and "Tracking Geometry C" are illustrated in Figures (2) and (3) respectively. The former represents a subset of nine short arcs typical of the GEOS-I satellite, while the latter represents a set of seven short arcs typical of the SECOR satellite. The actual distribution of these observations are given in Tables C and D . Use was again made of the special station selection algorithm for choosing the four "best" trackers on any given arc, and only those observations above ten degrees in elevation were utilized. The remarks made in the previous section with regard to parameter starting values also apply in these cases.

The final estimates, after convergence, for station surveys exercised in "Tracking Geometry B" (Case No. FQ-1), are listed in Table J. Based on an observation noise of .5 meters and a data rate of one observation every 20 seconds, the resultant standard deviations associated with the recovered surveys range from .4 to 1.4 meters. Again, as one would expect, there is a strong correlation between these results and the tracking geometry. For example, the tracker located at the site labeled ST9 provides more observations and is better situated geometrically, resulting in a sharper determination for its coordinates.

"Tracking Geometry C" was exercised in seven separate simulations in order to test such effects as gravity model, data rates, and parameter a priori uncertainties on the final survey error estimates. Final results for Case No. FQ-2 are listed in Table K , and may be considered as the nominal for this subset of seven simulations. The results obtained in this case are not quite as good as the ones for the previous case (FQ-1). There are two reasons for this behavior. The first is simply due to the poorer geometry as evidenced when comparing Figures (2) and (3). The second reason is due to the reduced number of observations for Case FQ-2 relative to Case FQ-1. Were we to increase the data rate for Case FQ-2 from one observation every 50 seconds to one observation every 20 seconds, we would expect a reduction in the survey uncertainties by a factor of $\sqrt{20/50}$ at the most. Actually, it would not be quite as good because of the existence of some constrained parameters such as bias and scale. Based on previous experience, we feel it safe to say that only about a 20% reduction in these survey uncertainties could be expected to result from such an increase in the data rate.

For Case FQ-3, we have made the assumption that there are no uncertainties associated with either the bias or scale parameters. That is, we know their values perfectly. The effect of such an (erroneous) assumption on final survey error estimates may be analyzed by comparing the corresponding entries in Tables K and L. We see that such an assumption leads to a reduction in survey uncertainties by a factor of 4.

To test the effect of gravity model errors, the estimation algorithm was provided with a gravity model different from that used in generating the observational material. In Case FQ-4, a spherical harmonic gravity field representation through 15th order and degree (SAO 15,15) was utilized, whereas for Case FQ-6, a field with only one zonal harmonic (J2) was considered. The model utilized in generating the data included spherical harmonics through 7th degree and order (NWL 7,7). Final survey estimates for these cases are given in Tables M and O . It can be seen that while there are no differences (within two significant figures) in the corresponding computed survey uncertainties, the differences in the estimated coordinates range within a few meters. The computed survey uncertainties, it should be recalled, are a function of the partial derivatives of the observations with respect to the parameters and these are very weakly dependent of gravity model perturbations. This explains why the computed uncertainties do not change. Inasmuch as we solve for a number of unknown parameters, the effect of errors in the gravity model is absorbed and distributed among these various parameters. Some of the errors appear in the recovered orbits, some in the bias and scale parameters, and some in our survey coordinates. For example, for Case FQ-2, where the correct gravity model was utilized, the tabulated correction to the height of the tracker at Austin (AUS V) is -5.0 meters. For Case FQ-6, where the "wrong" gravity model was utilized, the corresponding correction is +3.8 meters. The total variation of 8.8 meters is much larger than expected from the associated standard deviation of 3.2 meters.

These results indicate that, even for relatively short arc reductions, there is a need to use more sophisticated gravity models. Otherwise, the errors introduced may dominate and any improvement in the operational characteristics of the tracking instrument would not lead to a corresponding increase in the final geodetic accuracy of the system.

To test the influence of the data rate on the final survey error estimates, we repeated Case FQ-2 with a data rate of one observation every 100 seconds and labeled it Case FQ-5. Final error estimates are given in Table N . Comparing corresponding entries in Tables K and N , it appears that doubling the data rate results in an improvement by a factor of approximately 1.2. In Case FQ-7, the data rate was increased to one observation per second and at the same time, the a priori uncertainties associated with bias and scale were doubled (see Table A). This resulted in a reduction of final survey uncertainties by a factor of 2 (Table P). In Case FQ-8, a data rate of one observation every 5 seconds was chosen. Bias a priori uncertainty was increased to 100 meters effectively removing any constraints on this parameter. Survey recovery is comparable (Table Q) to that for Case FQ-2, where tighter a priori bias constraints were enforced. Actual bias recovery for this case is on the order of 5 meters or better. Thus, while meaningful bias recovery may not be possible, the overall effect of large a priori bias uncertainty on final survey uncertainties is relatively moderate and may be compensated for by increasing the data rates.

5.1.4 Analysis of Survey Errors for a Single Quad

Tracking configurations for single quad cases are illustrated in Figures (4), (5), (6), and (7). The same set of short arcs utilized in all four quad simulations were also utilized for single quad simulations except that there was no need to make use of the special station selection algorithm. Tracking geometries D (Figure (4)) and D.1 (Figure (5)) utilize simulated SECOR satellite observations, whereas for tracking geometries E and F, simulated GEOS-I data were utilized.

The distribution of observations for the large quad (LQ-1) and the small quad (SQ-1) are tabulated in Tables E and F respectively. Final estimates for station surveys appear in Tables R and S . Results for the small quad are somewhat better than for the large quad. This can be entirely accounted for by the better geometry of the former. Again, as in cases of four quad simulations, the uncertainties associated with the recovery of station heights are largest.

The effect of the total number of participating arcs may be analyzed by comparing results for Cases LQ-2 and LQ-5. Case LQ-5 utilizes a total of nine short arcs whereas for Case LQ-2, only a subset of four arcs was considered. The distribution of observations for these two cases are tabulated in Tables G and H .

Examination of the final results in Tables T and W , shows a relatively small improvement in the survey recovery when utilizing the larger data set. Taking into consideration the costs associated with the tracking and reduction of multiple arc data, it would appear that no more than four properly chosen arcs should provide sufficiently accurate estimates for the unknown station coordinates. The effect of doubling the a priori uncertainties for bias and scale is illustrated by means of Case LQ-6. Comparing the final results for this case (Table X) with those for Case LQ-2 (Table T) indicates an increase of about 50% in survey uncertainties.

Large quad simulation Cases LQ-3 and LQ-4, show the effect of errors in the fixed station coordinates on the final recovery. The results given in Table U show that, as expected, any uncertainty associated with the origin and orientation of the net will be propagated into all other survey uncertainties. We emphasize again, that all our results yield estimates of survey uncertainties relative to some known (by definition) origin and orientation.

LIST OF ILLUSTRATIONS

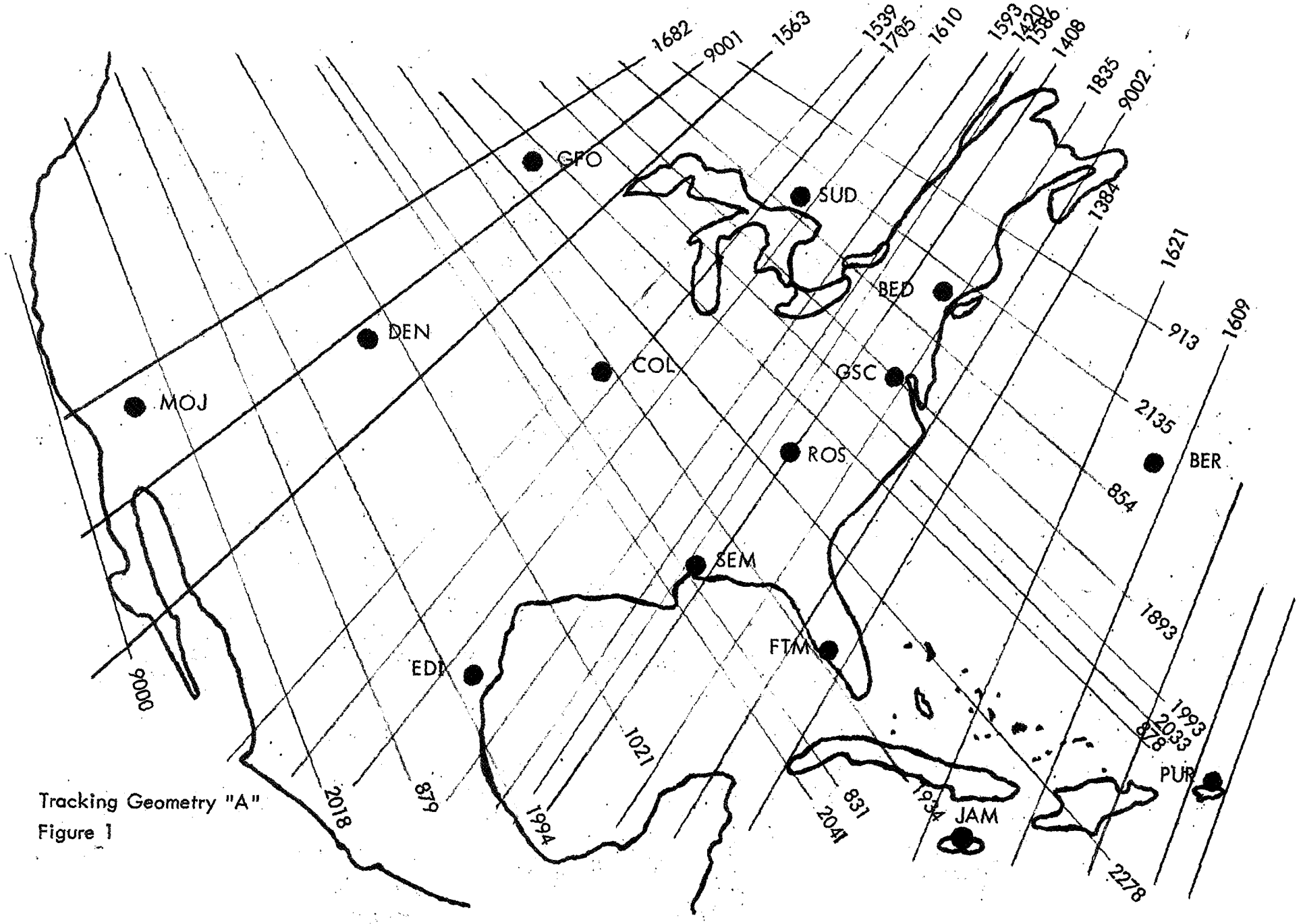

Tracking Geometry "A"
Figure 1

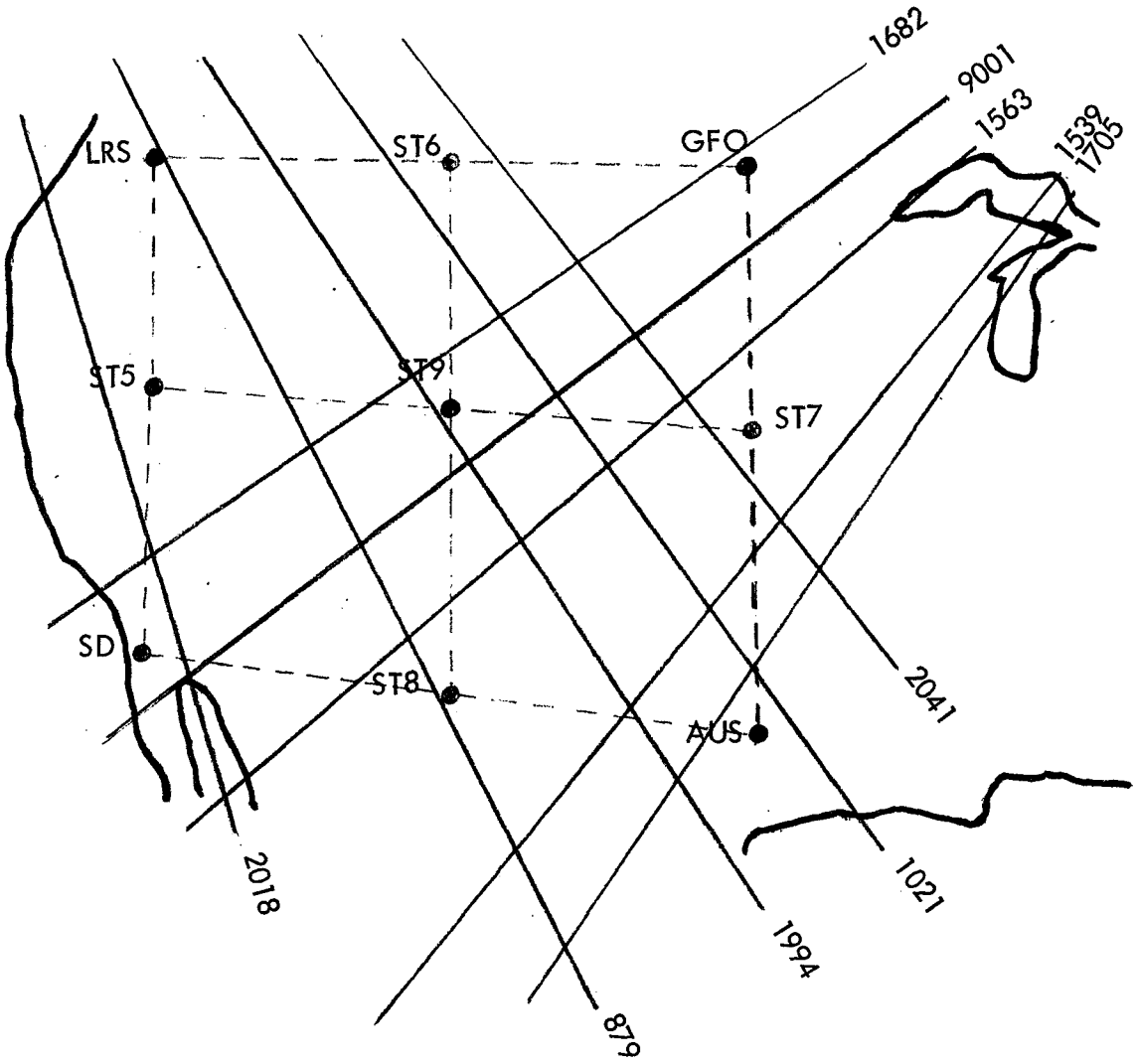

Tracking Geometry "B"
Figure 2

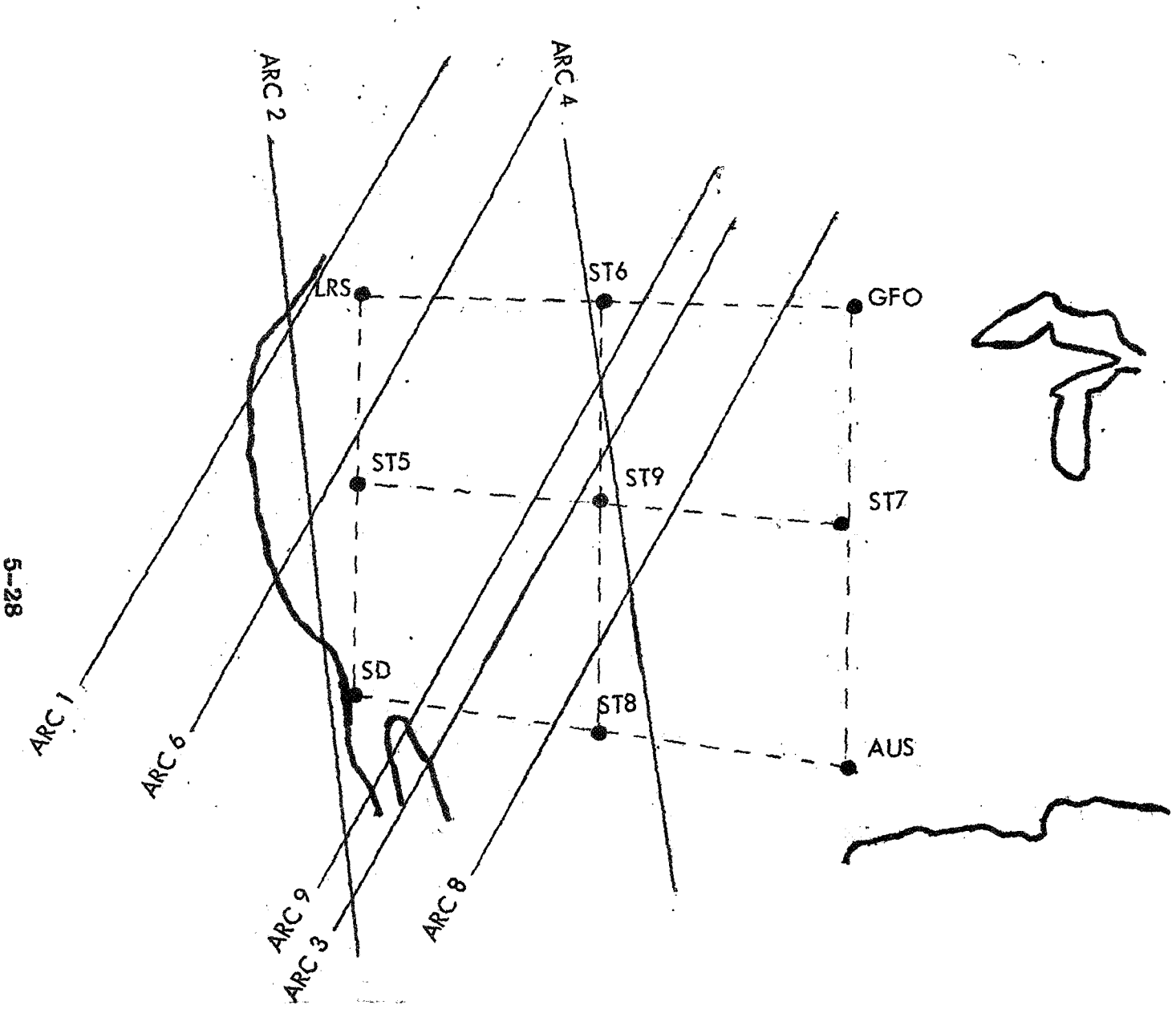

Tracking Geometry "C"

Figure 3

Tracking Geometry "D"

Figure 4

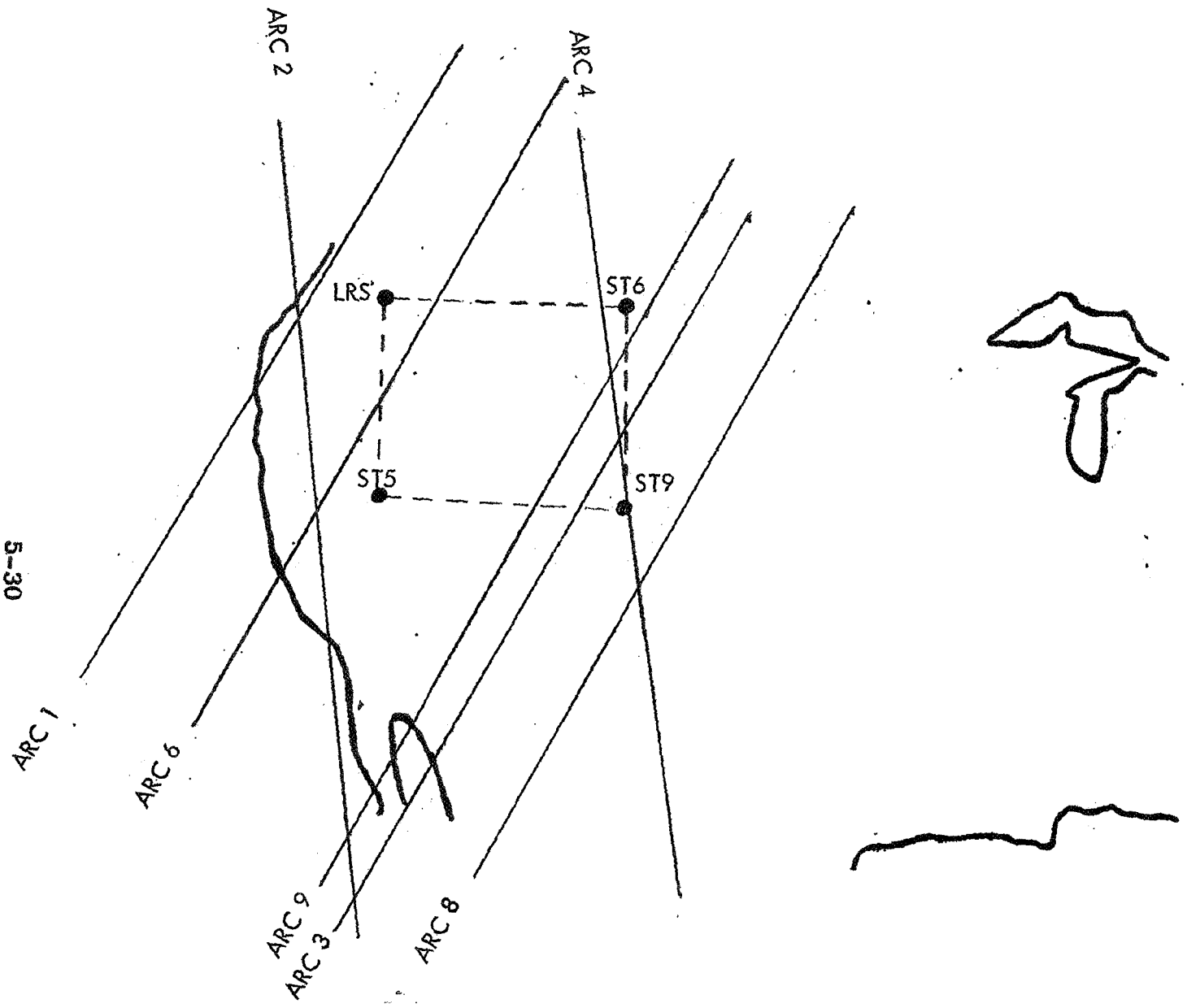

Tracking Geometry "D.1"

Figure 5

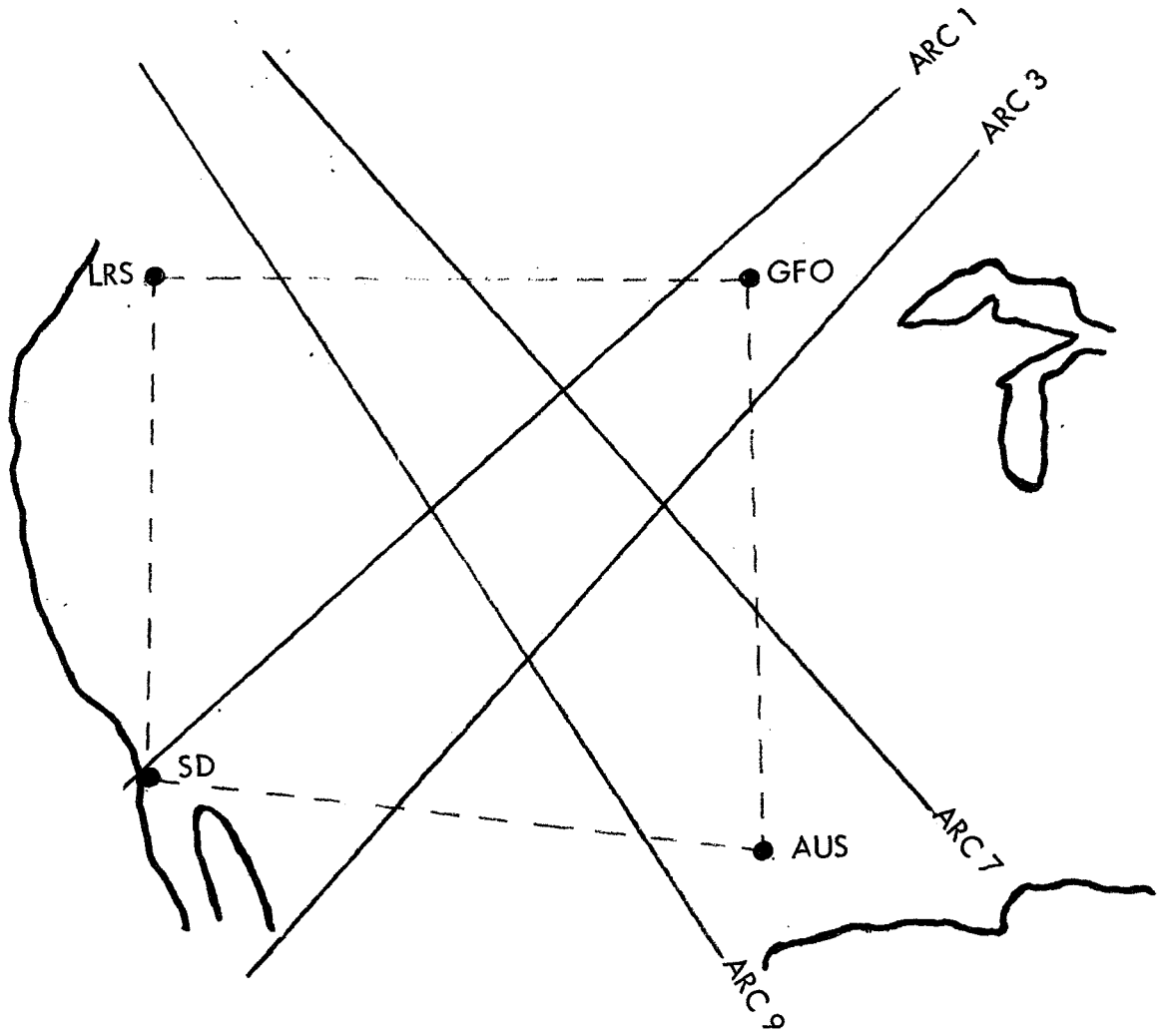

Tracking Geometry "E"

Figure 6

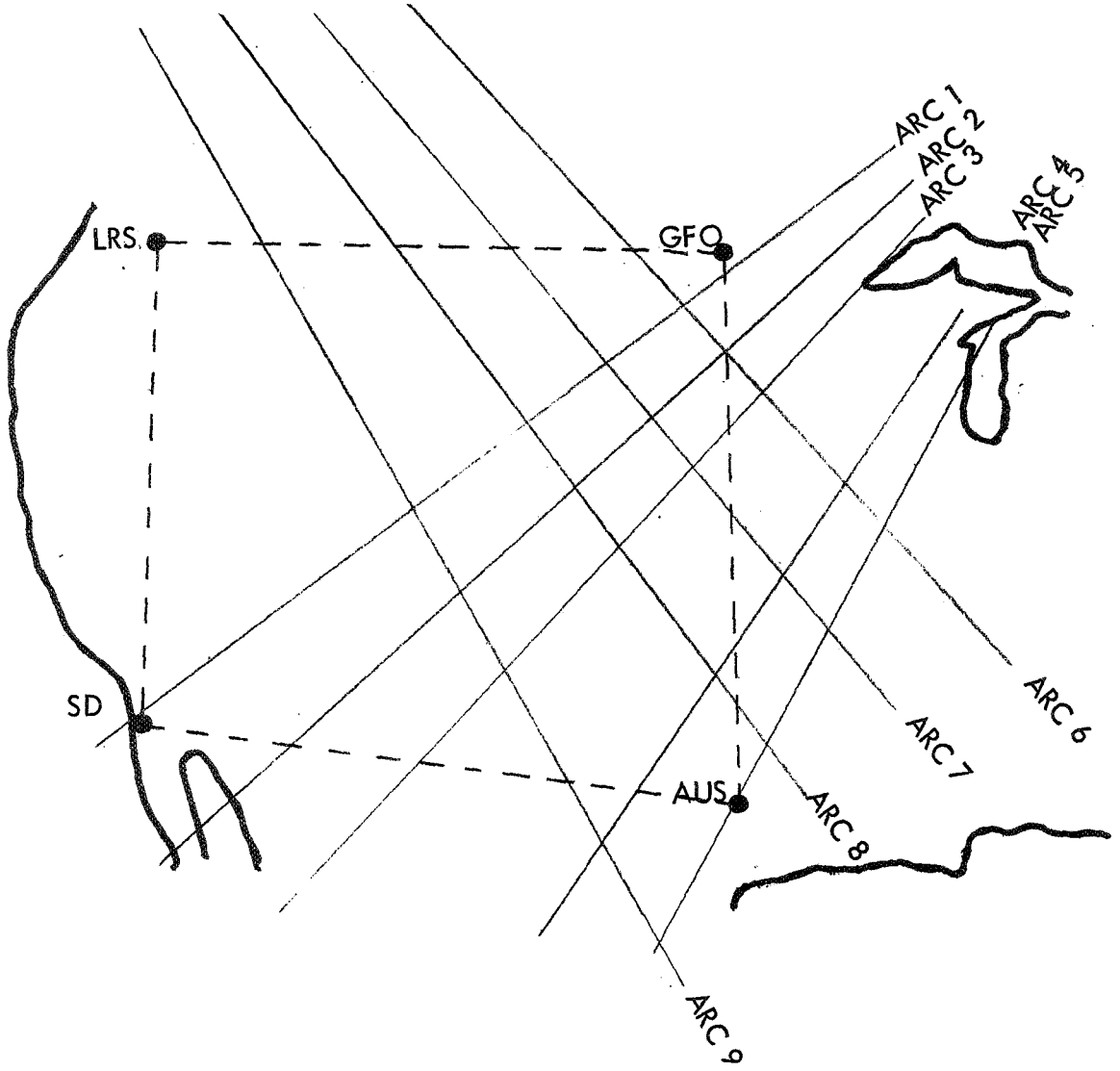

Tracking Geometry "F"

Figure 7

LIST OF TABLES

Table A

SUMMARY OF SIMULATIONS

Case No.	Tracking Geometry Type	Geopotential Model		Time Separation Between Observations	Error Model A Priori Uncertainties		Range Random Noise RMS In Meters
		Simulation Model	Estimation Model		Bias In Meters	Scale In Parts/10	
NET-1	A	Zonals To J7	Same	50 Seconds	1	1	.5
FQ-1	B	Zonals To J7	Same	20 Seconds	1	1	.5
FQ-2	C	NWL 7x7	Same	50 Seconds	1	1	.85
FQ-3	C	NWL 7x7	Same	50 Seconds	0	0	.85
FQ-4	C	NWL 7x7	SAO 15x15	50 Seconds	1	1	.85
FQ-5	C	NWL 7x7	Same	100 Seconds	1	1	.85
FQ-6	C	NWL 7x7	Zonals To J2	50 Seconds	1	1	.85
FQ-7	C	Zonals To J2	Same	1 Second	2	2	.5
FQ-8	C	Zonals To J2	Same	5 Seconds	100	2	.5
LQ-1	D	NWL 7x7	Same	50 Seconds	1	1	.85

(Continued on following page)

Table A

SUMMARY OF SIMULATIONS
(Continued)

Case No.	Tracking Geometry Type	Geopotential Model		Time Separation Between Observations	Error Model A Priori Uncertainties		Range Random Noise RMS In Meters
		Simulation Model	Estimation Model		Bias In Meters	Scale In Parts/10	
SQ-1	D.1	NWL 7x7	Same	50 Seconds	1	1	.85
LQ-2	E	NWL 7x7	Same	50 Seconds	1	1	.85
LQ-3	F	NWL 7x7	Same	50 Seconds	1	1	.85
LQ-4	F	NWL 7x7	Same	50 Seconds	1	1	.85
LQ-5	F	NWL 7x7	Same	50 Seconds	1	1	.85
LQ-6	E	NWL 7x7	Same	50 Seconds	2	2	.85

Table B

DISTRIBUTION OF OBSERVATIONS FOR TRACKING GEOMETRY TYPE A

	Tracking Stations														
Arc #	MOJ	FTM	JAM	BER	SEM	EDI	GFO	DEN	PUR	GSF	ROS	BED	SUD	COL	Total No. of Obs. per Arc
9000	21				1	9	14	19						11	75
9003		15	16	19	1				21	5		6			83
1657		9	3	7	10	5				16	11	12	11		84
1539	5				11	10	11	12		7	3	5	9	11	84
1682	10					4	20	15		4		6	11	14	84
1838				14			7		6	19		21	15	2	84
913	3			6			13	8	1	11	2	13	20	7	84
2018	18	3	1		7	12	10	20						13	84
1598		8			12	9	1	1		11	13	7	9	13	84
9001	14					10	11	18				2	7	17	79
1993		6	4	9			8	5	5	12	8	7	12	8	84
1420		14	6		17	13				6	10	3	4	11	84
1408		14	7		16	11				7	14	5	5	5	84
1502	9						12	1							22
1835		13	6	3	13	9				11	12	8	8	1	84
2278			8	7	7		6	4	6	7	11		7	10	73
1610	5				15	12	2	13		6	7	3	7	14	84
1586		13	6		15	11				8	15	5	6	5	84
1563	13				2	10	11	18		2		2	8	18	84
1384		7	4	15	6					17	10	14	11		84
2088		10	5	8			7	5	5	11	9	4	11	9	84
1609		15	14	14	6	1			17	7	2	6	2		84
1934		15	14	10	7		1		12	6	9		2	4	80
9002		11	7	9	10	5				14	8	11	9		84
1994	7	11	8		12	16	5	10	2		1			12	84

(Continued on following page)

Table B

DISTRIBUTION OF OBSERVATIONS FOR TRACKING GEOMETRY TYPE A
(Continued)

	Tracking Stations														
Arc #	MOJ	FTM	JAM	BER	SEM	EDI	GFO	DEN	PUR	GSF	ROS	BED	SUD	COL	Total No. of obs. per Arc
879	35	10	6		16	25	26	41						38	197
1705	4				12	9	10	11		7	5	5	9	12	84
2135				7			12	7	1	12	4	14	18	9	84
1021	6	10	8		13	11	7	9	4		4			11	83
1898		6	7	12			4	1	8	14	8	10	9	5	84
2017	8	1			3		16	15		5	6		10	19	83
1621		14	12	12	7	2			12	9	6	7	3		84
854		3	5	11			7	4	7	13	7	10	10	6	83
1597		15	15	16	4				20	6		6	1		83
878	1	8	5	7			9	7	5	9	7	3	13	10	84
2041	4	10	6		13		9	11	3		10		3	15	84
831	4	11	8		14		8	10	5		8		3	13	84
985	3	8	5	3	8		10	9	3	5	9		8	13	84
Total # of Obs. per Station	170	260	186	189	258	194	257	274	143	267	219	195	261	336	3209
% of total # of obs.	5.3	8.1	5.8	5.9	8.0	6.0	8.0	8.5	4.4	8.3	6.8	6.1	8.1	10.5	

Table C

DISTRIBUTION OF OBSERVATIONS FOR TRACKING GEOMETRY TYPE B

	Tracking Stations									
Arc No.	LRS	GFO	AUS	SD	ST5	ST6	ST7	ST8	ST9	Total No. of obs. per arc
1682	8	31		13	20	39	30	12	51	204
9001		21		26	28	25	23	30	51	204
1563		21	9	23	18	23	29	30	51	204
1539		27	51	11		20	40	24	31	204
1705		29	51	7		19	44	24	30	204
1021	7	10	31		4	13	32	26	35	158
2018	21		21	35	30	16	3	30	48	204
879	22		22	11	28	23	16	29	47	198
2041	7	45	34		1	17	44	25	23	196
1994	5		40		8	10	34	40	39	176
Total No. of Obs. per station	70	184	259	126	137	205	295	270	406	1952

Table D

DISTRIBUTION OF OBSERVATIONS FOR TRACKING GEOMETRY TYPE C

	Tracking Stations									
Arc No.	LRS	GFO	AUS	SD	ST5	ST6	ST7	ST8	ST9	Total No. of Obs. per Arc
1	20	7		10	16	12	3	5	7	80
2	12		4	14	19	9		11	22	91
3	11	12		10	12	14	11	11	15	96
4	12	9	12	6	13	14	14	13	11	104
6	16	10		10	13	15	7	7	15	93
7	12	12			8	12	4			48
8	5	11	11	9		12	14	12	18	92
9	13	11		11	13	13	8	11	16	96
Total No. of obs per Station	101	72	27	70	94	101	61	70	104	700

Table E

DISTRIBUTION OF OBSERVATIONS BY ARC AND STATION FOR TRACKING GEOMETRY TYPE D

	Tracking Stations				
Arc No.	LRS	GFO	AUS	SD	Total No. of Obs. per Arc
1	23	22	15	22	82
2	23	19	14	19	75
3	21	22	21	22	86
4	21	23	23	22	89
6	22	20	18	23	83
7	16	18			34
8	21	21	21	21	84
9	13	19	19	21	72
Total No. of Obs. per Station	160	164	131	150	605

Table F

DISTRIBUTION OF OBSERVATIONS FOR TRACKING GEOMETRY TYPE D.1

	Tracking Stations				
Arc. No.	LRS	ST5	ST6	ST9	Total No. of Obs. per Arc.
1	23	22	22	22	89
2	23	23	22	22	90
3	21	22	22	15	80
4	23	23	23	24	93
6	22	21	21	21	85
7	16	12	16		44
8	21	21	23	22	87
9	22	22	22	22	88
Total No. of Obs. per station	171	166	171	148	656

Table G

DISTRIBUTION OF OBSERVATIONS BY ARC AND STATION FOR TRACKING GEOMETRY TYPE E

	Tracking Stations				
Arc No.	LRS	GFO	AUS	SD	Total No. of Obs. per Arc
1	26	31	26	21	104
2					
3	28	28	31	31	118
4					
5					
6					
7	21	21	20	18	80
8					
9	30	27	27	28	112
Total No. of Obs. per Station	105	107	104	98	414

Table H

DISTRIBUTION OF OBSERVATIONS FOR TRACKING GEOMETRY TYPE F

	Tracking Stations				
Arc No.	LRS	GFO	AUS	SD	Total No. of Obs. per Arc
1	26	31	26	21	104
2	24	27	24	24	99
3	28	28	31	31	118
4	18	30	31	28	107
5	23	30	31	25	109
6	29	30	27	24	110
7	21	21	20	18	80
8	24	21	21	20	86
9	30	27	27	28	112
Total No. of Obs. per Station	223	245	238	219	925

Table I

FINAL ESTIMATES OF TRACKING STATION COORDINATES
CASE No. NET-1

Station Coordinate		* Estimated Correction to Nominal Values In Meters	Ratio of Sigmas Between Estimated Correction and Observation Noise
MOJ	E	-0.7	1.2
MOJ	N	-0.4	1.4
MOJ	V	C	-
FTM	E	C	-
FTM	N	C	-
FTM	V	-0.7	1.6
JAM	E	0.1	1.0
JAM	N	0.1	0.6
JAM	V	-0.3	2.2
BER	E	-0.2	1.0
BER	N	0.4	1.2
BER	V	0.1	2.2
SEM	E	-0.1	0.6
SEM	N	0.1	0.4
SEM	V	-0.6	1.0
EDI	E	0.1	1.0
EDI	N	-0.1	0.6
EDI	V	-0.4	1.4
GFO	E	-0.6	0.8
GFO	N	-0.0	0.6
GFO	V	0.3	1.2
DEN	E	-0.4	0.6
DEN	N	-0.1	0.6
DEN	V	0.1	0.6
PUR	E	0.7	1.6
PUR	N	-0.1	1.2
PUR	V	-0.1	2.8
GSF	E	0.0	0.8
GSF	N	0.3	0.6
GSF	V	-0.2	1.2
ROS	E	0.1	0.6
ROS	N	0.0	0.4
ROS	V	-0.3	1.0
BED	E	-0.4	1.0
BED	N	0.3	1.0
BED	V	0.1	1.6
SUD	E	-0.7	0.8
SUD	N	-0.3	0.8
SUD	V	-0.3	1.2
COL	E	C	-
COL	N	C	-
COL	V	C	-

* Based on observation noise sigma of .5 meters

C - Station coordinate constrained

Table J

FINAL ESTIMATES OF TRACKING STATION COORDINATES
CASE No. FQ-1

Station Coordinate		* Estimated Correction to Nominal Values In Meters	Ratio of Sigmas Between Estimated Correction and Observation Noise
GFO	E	1.3	2.0
GFO	N	0.0	1.4
GFO	V	-2.0	2.2
AUS	E	C	-
AUS	N	C	-
AUS	V	-3.4	2.8
SAN	E	-3.4	2.2
SAN	N	0.5	2.0
SAN	V	C	-
ST5	E	0.6	1.8
ST5	N	0.1	1.8
ST5	V	-0.1	1.2
ST6	E	0.7	2.0
ST6	N	0.1	1.2
ST6	V	-1.8	1.6
ST7	E	0.8	1.2
ST7	N	0.0	0.8
ST7	V	-2.3	2.2
ST8	E	0.0	1.2
ST8	N	0.3	1.2
ST8	V	-1.4	1.6
ST9	E	0.6	1.2
ST9	N	0.3	1.0
ST9	V	-1.4	1.2
LRS	E	C	-
LRS	N	C	-
LRS	V	C	-

* Based on observation noise sigma of .5 meters

C - Station coordinate constratined

Table K

FINAL ESTIMATES OF TRACKING STATION COORDINATES
CASE No. FQ-2

Station Coordinate		* Estimated Correction to Nominal Values In Meters	Ratio of Sigmas Between Estimated Correction and Observation Noise
GFO	E	0.3	1.6
GFO	N	0.4	1.8
GFO	V	-5.0	3.8
AUS	E	C	-
AUS	N	C	-
AUS	V	-5.1	5.8
SAN	E	2.7	2.4
SAN	N	-0.7	1.0
SAN	V	C	-
ST5	E	2.0	1.2
ST5	N	-0.6	0.6
ST5	V	-0.1	0.8
ST6	E	-0.5	1.0
ST6	N	0.6	0.8
ST6	V	-2.3	1.8
ST7	E	2.0	2.2
ST7	N	-0.7	1.2
ST7	V	-3.4	5.2
ST8	E	1.1	2.2
ST8	N	-0.3	1.0
ST8	V	-2.2	2.6
ST9	E	0.6	1.4
ST9	N	0.3	0.8
ST9	V	-1.7	2.0
LRS	E	C	-
LRS	N	C	-
LRS	V	C	-

* Based on observation noise sigma of .85 meters

C - Station Coordinate Constrained

Table L

FINAL ESTIMATES OF TRACKING STATION COORDINATES
CASE No. FQ-3

Station Coordinate		* Estimated Correction to Nominal Values In Meters	Ratio of Sigmas Between Estimated Correction and Observation Noise
GFO	E	0.0	0.6
GFO	N	0.3	0.4
GFO	V	-0.4	1.0
AUS	E	C	-
AUS	N	C	-
AUS	V	-0.4	1.4
SAN	E	-0.9	0.6
SAN	N	0.0	0.4
SAN	V	C	-
ST5	E	0.2	0.4
ST5	N	-0.2	0.2
ST5	V	0.3	0.2
ST6	E	-0.1	0.4
ST6	N	-0.2	0.2
ST6	V	-0.4	0.4
ST7	E	-0.7	1.2
ST7	N	-0.5	0.4
ST7	V	-0.9	1.4
ST8	E	-1.0	0.6
ST8	N	-0.1	0.4
ST8	V	-1.0	0.6
ST9	E	-0.6	0.4
ST9	N	-0.1	0.2
ST9	V	-0.4	0.4
LRS	E	C	-
LRS	N	C	-
LRS	V	C	-

* Based on observation noise sigma of .85 meters

C - Station coordinate constrained

Table M

FINAL ESTIMATES OF TRACKING STATION COORDINATES
CASE No. FO-4

Station Coordinate		* Estimated Correction to Nominal Values In Meters	Ratio of Sigmas Between Estimated Correction and Observation Noise
GFO	E	0.0	1.6
GFO	N	0.4	1.8
GFO	V	-2.7	3.8
AUS	E	C	-
AUS	N	C	-
AUS	V	-4.2	5.8
SAN	E	1.6	2.4
SAN	N	-1.0	1.0
SAN	V	C	-
ST5	E	1.4	1.2
ST5	N	-0.7	0.6
ST5	V	-0.2	0.8
ST6	E	-1.0	1.0
ST6	N	0.8	0.8
ST6	V	-1.3	1.6
ST7	E	1.7	2.2
ST7	N	-0.4	1.2
ST7	V	-2.1	5.2
ST8	E	0.1	2.2
ST8	N	-0.3	1.0
ST8	V	-2.3	2.6
ST9	E	-0.2	1.4
ST9	N	0.5	0.8
ST9	V	-1.4	2.0
LRS	E	C	-
LRS	N	C	-
LRS	V	C	-

* Based on observation noise sigma of .85 meters

C - Station coordinate constrained

Table N

FINAL ESTIMATES OF TRACKING STATION COORDINATES
CASE No. FQ-5

Station Coordinate		* Estimated Correction to Nominal Values In Meters	Ratio of Sigmas Between Estimated Correction and Observation Noise
GFO	E	1.3	2.0
GFO	N	0.4	2.2
GFO	V	-4.7	4.6
AUS	E	C	-
AUS	N	C	-
AUS	V	-6.1	6.8
SAN	E	2.9	2.8
SAN	N	-1.7	1.2
SAN	V	C	-
ST5	E	3.1	1.6
ST5	N	-0.9	0.8
ST5	V	-0.7	1.0
ST6	E	0.3	1.2
ST6	N	0.2	1.0
ST6	V	-2.3	2.0
ST7	E	3.6	2.6
ST7	N	-0.7	1.6
ST7	V	-2.3	6.0
ST8	E	2.8	2.6
ST8	N	-0.4	1.2
ST8	V	-2.4	3.0
ST9	E	1.5	1.8
ST9	N	0.1	0.8
ST9	V	-2.2	2.2
LRS	E	C	-
LRS	N	C	-
LRS	V	C	-

* Based on observation noise sigma of .85 meters

C - Station coordinate constrained

Table 0

FINAL ESTIMATES OF TRACKING STATION COORDINATES
CASE No. FQ-6

Station Coordinate		* Estimated Correction to Nominal Values In Meters	Ratio of Sigmas Between Estimated Correction and Observation Noise
GFO	E	-1.8	1.6
GFO	N	-2.5	1.8
GFO	V	0.3	3.8
AUS	E	C	-
AUS	N	C	-
AUS	V	3.8	5.8
SAN	E	1.7	2.4
SAN	N	-1.5	1.0
SAN	V	C	-
ST5	E	1.2	1.2
ST5	N	-1.2	0.6
ST5	V	-0.2	0.8
ST6	E	-1.4	1.0
ST6	N	-0.2	0.8
ST6	V	0.5	1.6
ST7	E	-0.8	2.2
ST7	N	-2.4	1.2
ST7	V	2.6	5.2
ST8	E	0.5	2.2
ST8	N	-0.5	1.0
ST8	V	0.9	2.6
ST9	E	-0.7	1.4
ST9	N	-0.3	0.8
ST9	V	0.9	2.0
LRS	E	C	-
LRS	N	C	-
LRS	V	C	-

* Based on observation noise sigma of .85 meters

C - Station coordinate constrained

Table P

FINAL ESTIMATES OF TRACKING STATION COORDINATES
CASE No. FQ-7

Station Coordinate		* Estimated Correction to Nominal Values In Meters	Ratio of Sigmas Between Estimated Correction and Observation Noise
GFO	E	-0.6	0.8
GFO	N	0.3	0.8
GFO	V	0.0	1.4
AUS	E	C	-
AUS	N	C	-
AUS	V	-1.7	2.4
SAN	E	0.6	1.0
SAN	N	0.1	0.6
SAN	V	C	-
ST5	E	0.1	0.4
ST5	N	0.1	0.2
ST5	V	-0.4	0.6
ST6	E	0.1	0.4
ST6	N	0.1	0.4
ST6	V	+0.3	0.8
ST7	E	0.3	0.6
ST7	N	+0.1	0.6
ST7	V	-0.4	2.0
ST8	E	0.1	0.8
ST8	N	-0.0	0.4
ST8	V	+0.2	1.2
ST9	E	-0.0	0.4
ST9	N	0.0	0.2
ST9	V	-0.0	1.0
LRS	E	C	-
LRS	N	C	-
LRS	V	C	-

* Based on observation noise sigma of .5 meters

C - Station coordinate constrained

Table Q

FINAL ESTIMATES OF TRACKING STATION COORDINATES
CASE No. FQ-8

Station Coordinate		* Estimated Correction to Nominal Values In Meters	Ratio of Sigmas Between Estimated Correction and Observation Noise
GFO	E	-1.8	2.2
GFO	N	2.8	2.0
GFO	V	-2.0	3.8
AUS	E	C	-
AUS	N	C	-
AUS	V	0.2	6.4
SAN	E	0.7	2.8
SAN	N	-0.3	1.2
SAN	V	C	-
ST5	E	0.3	1.2
ST5	N	-0.3	0.6
ST5	V	-0.7	1.4
ST6	E	0.1	1.0
ST6	N	0.5	0.8
ST6	V	-1.0	1.8
ST7	E	0.5	1.6
ST7	N	0.7	1.2
ST7	V	-3.9	5.2
ST8	E	0.7	2.0
ST8	N	-0.0	0.8
ST8	V	-0.6	3.0
ST9	E	0.6	1.2
ST9	N	0.3	0.4
ST9	V	-0.6	2.4
LRS	E	C	-
LRS	N	C	-
LRS	V	C	-

* Based on observation noise sigma of .5 meters

C - Station coordinate constrained

Table R

FINAL ESTIMATES OF TRACKING STATION COORDINATES
CASE No. LQ-1

Station Coordinate		* Estimated Correction to Nominal Values In Meters	Ratio of Sigma Between Estimated Correction and Observation Noise
GFO	E	-0.2	0.8
GFO	N	0.1	0.8
GFO	V	-0.7	2.4
AUS	E	C	-
AUS	N	C	-
AUS	V	0.2	3.6
SAN	E	0.2	1.2
SAN	N	-0.1	0.8
SAN	V	C	-
LRS	E	C	-
LRS	N	C	-
LRS	V	C	-

* Based on observation noise sigma of .85 meters

C - Station coordinate constrained

Table S

FINAL ESTIMATES OF TRACKING STATION COORDINATES
CASE No. SQ-1

Station Coordinate		* Estimated Correction to Nominal Values In Meters	Ratio of Sigmas Between Estimated Correction and Observation Noise
LRS	E	C	-
LRS	N	C	-
LRS	V	C	-
ST5	E	0.5	0.8
ST5	N	-0.4	0.4
ST5	V	0.3	0.8
ST6	E	-0.8	0.6
ST6	N	0.3	0.4
ST6	V	C	-
ST9	E	C	-
ST9	N	C	-
ST9	V	0.0	0.1

* Based on observation noise sigma of .85 meters

C - Station coordinate constrained

Table T

FINAL ESTIMATES OF TRACKING STATION COORDINATES
CASE No. LQ-2

Station Coordinates		* Estimated Correction to Nominal Values In Meters	Ratio of Sigma Between Estimated Correction and Observation Noise
GFO	E	-0.9	1.1
GFO	N	0.9	1.2
GFO	V	-0.9	1.3
AUS	E	C	-
AUS	N	C	-
AUS	V	-0.5	1.7
SAN	E	2.0	1.6
SAN	N	-0.9	1.1
SAN	V	C	-
LRS	E	C	-
LRS	N	C	-
LRS	V	C	-

* Based on observation noise sigma of .85 meters

C - Station coordinate constrained

Table U

FINAL ESTIMATES OF TRACKING STATION COORDINATES
CASE No. LQ-3

Station Coordinate		* Estimated Correction to Nominal Values In Meters	Ratio of Sigmas Between Estimated Correction and Observation Noise
GFO	E	-2.8	4.8
GFO	N	1.1	4.8
GFO	V	-3.0	3.8
AUS	E	CA	5.0
AUS	N	CA	4.9
AUS	V	-1.4	3.8
SAN	E	-0.1	5.2
SAN	N	0.0	5.1
SAN	V	CA	3.8
LRS	E	CA	4.5
LRS	N	CA	5.1
LRS	V	CA	3.8

* Based on observation noise sigma of .85 meters

CA - Station coordinate constrained with an a priori sigma of .5 meters

Table V

FINAL ESTIMATES OF TRACKING STATION COORDINATES
CASE No. LQ-4

Station Coordinate		* Estimated Correction to Nominal Values In Meters	Ratio of Sigmas Between Estimated Correction and Observation Noise
GFO	E	0.7	1.1
GFO	N	0.8	3.8
GFO	V	-1.1	1.2
AUS	E	CA	4.2
AUS	N	CA	4.2
AUS	V	0.4	1.6
SAN	E	0.6	3.8
SAN	N	1.0	0.9
SAN	V	CA	1.0
LRS	E	C	-
LRS	N	C	-
LRS	V	C	-

* Based on observation noise sigma of .85 meters

CA - Station coordinate constrained with a priori sigma of 5 meters

C - Station coordinate constrained

Table W

FINAL ESTIMATES OF TRACKING STATION COORDINATES
CASE No. LQ-5

Station Coordinate		* Estimated Correction to Nominal Values In Meters	Ratio of Sigma Between Estimated Correction and Observation Noise
GFO	E	0.1	0.7
GFO	N	-0.1	0.6
GFO	V	-1.1	1.0
AUS	E	C	-
AUS	N	C	-
AUS	V	-0.2	1.3
SAN	E	-0.0	1.0
SAN	N	0.7	0.6
SAN	V	C	-
LRS	E	C	-
LRS	N	C	-
LRS	V	C	-

* Based on observation noise sigma of .85 meters

C - Station coordinate constrained

Table X

FINAL ESTIMATES OF TRACKING STATION COORDINATES
CASE No. LQ-6

Station Coordinate		* Estimated Correction to Nominal Values In Meters	Ratio of Sigmas Between Estimated Correction and Observation Noise
GFO	E	-1.3	1.6
GFO	N	0.7	1.6
GFO	V	-1.1	1.6
AUS	E	C	-
AUS	N	C	-
AUS	V	-0.1	2.3
SAN	E	2.4	2.4
SAN	N	-0.6	1.5
SAN	V	C	-
LRS	E	C	-
LRS	N	C	-
LRS	V	C	-

* Based on observation noise sigma of .85 meters

C - Station coordinate constrained

REFERENCES

Reference 1 Hartwell, Lynn, McNellis, "Network Analysis Program Mathematical Analysis Document", Revision No. 2, NASA Contract NAS5-10588.

Reference 2 Garza-Robles, Guion, Lewis, "Network Analysis Program Documentation", Revision No. 2, NASA Contract NAS5-10588

Reference 3 Brown, D. C., "Advanced Techniques for the Reduction of Geodetic SECOR Observations", Final Report, July 1966, U. S. Army Contract DA-44-009-AMC-937(X).

Reference 4 Berbert, Brown, Lynn, "Short Arc Survey of the GEOS North American Network", presented at Symposium on Astrodynamics and Related Planetary Sciences sponsored by the American Geophysical Union, April 1969.

6.0 SUMMARY OF AROD FOR GEODETIC SURVEY

In the previous sections, the four principle sets of factors were studied which influence the capability of AROD to provide highly accurate geodetic survey. These were equipment performance and propagation effects on range accuracy and geometrical effects and data processing upon translation of range inaccuracy to position error.

A large number of potential range error sources were evaluated. Of these, most were shown to be reduced to negligible magnitude by proper reduction of available data. In these cases, the required data for the necessary corrections was determined and the method of range data adjustment obtained.

Other factors, which have resulted in error in other systems have been shown to have been reduced or eliminated by the AROD system.

Advanced data processing of available propagation data plus the proper choice of carrier frequency reduced both tropospheric and ionospheric propagation effects to small size. Any residuals can be lumped together along with calibration, scaling errors, and a small residual random error in a very simple range error model.

By constraining the error model of AROD somewhat less, then straight analysis of AROD indicates that a very simple error model encompassing all residual factors is possible. This model is $\alpha_o + \alpha_1 R + V$ where α_o is a bias constrained to 1 meter rms, α_1 is a scaling error held to 10^{-6} and V a random error of zero bias whose magnitude is 0.5 meters rms.

Using the geometry of previous geodetic survey system simulations

and used in actual field tests of optical systems and of SECOR, this error model was used to simulate the AROD performance. This was done by DBA Systems using the analytical methods developed for SECOR evaluations.

Three things evolved out of this evaluation. The AROD performance together with proper raw data reduction reduce ranging errors to a subsidiary role in survey error. A more important source is the adequate definition of the orbital parameters when using short arc analysis. This would be increasingly true if long arcs were used.

Secondly, the operational flexibility of AROD to rapidly interrogate a large number of stations greatly enhances its ability to provide both rapid and accurate geodetic survey. Positional accuracies of the order of 1 meter can be expected.

Lastly, using a limited number of passes, of order 10, and reasonable strength of figure or geometry, a large area can be surveyed using the AROD system.

The results of this AROD feasibility analysis study are sufficiently promising that a flight evaluation of AROD for geodetic survey is recommended.

7.0 BIBLIOGRAPHY

1. AROD System Description, Report No. 3065-2-1, Revision 5, 1 June 1966. Prepared for Instrumentations and Communications Division, Astrionics Laboratory George C. Marshall Space Flight Center, Huntsville, Alabama, Contract No. NAS8-11835. Motorola, Inc., Scottsdale, Arizona.

2. AROD System Test Model (Contract No. NAS8-11835) Final Report AROD Laboratory Test and Evaluation Program, 10 August 1967 for MSFC. Motorola, Inc.

3. AROD Vehicle Tracking Receiver Design. A. J. Kline, TM 3065-26 Contract No. NAS8-11835.

4. AROD Test and Feasibility Demonstration Program Definition, Contract No. NAS8-11835. S. W. Attwood, 31 March 1966.

5. Unpublished AROD Test Data. There are 63 files of such data with 1 to 50 tests per file on subsystem and system performance.

6. AROD Geodetic Feasibility Analysis - Technical proposal to Office of Grants and Research Contracts Code SC NASA Headquarters, 20 February 1967.

7. Addendum to Ref. 5, Section A.

8. The Propagation of Radio Waves Through the Standard Atmosphere, Vol. III, S. S. Attwood, Editor, NDRC-OSRD, Washington, D. C., 1946.

9. Clarke, R.H. and G. O. Hendry, "Prediction and Measurement of the Coherent and Incoherent Power Reflected from a Rough Surface", IEEE Transactions PGAP, May, 1964, pp. 353-363.

10. Thayer, G. D. and B. R. Bean, "Systematic Atmospheric Refraction Errors of Basehand-Type Radio Tracking Systems and Methods for their Correction", Paper given at "First Space Conference", Cocoa Beach, Florida, April, 1964.

11. Spann, R. G., "AROD Terrestial Multipath Effects", Report 11, February, 1967, Radiation Division Sperry Gyroscope Company, Great Neck, New York.

12. Wong, M. S., "Refraction Anomalies in Airborne Propagation", Proceedings of IRE, Vol. 46, September, 1958.

13. Clarke, R. H. and G. O. Hendry, "Prediction and Measurement of the Coherent and Incoherent Power Reflected from a Rough Surface," IEEE Transactions PGAP, May, 1964, pp. 353-363.

14. Bean and Dutton, Radio Meteorology, U. S. Department of Commerce, National Bureau of Standards, 1 March 1966.

15. Thayer, G. D. and B. R. Bean, " An Analysis of Atmospheric Refraction Errors of Phase Measuring Radio Tracking Systems", Part I, NBS Report 7254, U. S. Department of Commerce, NBS, Boulder, Colorado, 5 June 1962.

16. Brown, Duane C., "Advanced Techniques for the Reduction of Geodetic SECOR Observations", Contract DA-44-009-AMC-937(x), 29 July 1966, for U. S. Army Engineer GIMRADA.

17. "Report of the AD HOC Committee on Electromagnetic Propagation", Appendix B, 1962, A. F. Systems Command Contract AF 18 (600)-1895 ASTIA 296845.

18. Westwater, E. R., "An Analysis of the Correction of Range Errors Due to Atmospheric Refraction by Microwave Radiometric Techniques", March, 1967, Boulder, Colorado, U. S. Department of Commerce, ESSA ASTIA 651589.

19. Bean, B. R, B. A. Cahoon, and G. D. Thayer, "Tables for the Statistical Prediction of Radio Ray Bending and Elevation Angle Error Using Surface Values of the Refractive Index," Technical Note No. 44, U. S. Department of Commerce, NBS, Boulder, Colorado, 16 March 1960.

20. Dutton, E. J. and G. D. Thayer, "Techniques for Computing Refraction of Radio Waves in the Troposphere", Technical Note No. 97, U. S. Department of Commerce, NBS, Boulder, Colorado, 17 October, 1961, revised 15 July 1964.

21. Aslakson, C. I., The Shoran Manual, Two volumes prepared for Aeroservice Corporation.

22. Norton, K. A., "Refraction Corrections to Electrical Range Measurements", Proc. of the 3rd Tropospheric Refraction Effects Meeting, Vol. II, AD 628772, January 1966. (Motorola 20292)

23. AROD Test Model Hardware Final Report Contract NAS8-11835, 1 July 1967, Motorola, Inc.

24. Grant, W. B., "Extropolation of X-Band Measurements to Higher Frequencies", NBS Report 8882, Boulder Laboratories, Boulder, Colorado, 27 July 1965.

25. Lawrence, R. S., C. G. Little, and H.J.A. Chivers, "A Survey of Ionospheric Effects Upon Earth-Space Radio Propagation," Proc. of the IEEE, Vol. 52, January, 1964.

26. Interim Report, "Phase Difference Navigation Satellite Study", RCA Contract NAS-12-509, June, 1967, NASA Document N67-34257.

27. Weisbrod, S., and L. J. Anderson, "Simple Methods for Computing Tropospheric and Ionospheric Refractive Effects on Radio Waves," Proc. of IRE, Vol. 47, October, 1959, pg. 1770.

APPENDIX A

TYPICAL AROD ORBITAL PARAMETERS

Table A-1 is a compilation of typical simplified orbital equations. These are used only to estimate gross system parameters used for estimating general magnitudes of velocities, ranges, range rates, angles, and so forth to bound some of the factors that influence system performance.

Table A-2 is a list of relatively fixed parameter values for this general problem. Only circular passes directly over a station are considered.

TABLE A-1

Typical Orbital Parameters:

$$\frac{mv^2}{(a+h)} = \frac{mMk}{(a+h)^2}$$

$$\frac{mMk}{a^2} = mg$$

$$v^2 = \frac{a^2 g}{a + h} \qquad v = \left(\frac{a^2 g}{a + h}\right)^{1/2}$$

$$\sin \phi = \frac{h^2 + 2ah - r^2}{2ar}$$

$$\sin \alpha = \frac{h^2 + r^2 + 2(a + h)r}{2(a + h)r}$$

$$\dot{r} = v \cos \alpha$$

$\beta = \frac{vt}{a+h}$, t referenced to zenith

$r^2 = a^2 + (a + h)^2 - 2a\,(a + h) \cos \beta$, $r_{max} =$

$$\dot{r} = \frac{a\, v \sin \beta}{r}$$

$$\ddot{r}_{max} = \frac{av^2}{(a + h)h} = \left(\frac{a}{a + h}\right)^2 \frac{a}{h}\, g$$

TABLE A-2

Orbital Values:

$a = 6.367388 \times 10^6$ meters

$g \doteq 10$ m/(sec.)^2

$k = 6.66 \times 10^{17}$ $m^3/(Kg - sec.^2)$

If h = 1000 km

$v \doteq 7500$ m/sec.

$r_{max} = 9750$ km

$\dot{r}_{max} = 3500$ m/sec.

$\ddot{r}_{max} = 47$ m/sec.^{2}